SAPIENZA
UNIVERSITÀ DI ROMA

DEPARTMENT OF CIVIL ENGINEERING, BUILDING AND ENVIRONMENT
GEODESY AND GEOMATICS AREA

PH.D COURSE "INFRASTRUCTURES AND TRANSPORTATIONS"
XXX CICLO

Very Improved KINematic Gravimetry: a new approach to aerogravimetry

Candidate
Martina Capponi

Supervisor
Prof. Eng. Mattia Crespi

Co-supervisor
Emeritus Prof. Fernando Sansò

SAPIENZA
UNIVERSITÀ DI ROMA

DEPARTMENT OF CIVIL ENGINEERING, BUILDING AND ENVIRONMENT
GEODESY AND GEOMATICS AREA

PH.D COURSE "INFRASTRUCTURES AND TRANSPORTATIONS"
XXX CICLO

Very Improved KINematic Gravimetry: a new approach to aerogravimetry

Candidate
Martina Capponi

Supervisor
Prof. Eng. Mattia Crespi

Co-supervisor
Emeritus Prof. Fernando Sansò

Rome, February 21^{th}, 2018

To explain all nature is too difficult a task
for any one man or even for any one age.
'Tis much better to do a little with certainty
& leave the rest for others that come after you.

Isaac Newton

Contents

List of Figures

List of Tables

Abstract

The regional gravity field modeling by means of classical remove-compute-restore procedures is nowadays widely used in different contexts: from geodetic applications for the regional gravimetric geoid determination to exploration geophysics applications to extrapolate gridded or sparse points values of gravity anomalies (Bouguer, free-air, isostatic, etc.), useful to understand and map geological structures in a specific region. However, the accuracies and resolutions required for such exploration activity, do not consent the exploitation of satellite only gravity field data but need the integration with observation acquired at lower altitude.

Thanks to the development, in the late eighties and early nineties, of Global Navigation Satellite Systems (GNSS) and the consequent availability of accurate navigational data, techniques such as airborne gravimetry, that can provide this complementary information, started to spread worldwide. This technique represents nowadays one of the most efficient techniques ideal to collect gravity observations close to the Earth's surface, in a fast and cost-effective way. Airborne gravimetry is capable of providing gravity measurements also in challenging environments which can be difficult to access otherwise, such as mountainous areas, rain forests and polar regions.

However due to the relatively high acquisition velocity, the presence of atmospheric turbulence, aircraft vibration, instrumental drift, etc. airborne data are usually contaminated by a very high observation error. For this reason a proper procedure to filter the raw observations both in the low and high frequency should be applied to recover valuable information.

In this work a new methodology to process airborne gravity measurements, named Very Improved KINematic Gravimetry (VIKING) is presented.

The proposed procedure allows to pre-process the raw observations coming from both the GNSS receiver and the gravimeter, with the aim to optimally

combine the derived accelerations to compute gravity disturbances. Furthermore it consents to process by means of a filtering and gridding procedure these latter raw gravity disturbances to predict the signal on other points (grids or sparse points).

In details, the pre-processing deals with the manipulation of data acquired from the on board gravimeter and GNSS receiver to correct biases and derive gravity accelerations; while the processing regards the procedure to filter and grid the gravity accelerations data to obtain gravity anomalies/disturbances maps.

The developed algorithms used to pre-process raw GNSS acquired data are basically obtained by manipulating the classical GNSS observation equation to derive a new expression sensitive to the receiver acceleration (which corresponds to the vehicle acceleration) but almost insensitive to its actual position, by means of the implementation of the variometric approach. Regarding the pre-processing of the gravimeter data, the two principal aims of the method are the computation of all the corrections to properly combine gravimeter observations with GNSS observations and the optimal sampling of the gravimeter data, characterized by a very high observation rate, in such a way to not have loss of valuable information in terms of gravity accelerations.

The proposed solution to filter and grid raw airborne observations is a remove-compute-restore like procedure, and consists in a combination of an along track Wiener filter and a classical Least Squares Collocation technique. Basically the proposed procedure is an adaptation to airborne gravimetry of the Space-Wise approach, developed by Politecnico di Milano, to process data coming from the ESA satellite mission GOCE. Among the main differences with respect to the satellite application of this approach there is the fact that, while in processing GOCE data the stochastic characteristics of the observation error can be considered a-priori well known, in airborne gravimetry, due to the complex environment in which the observations are acquired, these characteristics are unknown and should be retrieved from the dataset itself.

The presented VIKING methodology is suited for airborne data analysis in order to be able to quickly filter and grid gravity observations in an easy fast and accurate way. Some innovative theoretical aspects focusing in particular on the theoretical covariance modeling are presented too.

An important part of the whole research project regarded the implementation of a suitable software for airborne gravity data processing. It has been developed in parallel C language and is organized in a set of toolboxes, which can be run independently from all the other ones, or in sequence to perform the whole processing. In order to evaluate the goodness of the whole procedure and its performances, various numerical tests have been performed on a real aerogravimetric dataset. The different tests were mainly focused on the analysis of the optimal choice of some parameters involved in the computation and on the performances

in terms of accuracy and computational times of the various modules. The final result of the whole VIKING procedure, once calibrated the different parameters accordingly to the numerical tests performed, shows a predicted signal with accuracies of about 1.3 $mGal$. The obtained result in term of accuracy is in line with the expectations derived from the specific survey characteristics.

Chapter 1

Introduction

1.1 Overview

The Earth's gravitational field has always been a matter of interest for the scientific community because of the valuable contribution that its knowledge can provide to the determination of the real shape of the Earth and also to various geosciences, in particular those involved with the study of mass transport in the Earth's system or the geology, the lithosphere and the Earth's interior. The science that deals with the measurement and representation of the Earth and of its gravitational field is geodesy. In the last decades the rapid development of technology has led to a noticeable improvement in geodesy due to the introduction of innovative instrumentation used to measure the gravitational field both at global and local scale.

The enhancements in satellite geodesy have allowed to reach accuracies never reached before at global level. The successful satellite missions like CHAMP (2000), GRACE (2002) and GOCE (2009), dedicated to the Earth's gravity field measurement, have revolutionized the mapping of this field on a global scale. These improvements have paved the way for important scientific applications such as the precise determination of the actual shape of the Earth, i.e. the geoid, the identification of the crust-mantle boundary surface or the modeling of geostrophic currents.

At regional and local level, the development in the late eighties and early nineties of Global Navigation Satellite Systems (GNSS) and the consequent avail-

ability of accurate navigational data, have led to the spread of techniques such as airborne or shipborne gravimetry. These type of gravity measurements are capable of providing accurate data at a much higher resolution that the one obtained from satellite observations. Local gravity data can be used for scientific applications, like the regional gravity field modeling or gephysical studies, but can also be used for commercial applications such as resources exploration. For exploration purposes much higher resolution and accuracy than that obtained from satellite-only gravity data are required and a complementary information can be provided by airborne gravity data.

Airborne gravimetry is nowadays one of the most efficient techniques ideal to collect gravity observations close to the Earth's surface, in a fast and cost-effective way. One of the main reason of its wide spread is the capability of providing gravity measurements also in challenging environments which can be difficult to access otherwise, such as mountainous areas, rain forests and polar regions. In principle, to measure gravity with this technique, several components are required: an accelerometer for measuring the specific force (gravimeter), a system to compute the accelerometer attitude and a system that measures the inertial acceleration of the aircraft. This latter acceleration is nowadays derived from GNSS observations. By combining the acceleration from the two systems, accelerometer and GNSS, gravity observations can be obtained.

One of the negative aspects of this technique is that in general the data acquired are characterized by extremely large noise, due to the fact that measurements are taken in a complex and dynamic environment. This large noise is both a high frequency noise caused by aircraft vibration, and a low frequency one, due to drifts and systematic errors which affect the accelerometers and the attitude measurements. Typically the noise-to-signal ratio is of the order of 1000 or even more. Another critical issue is the processing of GNSS raw data to compute accelerations, which can led to an increase of the high frequency noise that is reflected in a degradation of the derived gravity observations.

Two possible ways to improve the resolution and accuracy of airborne gravimetry are: the improvement of the sensors used or the development of innovative methodologies for the processing of existing data. The research here presented is focusing on the latter solution.

1.2 The main contributions of the present research

In this framework, this research presents an innovative methodology, called VIKING - Very Improved KINematic Gravimetry for the processing of airborne gravity data. The research project aims to improve performances of airborne kinematic

gravimetry in terms of accuracy and spatial resolution of the retrieved local gravity field, with exploitation of current state of the art satellite technology and innovative processing capabilities.

Within the current research, we will make a distinction between pre-processing and processing of airborne observations: the former deals with the manipulation of data acquired from the on board gravimeter and GNSS receiver to correct biases and derive gravity accelerations; the latter regards the procedure to filter and grid the gravity accelerations data to obtain gravity anomalies/disturbances maps. The objective of the present research is to define a new procedure to pre-process the raw observations coming from both the GNSS receiver and the gravimeter with the aim to optimally combine the derived accelerations. Furthermore, some innovative aspects related also to the processing of the gravitational accelerations, i.e. the filtering, the covariances estimation and the Least Squares Collocation (LSC) adjustment steps, are presented too.

In particular, the method used for the pre-processing of raw GNSS observations is based on the manipulation of the classical GNSS observation equation in such a way that a new observable sensitive to the antenna acceleration at the considered epoch but almost insensitive to the actual antenna position is derived. Regarding the pre-processing of the gravimeter data, the two principal aims of the method are the computation of all the corrections to properly combine gravimeter observations with GNSS observations and the sampling in an effective way of gravimeter data, characterized by a very high observation rate, so that there is no loss of valuable information in terms of gravity accelerations. The first problem is related to the geometry of the instruments on-board and if not properly treated can cause the two instruments to sense different accelerations.

The procedure presented in this work to process (filter and grid) airborne observations consists in a combination of an along-track Wiener filter with a classical Least Squares Collocation adjustment. This algorithm is similar to the GOCE space-wise approach, one of the ESA official solution for the GOCE mission developed by Politecnico di Milano. Among the main differences with respect to the GOCE space-wise solution is worth to be mentioned the fact that, when dealing with airborne observations, the stochastic properties of the observation error are in general unknown and should be therefore estimated by the dataset itself. This last issue has been solved using the crossover analysis in an innovative way, i.e. to sample the airborne system observation error, as described in the following.

1.3 Outline

The present work is organized in 8 chapters. Apart from this first one, meant as a general introduction to the applications of gravity field data and in particular to airborne gravimetry the other ones are organized as follow.

In Chapter 2 the principal laws and definitions of the gravitational potential theory are presented to give to the reader a summary of the basic theory related to the Earth's gravitational field. At the beginning of Chapter 3 a historical overview of the development and spread of airborne gravimetry technique is given. In the second part, the gravity measurement principle is presented together with the standard procedure used to pre-process the gravity data acquired during a survey. Finally a brief description of typical applications for these local gravity data are outlined too.

Chapter 4 presents the VIKING algorithm implemented into a software within this work. In the first part of this chapter the variometric approach for GNSS processing is introduced, followed by the description of the methodology for deriving accelerations from both GNSS and gravimeter data. A brief overview of all the other correction terms that have to be computed to correctly take into account the geometry and the dynamic during the aircraft survey is reported too.

In Chapter 5 the innovative aspects introduced in the classical procedure remove-compute-restore for processing airborne gravimetric accelerations are presented. The advantages of using a Wiener filter and a crossover analysis are highlighted. To conclude, the Least Squares Collocation gridding solution is exposed too.

Chapter 6 is dedicated to the description of the general features of the implemented software for the whole processing of aerogravimetric data. Chapter 7 instead presents the results achieved from different tests performed to calibrate some parameters of the methodology and also the results of the analysis of the data from a real airborne gravity survey, acquired in $2014 - 2015$ by one of the major operator providing airborne geophysical surveys for petroleum and mineral exploration, within an exploration survey committed by Eni S.p.A.. To preserve confidentiality all the geographical information about the area have been removed. In this Chapter the capability of the variometric approach to work with multi-constellation GNSS data has been also investigated and discussed.

The last chapter summarizes the main innovative aspects of this work, the results achieved and the issues to be further investigated.

Chapter 2

Elements of potential theory

To study the Earth's gravitational field it is fundamental to introduce the potential field theory that includes mathematical laws which can be used to describe not only the gravitational attraction but also several other phenomena, like magnetic and electrostatic fields, the fields generated by electrical currents or steady flow of ideal fluids. In this chapter some general aspects of potential theory, with a particular focus on practical geophysics application problems will be presented. In detail, the meaning of a potential field and its principal equations will be exposed in Section 2.1. The spherical harmonic functions, which can be used to describe the Earth's gravity field, will be described in Section 2.2. Moreover some definitions useful for geophysical problems related to the Earth's gravity field measurement and representation will be presented in Sections 2.3 and 2.4.

2.1 The gravitational potential

To understand the meaning of the gravitational potential, the definition of the general term potential field is needed. Generally speaking a field is a set of functions of space and time; it can be of various kind but within this work we will focus on a force field, which describes the forces acting at each point of space at a certain time [5]. This kind of field is regarded to also as a vector field that to be fully described must be characterized by three functions of space and time, corresponding to the respective components of the field in three orthogonal directions. An important characteristic of a vector field is given by its field lines

or lines of force, that are tangent at every point to the vector field.

The Universal Law of Gravitation formulated by Isaac Newton in 1687 in his work "Philosophiae Naturalis Principia Mathematica" together with the Newton's second law of motion should be recalled before the definition of the gravitational potential. The former states that each mass particle in the universe attracts all the others with a force directly proportional to its mass and inversely proportional to the square of its distance. Given two particles with masses m and M, as represented in Fig. 2.1:

$$\underline{F} = G\frac{Mm}{l^2}\underline{n} \tag{2.1}$$

where G is the Newton's gravitational constant $G = 6.67 \cdot 10^{-11} \frac{m^3}{kg\ sec^2}$, l is the distance between the two masses, and $\underline{n}$ is the unit vector in the direction of the geometric distance l. The Newton's second law of motion instead states that the

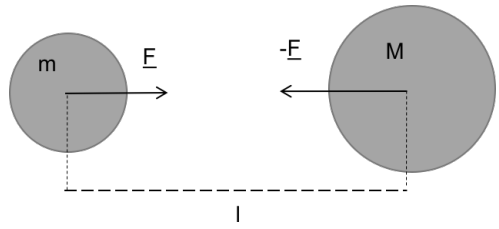

Figure 2.1: Universal law of gravitation

acceleration of a proof mass depends on the force acting upon the body and the inertial mass of the object itself:

$$\underline{F} = m\underline{a} \tag{2.2}$$

where m is the proof mass, $\underline{a}$ represents the acceleration and $\underline{F}$ is the force acting upon the mass. Now, considering both Eq. 2.1 and Eq. 2.2, we have that the acceleration of the particle with mass m under the gravitational attraction of the particle M is given by:

$$\underline{a} = \frac{GM}{l^2}\underline{n} = \frac{\underline{F}}{m} = \underline{f}. \tag{2.3}$$

The force per unit mass $\underline{f}$ at a certain point is also defined as the gravitational field strength or intensity.

The *gravitational potential* of the force field generated by a point of mass M is defined as:

$$V = \frac{GM}{l} \tag{2.4}$$

being V a scalar quantity. It is the work done in bringing a unit mass from infinity to a certain point inside the field distant l. As a consequence, the change in gravitational potential (ΔV) is the change in energy per unit mass when this mass is moved from one point to another in the field. By definition, the gravitational potential gradient is the rate of change of gravitational potential with distance in the field and this is equal to the gravitational field intensity at that point. This means that the derivatives of the potential in any direction are equal to the components of the force per unit mass $\underline{f}$ in that direction, which can be written as:

$$\underline{f} = \begin{bmatrix} \underline{f}_x \\ \underline{f}_y \\ \underline{f}_z \end{bmatrix} = \begin{bmatrix} \frac{\partial V}{\partial x} \\ \frac{\partial V}{\partial y} \\ \frac{\partial V}{\partial z} \end{bmatrix} = grad\ V = \nabla V. \tag{2.5}$$

In mathematics the gradient of a scalar field is defined as the vector which components are the partial derivatives of the field. It represents the direction of maximum increase of the function $\underline{f}$.

After having clarified the relation between the gravitational potential and the gravitational attraction force, applying the superposition principle, it is possible to evaluate the gravitational potential generated by a system composed by n point masses. The superposition principle states that the gravitational potential (or equally the attraction) of a collection of masses equals to the sum of the gravitational potentials of the individual masses [5]:

$$V = \frac{GM_1}{l_1} + \frac{GM_2}{l_2} + \cdots + \frac{GM_n}{l_n} = G \sum_{i=1}^{n} \frac{M_i}{l_i}. \tag{2.6}$$

Moreover, the gravitational potential at point $P = (X, Y, Z)$ generated by masses distributed inside a volume Ω is:

$$V(X,Y,Z) = G \iiint_{\Omega} \frac{\rho d\nu}{l} = G \iiint_{\Omega} \frac{\rho(x,y,z)}{l(x,y,z,X,Y,Z)} dx\ dy\ dz \tag{2.7}$$

where ρ represents the density of the mass element $dm = \rho d\nu$, $d\nu$ is the unit

element of the volume Ω, $d\nu = dx\ dy\ dz$ and l is the distance between the integration point (x, y, z) and P.

The principal properties of the gravitational potential are summarized in the following. For more details the interested reader can refers to [30], [60].

- V is a continuous function in space;
- V zeroes at infinity as $\frac{1}{r}$, r being the distance from the origin;
- the first derivatives of V (the components of the gravitational force per unit mass $\underline{f}$) are continuous functions in space;
- the second derivatives of V are not continuous everywhere (e.g. where the mass density changes with discontinuities, the second derivatives are discontinuous too).

Speaking of gravitational potential, three fundamental equations require to be mentioned: the Poisson's equation, the Laplace's equation and the Gauss's formula.

We define the Laplace operator of the potential field as follow:

$$\nabla^2\ V = \frac{\partial^2 V}{\partial x^2} + \frac{\partial^2 V}{\partial y^2} + \frac{\partial^2 V}{\partial z^2} \tag{2.8}$$

being ∇^2 the Laplace operator that in mathematics is a differential operator of second order that can be applied to scalar or vectorial fields. This operator in Cartesian coordinates corresponds to the sum of all the unmixed second partial derivatives. The Poisson's equation asserts that the gravitational potential assumes the following value:

$$\nabla^2\ V = -4\pi G\rho \tag{2.9}$$

of course outside the masses $\rho = 0$ and the Laplace's equation follows:

$$\nabla^2\ V = 0. \tag{2.10}$$

The harmonic functions solve this last equations and this means that outside the masses that generate the gravitational field, the potential V is a harmonic function. By definition, any real function with continuous second partial derivatives which satisfies Laplace's equation is called harmonic function and the properties of this kind of functions will be investigated more in details in the following section.

The other fundamental relation, valid for every vector field, is Gauss's formula, applied to the volume Ω enclosed by the surface S_Ω:

$$\iiint_\Omega \mathrm{div}\underline{f} d\nu = \iint_{S_\Omega} f_n dS_\Omega \tag{2.11}$$

where f_n is the component of $\underline{f}$ in the normal direction with respect to the surface S_Ω, while the $div\underline{f}$ corresponds to:

$$div\underline{f} = \frac{\partial f_x}{\partial x} + \frac{\partial f_y}{\partial y} + \frac{\partial f_z}{\partial z} = \nabla \underline{f} = \nabla^2 V = -4\pi G\rho \tag{2.12}$$

and it measures the "intensity" of the sources (enclosed in the volume Ω) generating the field. The left-hand term of Eq. 2.11 represents the sum of the sources in the volume Ω and the right-hand side represents the total flow across the boundary surface S_Ω. So the masses can be associated to the sources generating the field; the "strength" of the sources corresponds to the $div\underline{f}$ directly proportional to the density ρ and the surface integral is the total gravitational flow through S_Ω. Since the components of the vector $\underline{f}$ can be easily derived from the gravitational potential V, the Gauss's formula can be expressed also as:

$$\iiint_\Omega \nabla^2 V d\nu = \iint_{S_\Omega} \frac{\partial V}{\partial n} dS_\Omega. \tag{2.13}$$

In potential theory, we can assert that it is possible to identify basically two kinds of problems: the forward and inverse problem. The former, applied to the geophysical interpretation of measured gravity field, consists in determining the gravitational potential values from a certain known distribution of mass sources. The solution to this problem is unambiguous since the harmonic function V outside the surface S_ν, being ν the volume determined by the known distribution of mass sources, is univocal determined from its value on S_ν. The latter, namely the inverse problem, regards the direct computation of the distribution of masses from observations of the gravity field. Differently from the forward problem, this one has not an univocal solution, since, in general, infinite mass distributions exist that can generate an external potential V.

2.2 Spherical harmonic functions

The Laplace's equation (Eq. 2.10), once converted from Cartesian to spherical coordinates, can be solved and the general expression of the spherical harmonic functions can be derived, as presented in the following. The relation between

Cartesian and spherical coordinates is:

$$\begin{cases} x = r\ cos(\varphi)\ cos(\lambda) \\ y = r\ cos(\varphi)\ sin(\lambda) \\ z = r\ sin(\varphi) \end{cases} \tag{2.14}$$

where r is the radius of the sphere, φ is the spherical latitude and λ is the spherical longitude. Applying these conversion relations to Eq. 2.10, firstly the expressions for dr, $d\varphi$, $d\lambda$ in terms of dx, dy, dz can be derived and then the second derivatives of the potential V can be computed as well. After a few steps, the Laplace's equation in spherical coordinates results as:

$$\nabla^2 V = \frac{\partial^2 V}{\partial r^2} + \frac{1}{r^2}\frac{\partial^2 V}{\partial \varphi^2} + \frac{1}{r^2}\frac{1}{cos^2(\varphi)}\frac{\partial^2 V}{\partial \lambda^2} + \frac{2}{r}\frac{\partial V}{\partial r} - \frac{1}{r^2}\frac{sin(\varphi)}{cos(\varphi)}\frac{\partial V}{\partial \varphi} = 0. \tag{2.15}$$

As stated previously, a function is harmonic in a certain region if it satisfies the Laplace's equation at every point of that region. A harmonic function is analytic inside the region in which satisfies the Laplace's equation (i.e. it is a function that is locally given by a convergent power series) and this means that it is continuous and its derivatives of every order are continuous as well. The gravitational potential, satisfying the Laplace's equation outside the masses, is a harmonic function in this region. The simplest harmonic function is the inverse of the geometrical distance between two points of coordinates (x, y, z) and (ξ, η, ζ):

$$\frac{1}{l} = \frac{1}{\sqrt{(x-\xi)^2 + (y-\eta)^2 + (z-\zeta)^2}}. \tag{2.16}$$

Eq. 2.16 can be seen as the potential of a point with mass $M = \frac{1}{G}$ placed at $(\xi,\ \eta,\ \varsigma)$, computed at $(x,\ y,\ z)$, in this case $V = \frac{1}{l}$.

Coming back to Eq. 2.15, the complete real solution of the form $V(r, \varphi, \lambda)$, by separation of variables, results as:

$$V = \sum_{\ell=0}^{\infty}\sum_{m=0}^{\ell}\frac{1}{r^{(\ell+1)}}P_{\ell m}(sin(\varphi))[C_{\ell m}\ cos(m\lambda) + S_{\ell m}\ sin(m\lambda)] \tag{2.17}$$

where $C_{\ell m}$, $S_{\ell m}$ are numerical coefficients that characterize the values of V on the sphere of radius R centered at the origin, $P_{\ell m}(sin(\varphi))$ are the Legendre's associated functions of degree ℓ and order m. In particular, for each couple (ℓ, m) these functions' expression is:

$$P_{\ell m}(sin(\varphi)) = cos^2(\varphi) \sum_{t=0}^{k} T_{\ell m t}\ sin^{\ell - m - 2t}(\varphi) \tag{2.18}$$

with k equal to the integer part of $\frac{(\ell - m)}{2}$ and the coefficients $T_{\ell m t}$ which can be determined using recursive formulas, as proposed by [36], starting from:

$$T_{\ell m t} = \frac{(-1)^{\ell}(2\ell - 2t)!}{2^{\ell}(\ell - t)!(\ell - m - 2t)!}. \tag{2.19}$$

An example of Legendre's associated functions is shown in Fig. 2.2.

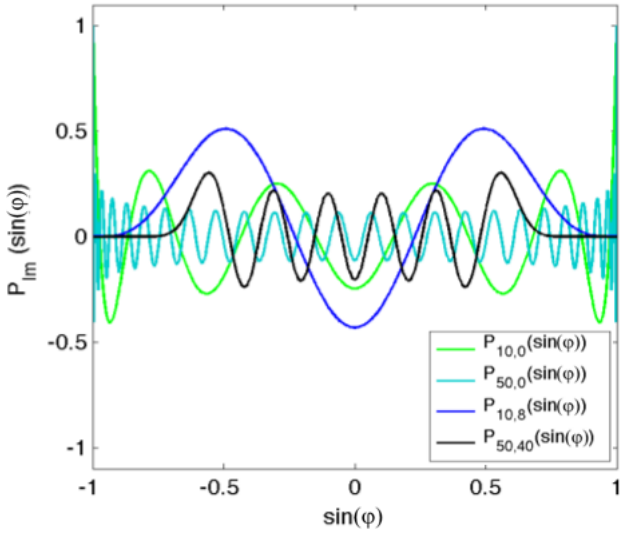

Figure 2.2: Legendre's associated functions $P_{\ell m}(sin(\varphi))$

In Eq. 2.17 it is possible to identify a particular kind of functions, namely the Laplace's spherical harmonic functions, defined as follow:

$$Y^{C}_{\ell m}(\varphi, \lambda) = P_{\ell m}(sin(\varphi))\ cos(m\lambda) \qquad \text{(cosine harmonic)}$$
$$Y^{S}_{\ell m}(\varphi, \lambda) = P_{\ell m}(sin(\varphi))\ sin(m\lambda) \qquad \text{(sine harmonic)}$$

The spherical harmonics are a complete set of base functions on the sphere, that can be used to represent functions defined on the surface of a sphere. They

can be considered the equivalent of Fourier series in one dimension, applied to the sphere.

The spherical harmonics can be divided in: *zonal*, *tesseral* and *sectoral* harmonics. The *zonal* spherical harmonics are those characterized by order $m = 0$ and they are invariant under the rotation through the z axis. This means that they are invariant with respect to λ. Another characteristic of these function is that they have ℓ zeros in the interval $-\frac{\pi}{2} \leq \varphi \leq \frac{\pi}{2}$. The spherical harmonics with order $m \neq 0$ are divided in *tesseral*, if $m \neq \ell$, and *sectoral*, when $m = \ell$. Those two types of harmonics are characterized by $(\ell - m)$ change of sign in the interval $-\frac{\pi}{2} \leq \varphi \leq \frac{\pi}{2}$. Moreover the functions $cos(m\lambda)$ and $sin(m\lambda)$ have $2m$ zeros in the interval $0 \leq \lambda \leq 2\pi$. These three types of harmonics are shown in Fig. 2.3. The

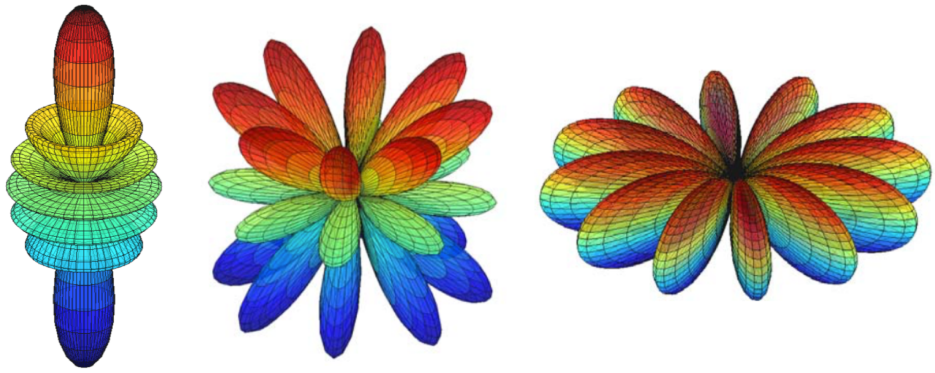

Figure 2.3: Zonal, tesseral and sectoral spherical harmonics: the harmonic on the left is the zonal harmonic with $\ell = 6$ and $m = 0$; the one in the middle is the tesseral harmonic with $\ell = 6$ and $m = 4$, the one on the right corresponds to the sectoral harmonic with $\ell = 6$ and $m = 6$

spherical harmonics are orthogonal functions that satisfy the following relations:

$$\iint_\sigma Y^C_{sr}(\varphi,\lambda) Y^C_{\ell m}(\varphi,\lambda) d\sigma = \iint_\sigma Y^S_{sr}(\varphi,\lambda) Y^S_{\ell m}(\varphi,\lambda) d\sigma = 0 \qquad s \neq \ell \text{ and } r \neq m$$

$$\iint_\sigma Y^C_{\ell m}(\varphi,\lambda) Y^S_{\ell m}(\varphi,\lambda) d\sigma = 0 \qquad \text{always}$$

$$\iint_\sigma [Y^C_{\ell 0}(\varphi,\lambda)]^2 d\sigma = \frac{4\pi}{2\ell+1} \qquad \text{zonal harmonics}$$

$$\iint_\sigma [Y^C_{\ell m}(\varphi,\lambda)]^2 d\sigma = \iint_\sigma [Y^S_{\ell m}(\varphi,\lambda)]^2 d\sigma = \frac{2\pi}{2\ell+1} \frac{(\ell+m)!}{(\ell-m)!}$$

All the above orthogonal relations allow to estimate the coefficient $C_{\ell m}$ and $S_{\ell m}$ to describe the gravitational potential. A Global Gravity Model (GGM) in fact, basically consists in a set of coefficients $C_{\ell m}$ and $S_{\ell m}$ for each degree ℓ and order m, till a maximum degree equal to $\ell = L_{max}$. The maximum degree L_{max} is usually chosen from an analysis of the "degree variance" which expresses the power of a certain degree ℓ. It can be approximately calculated by means of Kaula relation's [36]:

$$\sigma_\ell^2 = \sum (C_{\ell m}^2 + S_{\ell m}^2) \cong 160 \frac{10^{-12}}{\ell^3}. \tag{2.20}$$

2.3 Earth's gravity field, geoid, ellipsoid

The Earth's gravity field is the field generated by the forces that act on a body in quiet on the Earth's surface. It is given by the sum of two acting forces, considered applied to a unit mass: the gravitational force (Newton's attraction force) and the centrifugal one, due to Earth's rotation:

$$\underline{g} = \underline{f} + \underline{c} \tag{2.21}$$

where $\underline{f}$ is the gravitational force, $\underline{c}$ represents the centrifugal force, equal to $\omega^2(r\ cos(\varphi))$, with ω the Earth's rotation velocity. The gravity force per unit mass, that corresponds to an acceleration, is measured generally in *gal*:

$$1\ gal = 1\ cm\ s^{-2} \tag{2.22}$$

and its direction is defined by the plumb line, so it coincides with the direction of the vertical. The gravity force is not constant on the Earth's surface and it can vary from about 978 *gal* at the Equator to about 983 *gal* in correspondence to the North and South poles.

The field generated by the Earth's gravity force admits a potential which results in:

$$\underline{g} = \nabla W \tag{2.23}$$

with W the gravity potential. It can be written as the sum of two potential field:

$$W = V + \frac{1}{2}\omega^2 r^2 cos^2(\varphi) \tag{2.24}$$

where the right terms of Eq. 2.24 correspond to the gravitational and centrifugal potentials, respectively; r is the sphere radius, φ the latitude. All these surfaces that correspond to $W = const$ are referred to as equipotential surfaces (see Fig. 2.4) of the gravity field and the gravity vector is always perpendicular to them, passing through each point belonging to their surfaces.

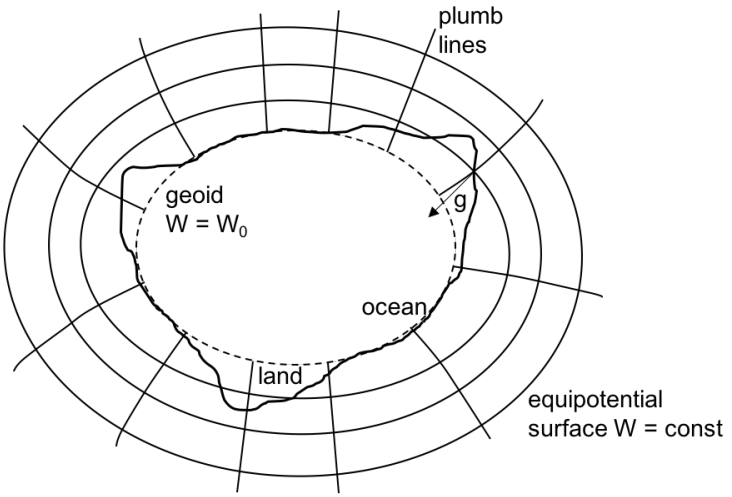

Figure 2.4: Simplified example of the Earth's equipotential surfaces

The *geoid* by definition is the equipotential surface that coincides with the mean sea level in the ocean and its ideally continuation through the continents. It is basically the shape that the surface of the oceans would take, hypothetically in absence of winds and tides, under the effect of the Earth's gravity and centrifugal force. Constituting an equipotential surface, all the points on the geoid have the same potential. The shape of the geoid is influenced by the underlying (and overlying in continental areas) masses and because of the complexity of the Earth's internal mass distributions it is not a simple and smooth geometrical surface. Due to this complex geometry, another surface is generally adopted as reference, the one defined by an ellipse of revolution. [30, 60]

The reference ellipsoid is symmetric through its center and with respect to the rotation axis. Its shape can be described with two parameters: the equatorial radius a and the polar radius c, which are in a relation described by the flattening

parameter

$$f = \frac{a - c}{a} \tag{2.25}$$

or alternatively by the first eccentricity

$$e^2 = \frac{a^2 - c^2}{a^2}. \tag{2.26}$$

Once introduced this reference surface it is possible to split the Earth's gravity field as the sum of two separate contribution: the *"normal"* field (i.e. the reference one) and the *"residual"* field (i.e. the anomalous one). The former is the field that assumes constant values in correspondence of the reference ellipsoid. The normal gravity $\underline{\gamma}$ can be expressed in terms of the normal potential U:

$$\underline{\gamma} = \nabla U. \tag{2.27}$$

The normal potential is the sum of a gravitational potential term U_g and a rotational term U_r [30, 60],

$$U = U_g + U_r \tag{2.28}$$

where

$$U_r = \frac{1}{2}\omega^2 r^2 cos^2(\varphi) \tag{2.29}$$

with ω the angular velocity and φ the latitude. [30] The normal gravitational potential, for symmetry reasons, can in general be expressed as the sum of zonal spherical harmonics:

$$U_g = \frac{GM}{r}\left[1 + \sum_{\ell=1}^{\infty} C_{2\ell,0}\left(\frac{a}{r}\right)^{2\ell} P_{2\ell,0}(sin(\varphi))\right] \tag{2.30}$$

with M the total mass and a the equatorial radius. It is harmonic outside the ellipsoidal surface and it can be uniquely determined everywhere outside by its values on the surface. Moreover, on the surface itself, it is determined by the flattening f parameter, the ellipse equatorial radius a, the total mass of the Earth M and the angular velocity ω. Therefore, the knowledge of these four

parameters allows to evaluate the total normal potential anywhere on or above the surface.

The anomalous potential T is given by the difference between the Earth's gravity potential and the normal one. Globally it is small compared to the normal field with variations smaller than 10^{-5}. [60]

$$T = W - U. \tag{2.31}$$

The functionals of the anomalous potential T are usually adopted for regional or local gravity models. One of the most common used is the gravity anomaly which represents the difference between the gravity computed at one point P on the geoid and the relative gravity on the ellipsoid (see Fig. 2.5).

$$\Delta g = g(P) - \gamma(Q) \tag{2.32}$$

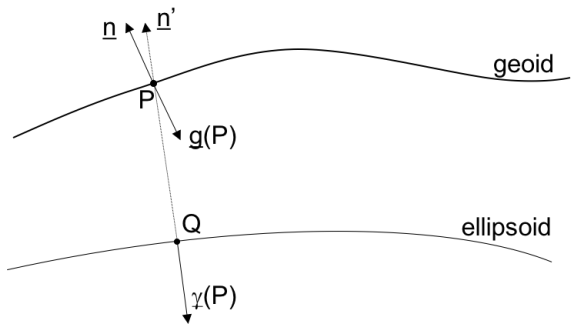

Figure 2.5: Gravity anomaly schematic representation

In other cases the functional adopted instead of the gravity anomaly can be the gravity disturbance, which is simply defined as the difference between the gravity at a certain point P and the correspondence value of the normal gravity at the same point; or it can be the geoid undulation that can be easily derived in the following way:

$$N = \frac{T}{\gamma} \tag{2.33}$$

known as Brun's relation.

2.4 Gravity anomalies

The local density variations produce gravity anomalies with respect to the normal gravity field, that if properly isolated inside the observed gravity measurement, can be useful for geophysical applications, as resources exploration. As proposed in [5], an easy way to describes all these correction is to consider them as contributions to the observed gravity:

obs. gravity = attraction of the reference ellipsoid
+ effect of elevation above sea level (free-air)
+ time-dependent variations (tidal)
+ effect of moving platform (Eötvös)
+ effect of the "normal" mass above sea level (Bouguer and terrain)
+ effect of the masses that support topographic loads (isostatic)
+ effect of crust and upper mantle density variations (geology)

To identify the gravity anomalies means to separate the last quantity of this sum from all others terms. The effect of the elevation above or below the sea level is a correction that has to be applied to all those gravity measurements taken over land or in the air. If $g(r)$ represents the gravity attraction on the geoid, its correspondent value at an altitude $r + h$ above the geoid is given by a Taylor's series expansion:

$$g(r+h) = g(r) + h\frac{\partial g(r)}{\partial r} + \cdots \tag{2.34}$$

with this last term, i.e. $h\frac{\partial g(r)}{\partial r}$, being the one that takes into account the difference in elevation between $g(r)$ and $g(r+h)$. Neglecting the high-order terms and rearranging the Eq. 2.34, assuming a spherical and uniform Earth with $g(r) = \frac{-GM}{r^2}$, we get:

$$g(r) = g(r+h) - h\frac{2g(r)}{r}. \tag{2.35}$$

This last term is known as the free-air correction because it is only an elevation adjustment. The application of this correction provides the *free-air anomaly* given by:

$$\Delta g_{fa} = g_{obs} - g_{fa} - g_0 \tag{2.36}$$

where g_{obs} is the observed gravity and g_0 represents the attraction of the reference ellipsoid.

The tidal correction is applied to remove from the observed gravity the effect of Earth's tides. It is both time- and latitude-dependent and its order of magnitude is of 0.1 $mGal$. [5] This correction term can be computed at any time and place on the Earth's surface using well known formulas (e.g. [43]). The Eötvös effect is a motion-related effect that has to be properly taken into account for gravity measurements made on moving platforms, like ships or aircrafts. It will be investigated more in details in the following chapters.

After the application of the free-air correction and the removal of the reference gravity from the observed gravity, all the masses between the level of observation and sea level are still affecting the measured gravity. The simple Bouguer correction accounts for these masses. To compute this term, the principal hypothesis consists in approximating all the masses between the observation point and the sea level with infinitely extended flat slab of homogeneous density and thickness equal to the height of the observation point height above the sea level. The attraction due to an infinite slab of constant density can be computed by the following equation:

$$g_{sb} = 2\pi G\rho h \tag{2.37}$$

where ρ is the density and h is the thickness of the slab. Removing this correction term from the *free-air anomaly* it is possible to derive the *simple Bouguer anomaly*:

$$\Delta g_{sb} = g_{obs} - g_{fa} - g_{sb} - g_0. \tag{2.38}$$

In the *simple Bouguer anomaly* the actual shape of the terrain is not considered: mountains and valleys are in fact ignored by the slab approximation. This problem is solved computing the terrain correction g_t adjustment that is fundamental to take into account the gravitation effect of the actual topography. Adding this term the *Bouguer anomaly* is obtained as:

$$\Delta g_b = g_{obs} - g_{fa} - g_{sb} - g_t - g_0. \tag{2.39}$$

The terrain correction is traditionally computed by approximation the topography with a digital terrain model and computing the gravitational attraction of the model with the uses of various numerical or analytical methods as those proposed in [44], [46], [23], [72], [56]. Both the *simple Bouguer anomaly* and the

Bouguer anomaly are generally adopted for geophysical applications since they reflect the "anomalous masses" with different density from the one considered for the Bouguer slabs. This means that they highlight the density contrasts of the anomalous masses.

The last correction term to be analyzed is the isostatic correction. It is calculated on the basis of the isostasy hypothesis that considers the lighter crust as a floating mass on the denser underlying mantle (isostatic equilibrium), in the absence of disturbing forces [75]. The three principal models of isostasy used to compute this correction term are the Airy-Heiskanen model (in which the crust is considered with a constant density and the different topographic heights are associated to changes in crustal thickness), the Pratt-Hayford model (where different topographic heights are accommodated by lateral changes in rock density) and the Vening-Meinesz or flexural isostasy model (in which the lithosphere is considered as an elastic plate that distributes local topographic loads over a broad region by bending) [5, 30]. The application of this correction term to the *Bouguer anomaly* provides the *isostatic anomaly*:

$$\Delta g_i = g_{obs} - g_{fa} - g_{sb} - g_t - g_{is} - g_0. \tag{2.40}$$

The computation of all these correction terms allows to separate the various gravitational contributions and provides valuable information which can be used for a better understanding of the geological structure of the Earth's interior.

Chapter 3

Airborne gravimetry

The airborne gravimetry technique is one of the most promising technique for the retrieval of local gravity field data. Differently from pointwise ground measurements, that are quite time consuming, this technique allows to investigate with a few days survey, wide areas of about one hundred of km^2 at a relatively low cost. Another advange of using the airborne gravimetry technique is related to the fact that this type of survey can be conducted in every kind of challenging environment.

This chapter provides an introduction to the airborne gravimetry technique. In Section 3.1 a brief history about the first ideas and experiments in the late 1950s is given. The Subsection 3.1.1 is dedicated to the development of GNSS. The general principle of measurement is discussed in Section 3.2, with particular focus on all the sensors required on board and the importance of the separation of kinematic and gravitational accelerations. The standard procedure to pre-process "raw" aerogravimetric data is explained in details in Section 3.3. The chapter concludes with a discussion of the various applications of airborne gravimetry, from geodetic to geophysical ones, and future developments.

3.1 Historical overview

In the first half of the 20^{th} century various experiments have been conducted to test gravimeters in dynamic environments. During this period the technological evolution has led to a natural evolution of successes with ocean bottom, submarine and shipboard gravimeters. As a consequence, already in the 1950s, both

geodesists and geophysicists were looking for a system to measure gravity from the sky. Airborne systems in fact were considered capable of providing rapid regional gravity maps which could be useful for exploration purposes and geodetic applications.

In 1957 a Canadian geophysicist Hans Lundberg conducted one of the first test of airborne gravimetry measurements, with a system based on the principle of gradiometry, but the experiment was received with skepticism especially in the exploration industry [28]. Another attempt to measure gravity from an aircraft was conducted in the 1958 by the U.S. Air Force Geophysics Lab and this is considered the first fixed-wing airborne gravimetry test. The fixed-wing aircraft was flying at an altitude of 6-9 km to reduce the effect of turbolence in the lower layer of the atmosphere. The gravimeter used was a LaCoste and Romberg sea gravimeter (Model "S") and for navigation a Doppler system was used, which determined the elevation above the mean sea level from the tracking range data on the ground [70]. Additional tests, mainly focused on exploration purposes, were conducted in the following years sponsored by various United States and Russian agencies in collaboration with oil companies, which did sponsor some tests to be aware of the developments [48].

At the time, one of the main problems for airborne gravimetry was the navigation of the aircraft and, to reduce the errors in position estimation, various techniques were exploited such as the Doppler system or a mapping camera and a radar altimeter. These first years of experiments have led to the conclusion that about 10 $mGal$ of accuracy could be reached using the existing navigation systems, coupled with an accurate ground control technique. Moreover, it appeared clear that to reduce the in-flight accelerations of the aircraft, which are the main source of errors in the airborne gravity measurements, large aircrafts flying at high altitudes would be suitable, smoothing the flight conditions. The Eötvös effect, directly related to the aircraft velocity, was initially considered another major issue to be solved to improve the precision of airborne gravity measurements but it was demonstrated that a proper flight programming could allow the estimation of accurate corrections.

Throughout the 1960s and 1970s other successful tests were conducted by the U.S. Naval Oceanographic Office using an helicopter instead of a fixed-wing aircraft, the first one in the 1965 with on board a gimbal-suspended LaCoste and Romberg sea gravimeter. The accuracy range for the measurements, once reduced to the ground, was within ± 5 $mGal$ with respect to the known values [27]. The improved results were related to the fact that the helicopter, differently from the aircraft, has a better capability in following the terrain and flying at lower altitudes and speeds so it is less affected by turbulence conditions.

Despite the improvements in the gravimeters technology and the development of stabilized platform systems, airborne gravimetry did not become fully opera-

tional until the advent of Global Positioning System (GPS) (1980s-1990s). This innovative technology permitted to solve the major problem of the precise estimation of the aircraft position and led to the improvement of existing measurement systems and the consecutive spread of the airborne gravimetry for both geophysical exploration and geodetic applications. The development of GPS technology allowed on the one hand to improve existing gravimeter systems, on the other hand also to develop a new system used to determine the gravity vector by the combination of GPS with Inertial Measurement Units (IMU)[1].

In the 1990s, the academic community (i.e. the University of Calgary, the University FAF Munich, the National Survey ad Cadastre of Denmark, the Swiss Federal Institute of Technology...) in collaboration with industries and governments started the first large-scale airborne gravity campaigns to assess the capabilities of this technique to measure gravity field at a resolution of few km. In 1991-1992 one of the first wide-area survey was conducted in Greenland [7], [18] and with various joint projects other surveys were conducted in the same years and in the following ones over the Antarctic region and in Switzerland. The new accuracies reachable after the advent of GPS were of few $mGal$ at 5-6 km of spatial resolution.

Concurrently to the spread of airborne gravimetry with gravity measured using a stabilized platform system, in the 1990s another type of system was deployed: the Strapdown Inertial Navigation System (SINS). It consists in a set of three orthogonal accelerometers and three gyroscopes. The objective of this system is the determination of the full gravity disturbance vector along the aircraft trajectory and when used, the technique is referred to as airborne vector gravimetry. The first tests and developments of this technique were conducted by the University of Calgary [63] and showed that comparable accuracies at the same spatial resolution of few kilometers could be achieved [77]. For geophysical applications as resources exploration nowadays the classical technique adopted is the stabilized platform system however, in recent years, vector gravimetry surveys begin to be employed by various geophysics companies. Strapdown gravimetry systems are raising the interest of the scientific community due to the potential evolution of IMU [21] [47] [66].

3.1.1 The development of GNSS

With the acronym GNSS we refer to artificial satellites constellations developed for navigational purposes. These systems in fact allow to determine the positions (and velocities/accelerations) of a passive user receiver by a proper processing of signals broadcast by satellites.

The first system to be developed and deployed was the United States (US) NAVigation Satellite Time and Ranging (NAVSTAR) GPS. The first satellite of

this NAVSTAR GPS was launched in 1978 and the Full Operational Capability (FOC) was reached in 1995 with 24 satellites orbiting around the Earth. Initially it was set up for military purposes and to prevent that signals were used in real-time positioning by anyone outside the US Army, these signals were encrypted (Selective Availability S/A). In this way only the US military were able to fully use the system. But in year 2000 the US president Bill Clinton decided to remove the Selective Availability and the position accuracy reached roughly 10 m, against previous 100 m. From that moment there has been a strong development of commercial GPS. For a long period, GPS has been the most used navigation system both for civilian and scientific applications.

In the meanwhile, other countries started to develop similar systems for navigational purposes and the ensemble of all these systems is referred to as GNSS. The aim of the development of other systems was to ensure access to GNSS signals that were not under control of a single nation, both for military but also civilian reasons. The Russian GLObal'naya NAvigatsionnay Sputnikovaya Sistema (GLONASS) reached the fully operation in 1996 with 24 satellites but the economic crisis that hit the country blocked the launch of new satellites and in few years the number of GLONASS operational satellites rapidly decreased to less than 10. Nowadays the available satellites constellations have grown and in addition to the GPS constellation and GLONASS (again fully operational), other systems were launched such as the European Galileo and the Chinese Compass (today Beidou). More information about satellites-based navigation systems can be found in [32].

A GNSS consists of three segments: the Space segment, the Control segment and the User segment.

The GNSS Space segment consists of a constellation of artificial satellites, flying in specific orbits specially designed to ensure the availability of (at least) four satellites in view from virtually any point on the Earth. The satellites are equipped with atomic clocks, radio transceivers and continuously broadcast messages that includes the time the message was transmitted and the satellite position. These information are in general used to estimate the three-dimensional position of the receiver.

The Control segment consists of a global network of ground facilities that track satellites, monitor their transmissions, perform analysis and send commands and data to the constellation. The Master Control Station (for GPS constellation is located in Colorado, for GLONASS in Moscow) generates and uploads navigation messages and ensures the health and accuracy of satellites constellation. The Master Control Station receives navigation information from monitoring stations, it utilizes this information to compute the location of the GNSS satellites in space and then uploads this data to the satellites.

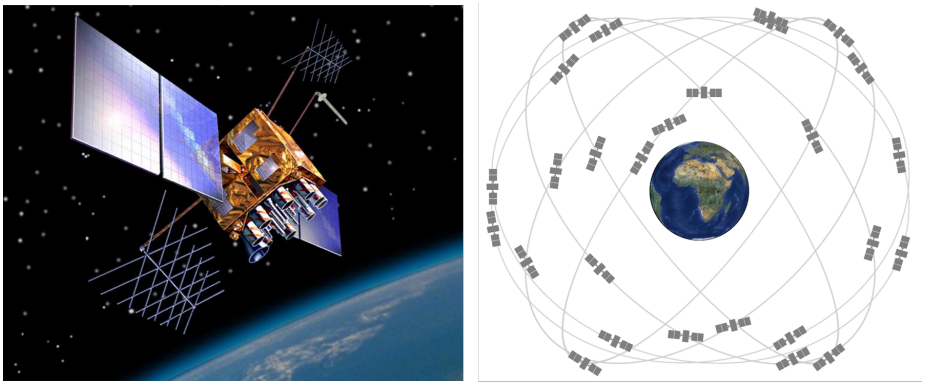

(a) GPS IIR-M satellite (b) GPS constellation

Figure 3.1: GPS Space Segment (*http://www.gps.gov*)

The User segment consists of the GNSS receiver equipment, which receives the signals from the satellites and uses the transmitted information to calculate the user's three-dimensional position and time. The GNSS users can be civilian and military ones: the military service have access to the system up to its full capability; the civilian service is freely available to all users on a continuous, worldwide basis, but limited only to certain signals broadcast by satellites. Various services have been established to deliver GNSS data and products to the user: one of these services is the International GNSS Service (IGS) [17]. The IGS is an international activity, officially established in January 1994 as a service of the International Association of Geodesy. The main role of this activity is to support scientific research based on highly precision and accurate Earth observations using the technologies of GNSS. The IGS collects, archives and distributes GPS and GLONASS observation datasets of sufficient accuracy to meet the objectives of a wide range of scientific and engineering applications and studies. IGS products support scientific activities such as improving and extending the International Terrestrial Reference Frame maintained by the International Earth Rotation and Reference Systems Service, monitoring deformations of the solid Earth and variations in the liquid Earth and in Earth's rotation, determining orbits of scientific satellites, and also monitoring the troposphere and ionosphere. Some of IGS products are: GPS satellite ephemerides (satellite and station clocks), Earth's rotation parameters and atmospheric parameters as the tropospheric Zenith Total Delay with different accuracy or the ionospheric Total Electron Content (TEC) [16].

3.2 The principle of airborne gravimetry

Airborne gravimetry is used to measure the gravity field and various measurement systems can be adopted. The instrument used to measure the gravity field is the gravimeter, which in principle is a highly sensitive accelerometer. Generally airborne gravimetry is classified in scalar gravimetry, vector gravimetry and gradiometry. When dealing with scalar gravimetry, the quantity that has to be determined is the magnitude of the gravity vector. In this case the system used for measurements can be the stabilized platform or the strapdown system. In vector gravimetry all the components of the gravity vector are measured using in general a strapdown system with a triad of accelerometers and another triad of gyroscopes. The quantities observed in airborne gradiometry instead are the second derivatives of the gravity field. In this latter case the designed system consists in opposing pairs of accelerometers on a rotating platform [64]. In this work we will focus just on classical scalar gravimetry by means of stabilized platform systems however some of the proposed procedures can be easily adapted to other measurement principles.

In the following the basic theory of measurement on a vehicle in movement will be presented. The three fundamental laws of physics which govern airborne gravimetry and gradiometry are: the Newton's second law of motion, the Newton's law of gravitation and Einstein's equivalence principle. These three laws are valid in an inertial reference frame, this means a fixed system of coordinates that does not rotate.

The Newton's second law of motion, as reported in the previous chapter, states that the acceleration of a proof mass into an inertial reference frame depends on the force acting upon the body and the inertial mass of the object itself:

$$m_i \underline{\ddot{x}} = \underline{F} \tag{3.1}$$

where m_i is the proof mass, $\underline{\ddot{x}}$ represents the second derivative in time of the position vector $\underline{x}$ and $\underline{F}$ is the force acting upon the mass. The acceleration is directly proportional to the acting force and inversely proportional to the mass of the object. On the Earth, in presence of the Earth's gravitational field the law is modified as follow:

$$m_i \underline{\ddot{x}} = \underline{F} + \underline{F}_g \tag{3.2}$$

with $\underline{F}_g$ the gravitational force ideally due to the field generated by all masses in the universe, according to Newton's law (see Eq. 2.1).

The Einstein's equivalence principle, formulated within his theory of relativity in early 1990s, states that " we [...] assume the complete physical equivalence of a gravitational field and a corresponding acceleration of the reference system.", which means that no experiment or exploitation of the laws of physics performed in a closed system can distinguish between a reference frame in a gravitational field and an accelerated reference frame. As a consequence of this principle the inertial mass is considered equivalent to a gravitational mass and the complete equation of motion into an inertial reference frame can be expressed as follow:

$$\underline{\ddot{x}} = \frac{\underline{F}}{m} + \underline{g} = \underline{f} + \underline{g} \tag{3.3}$$

where $\underline{\ddot{x}}$ is the total kinematic acceleration, $\underline{f}$ is the specific force or the acceleration resulting from an active force applied to the body; $\underline{g}$ is the gravitational specific force. Among these accelerations the one sensed by the accelerometer is $\underline{f}$, i.e. the one generated by the action forces and not the gravitational one. The only case in which it is possible to directly measure the gravitational acceleration $\underline{g}$ is in case of $\ddot{x} = 0$, which means if the measurement is conducted in static conditions on the Earth's surface, with the gravimeter properly oriented along the direction of the gravity vector (with sensitive axis along the plumb line). This kind of gravimeters, which are sensitive to $\underline{f}$, are commonly used for any type of moving vehicle gravimetry survey. To measure the kinematic acceleration another instrument has to be used and since the advent of GNSS all airborne systems use a GNSS receiver to track the vehicle movements and determine the motion.

Actually the equation for airborne gravimetry is more complicated than Eq. 3.3 because of the dynamic condition in which the measurement is done. First of all it has to be considered that the acceleration sensed by the gravimeter is measured in a non-inertial frame attached to a moving vehicle. Moreover, the specific forces and kinematic accelerations are referred to different measurement points of the vehicle and finally the gravitational acceleration is usually required in a local, Earth-fixed reference frame. All these reasons led to the necessity to properly take into account different reference frames, rotations and level-arm effect due to the moving vehicle. In particular, the specific frames to be considered are:

- the *body frame* which axes are defined by principal axes of the vehicle: forward, to-the-left and up;
- the *navigation reference frame* in which the navigation equation are formulated; this frame is a local Cartesian reference frame with origin in a point P with known coordinates with respect to the reference ellipsoid, z-axis

aligned with the normal to the ellipsoid, the x-axis pointing toward east and y-axis toward north, forming North-East-Up frame (l-frame);

- *Earth-centered Earth-fixed reference frame* with origin in the Earth's center of mass and axes defined by conventional pole and Greenwich meridian (e-frame).

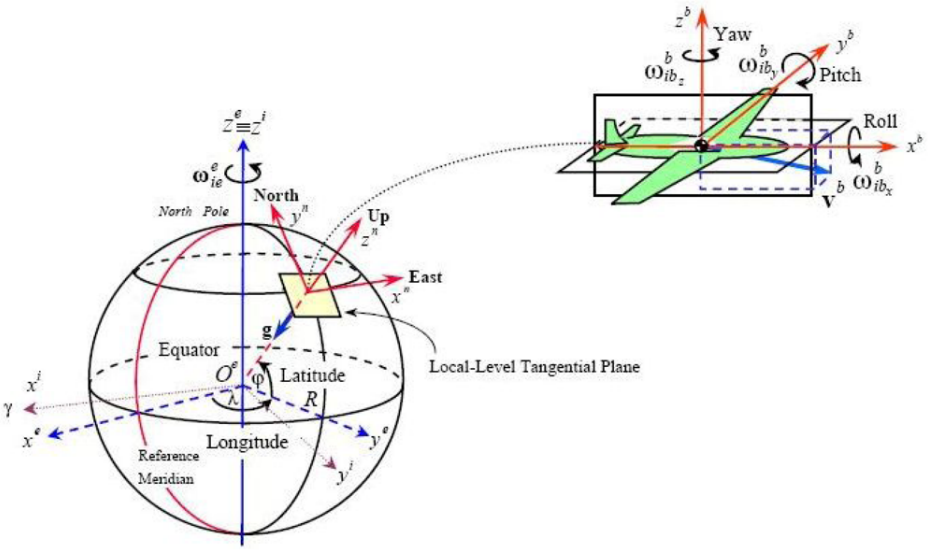

Figure 3.2: Reference frames adopted in airborne gravimetry (from [33])

In the navigational frame (*l-frame*) the general equation to obtain the gravity vector from airborne gravity measurements can be written in the following way [64]:

$$\underline{g}^l = \underline{\ddot{x}}^l - \underline{f}^l + (2\mathbf{\Omega_{ie}}^l + \mathbf{\Omega_{el}}^l)\underline{\dot{x}}^l \tag{3.4}$$

where the superscript $\cdot^l$ is referred to the reference frame in which the equation is valid. In Eq. 3.4 $\underline{\ddot{x}}$ is the aircraft acceleration vector, $\underline{f}$ is the specific force measured by the gravimeter, $\mathbf{\Omega_{ie}}$ and $\mathbf{\Omega_{el}}$ are the skew-symmetric matrices of the angular velocities due to the Earth-rate and aircraft-rate over the ellipsoid, $\underline{\dot{x}}$ is the vehicle velocity vector. The third right-hand term of this expression represents the Coriolis acceleration vector.

Eq. 3.4 is valid in case of a stabilized platform system in which a mechanism based on a gyros and two horizontal accelerometers maintains the original

orientation of the platform. In case of a strapdown system instead the accelerometers measurements ($\underline{f}^b$) refers to the body reference frame so Eq. 3.4 has to be modified introducing the rotation matrix from the body-frame (*b-frame*) to the navigational frame (*l-frame*) [64].

$$g^l = \underline{\ddot{x}}^l - \mathbf{R}_b^l \underline{f}^b + (2\mathbf{\Omega_{ie}}^l + \mathbf{\Omega_{el}}^l)\underline{\dot{x}}^l. \tag{3.5}$$

This rotation matrix R_b^l basically replaces the stabilized platform mechanism. The previous Eq. 3.4 and 3.5 are in vector form but can be applied to scalar gravimetry too, considering just the vertical component of interest. In this latter case Eq. 3.4 becomes:

$$g_U^l = \ddot{x}_U^l - f_U^l - \left(\frac{v_E^2}{R_1 + h} - 2\omega_{ie} v_E cos\varphi - \frac{v_N^2}{R_2 + h}\right) \tag{3.6}$$

with v_E, v_N, v_U the velocity components in the East, North,Up axis of the navigational frame, R_1 and R_2 are the prime vertical and the meridian radii of curvature. The third term in parenthesis represents the so called Eövös correction term to consider the centripetal acceleration generated by the movement of the aircraft over a curved and rotating Earth [64]. To complete the general equation of airborne gravimetry, another couple of correction terms need to be considered: the correction terms for tilt effect and lever-arm. The tilt effect is due to a misalignment of the stabilized platform which can results in gravity measurements errors due to the horizontal accelerations. It can be modeled using a combination of three acceleration components as reported in [50]:

$$\epsilon_g^{tilt} = \sqrt{g_m^2 + A^2 - a^2} - g_m \tag{3.7}$$

with $A^2 = (A_X^2 + A_L^2)$, where A_X and A_L are the accelerometer outputs along the cross and long axis and with $a^2 = (a_E^2 + a_N^2)$, where a_E and a_N are horizontal kinematic accelerations in the East and North directions derived from navigational data, and g_m is the gravimeter reading. However in airborne gravimetric surveys this effect is automatically corrected hence it will not be introduced in the following equations.

The lever arm effect is a consequence of the fact that the gravimeter and the GNSS receiver observations are referred to two different physical points so the vertical accelerations sensed by the two instruments can differ due to the aircraft attitude variations (i.e. its orientation relative to Earth's horizon). The correction is usually applied to the kinematic acceleration derived from GNSS tracking. In the inertial reference frame it has to be considered that

$$x_{antenna} = x_{gravimeter} + b \tag{3.8}$$

where b is the GNSS antenna offset with respect to the gravimeter (considered the center of mass of the vehicle). This effect can be modeled if the aircraft orientation and the on-board instruments geometry are available or may be neglected if the offset between the GNSS antenna and the gravimeter is small. A stable and accurate formula to compute the lever-arm effect is given in [34], assuming to know the lever-arm position in the inertial reference frame:

$$LA = \frac{d^2}{dt^2}\left(\mathbf{R}_b^i b^b\right) \tag{3.9}$$

where LA is the lever-arm effect, $\mathbf{R}_b^i$ is the rotation matrix to transform the lever-arm coordinates from the body frame, b^b, to the inertial one. So in conclusion the general equation for gravity at a certain altitude is:

$$\underline{g} = \underline{\ddot{x}} - \underline{f} - \underline{E\ddot{o}} - \underline{LA} \tag{3.10}$$

with $\underline{\ddot{x}}$ the result of GNSS data processing, $\underline{f}$ the output of the gravimeter, $\underline{E\ddot{o}}$ the Eötvös correction term, $\underline{LA}$ the lever arm term.

Actually in a real aerogravimetric survey the gravimeter does not measure $\underline{f}$ but its variations with respect to the value measured at a certain calibration point. The instrument calibration is generally done in static conditions at the airport before the departure and the measured value is assumed as a reference for all the following data acquired during the survey. Classically the reference gravity measure is a gravity disturbance, obtained as the difference between the gravity acceleration $\underline{g}$ at a certain point P and the normal gravity $\underline{\gamma}$ at the same point, being the normal gravity field the field that admits as equipotential surface the reference ellipsoid (see Chapter 1). This means that Eq. 3.10 in classical airborne gravimetery is modified in:

$$\underline{\delta g} = \underline{\ddot{x}} - \underline{f} - \underline{E\ddot{o}} - \underline{LA} - \underline{\gamma} - \underline{\delta g_0} \tag{3.11}$$

with $\underline{\delta g}$ the gravity disturbance, $\underline{\gamma}$ the normal gravity and $\underline{\delta g_0} = g_0 - \gamma_0$ the gravity disturbance measured at the calibration point.

3.3 Classical pre-processing of airborne gravity data

The objective of this section is to expose the standard procedure to pre-process raw aerogravimetric data acquired with the GNSS receiver and the gravimeter. With the term "raw" data we refer to the direct output of the on-board instrumentation without any processing: for GNSS data, these data are in RINEX format together with the corresponding ephemerides in navigational RINEX format; for gravimeter data, they are usually in ASCII format with the accelerations sensed by the on-board gravimeter together with all the ancillary informations required to exploit the data.

3.3.1 GNSS processing

The GNSS observables are used for navigational purposes to derive the aircraft trajectory, velocity and acceleration. For airborne gravimetry, the observable generally used is the carrier phase, obtained from the difference between the incoming carrier wave and the phase of a signal generated internally by the receiver. In case of absence of the Earth's atmosphere, the GNSS signal would travel in vacuum and the general expression in leght unit for the carrier phase would be:

$$L^s_{r,i}(t_r) = \rho^s_r(t^s) + \lambda_i N^s_{r,i} + c(\delta t_r - \delta t^s) \tag{3.12}$$

where ρ is the geometric distance between the receiver position at epoch t_r and the satellite position at t^s, λ is the wavelength of the carrier phase i, N is the integer ambiguity (number of cycles between the satellite and the receiver at epoch t_0), c is the speed of light and δt_r and δt^s are the receiver and satellite clock errors. The integer ambiguity remains constant if there is no loss of lock of signals between the receiver and the satellite. In case the tracking of the satellite is interrupted, the observations present a jump referred to as cycle slip and another unknown has to be introduced [6].

Now, considering that the signals travel in the atmosphere and not in vacuum, other terms need to be added to Eq. 3.12 to consider the systematic biases that affect the signals. The new expression for carrier phase became:

$$L^s_{r,i}(t_r) = \rho^s_r(t^s) + \lambda_i N^s_{r,i} + c(\delta t_r - \delta t^s) + T^s_r(r_r) - I^s_r(r_r) + m^s_r(t_r) + \epsilon^s_{r,i,L}. \tag{3.13}$$

A brief description of the added biases is given in the following:

- T_r^s is the tropospheric delay due to the neutral part of the Earth's atmosphere (first 50 km from the surface). This delay is dependent on the tropospheric conditions along the ray path and various models can be implemented to account for it [55].
- I_r^s is the ionospheric delay and depends on the free electron content in the ionosphere (about 70 to 100 km above the Earth). To eliminate this error, which is frequency dependent, a linear combination of two frequencies called iono-free combination, is generally used [32].
- m_r^s is the multipath effect, caused by the signals that reach the receiver after being reflected and not from the direct path. In general in case of an aerogravimetric survey this effect is reduced due to the fact that the measurements are done hundreds of meters above the topography and moreover the GNSS instrumentation used are well screen from these reflected signals. However since it is frequency dependent it can be modeled using a combination of observables (pseudorange and carrier phase) on different frequencies [32].
- ϵ_r^s is the observation error; it can depend on the hardware and the wavelength of the signal.

To estimate the receiver position, reducing as much as possible these errors which affect the observations, the double differences of carrier phase are commonly used. Given two receivers r and l, observing simultaneously two satellites s and u, it is possible to combine the general carrier phase observable (L_i) to form a new observable, called double difference of carrier phase, which displays as follow:

$$\begin{aligned} L_{rl,i}^{su}(t) &= L_{rl,i}^{s}(t) - L_{rl,i}^{u}(t) = \\ &= \rho_{rl,i}^{su}(t^s) + \lambda_i N_{rl,i}^{su} + T_{rl}^{su} - I_{rl,i}^{su}(t) + m_{rl,i}^{su}(t) + \epsilon_{rl,i}^{su} \end{aligned} \tag{3.14}$$

where the notation stands for:

$$\cdot_{rl}^{su} = (\cdot_{l}^{s}(t) - \cdot_{r}^{s}(t)) - (\cdot_{l}^{u}(t) - \cdot_{r}^{u}(t)). \tag{3.15}$$

The use of this differentiated observable prevents the estimation of the absolute position of the receiver and consents only to determine its relative position with respect to another station. Generally the reference station is chosen among the ground permanent stations (continuously operating network). In case this

is not possible, a ground point is used as reference station, measured in static conditions and post-processed in Precise Point Positioning (PPP - an absolute positioning method). Despite this aspect of relative position, the double difference of carrier phase remains nowadays the fundamental observable used for positioning because it brings some important benefits in the reduction of the unknown terms and of the errors afflicting the signal. The double differentiation in fact eliminates the receivers clock unknowns and very important, it removes the fractional part of the initial ambiguity, leaving as unknown just the integer part. Various algorithms exist in literature [35] for fixing ambiguities.

In practice, the GNSS observations acquired during an aerogravimetric survey are processed using commercial software which provide to detect and repair cycle slips, model and remove tropospheric and ionospheric errors, fix initial ambiguities and determine the double differences estimates for each flight line. To obtain the optimal solution for each flight line, in the processing of GNSS data various different signal combinations are used to estimate the trajectory. All the solutions are then classified according to the accuracy and smoothness of the trajectory and for each single flight line the best solution is chosen.

Once estimated the positions, the aircraft accelerations are generally obtained with two numerical differentiations.

3.3.2 Gravimeter processing

The inertial accelerations measured by the gravimeter, before the combination with GNSS acceleration, are processed with the principal aim of reducing the observation noise. The gravimeter's recording rate is usually extremely higher than the GNSS one so data have to be filtered and downsampled to match GNSS measurements. The filters have to be carefully chosen to avoid and reduce at minimum biasing the data. In general the standard filtering procedures for gravimeter data are based on the a priori knowledge of the error spectrum. Before computing gravity, these gravimeter accelerations are corrected for the Eötvös effect and for normal gravity. Some improvements in the computation of these correction terms as the use of GNSS phase angle corrections and the advanced analysis of the system uncertainties allow to improve the quality of gravity data, reducing the observations noise. In the end gravity is calculated by subtracting the GNSS derived aircraft accelerations from the inertial accelerations, according to Eq. 3.11.

3.4 Applications

Airborne gravimetry is widely used for various applications in both geodesy and geophysics. The type of application is important because influences the survey

design. The type of observation and accuracy required, the area coverage, the resolution and the flight path definition as well as the definition of the instrumentation to be used are all part of the survey design and depend on the scope of the gravity data acquired.

One of the most important geodetic application of airborne gravimetry is the local geoid determination. Removing tides and currents from the ocean, the remaining smoothly undulating shape is referred to as "the geoid" and it corresponds to the equipotential surface of the gravity field at the mean sea level. It is the conventional surface which defines the zero elevation level. For these type of applications usually airborne gravimetry data are combined with satellite gravimetry data which provide accurate low-frequency information. Exploiting airborne gravimetry the accuracy reachable for the geoid are few centimeter (2-5 cm) at a spatial resolution of 5-10 km [9]. In this respect one of the first important and successful campaign is the one conducted in Greenland in mid 1990s by the Naval Research Laboratory (NRL) [8]. In the latest decades other campaigns have been conducted in various regions that lack accurate gravity data all over the world like the ones still in process done within the "grav-D" project, led by the National Geodetic Survey, to re-define the vertical datum of the US by 2022 [68].

Another important geodetic application of airborne gravimetry is the filling of polar gaps. The gravity field of the polar regions is in fact of prime importance for Earth's global gravity field models, but also for providing information on the geology of those regions and for navigation and orbit determination. Satellite gravity field missions such as CHAMP, GRACE and GOCE were all strongly affected by the gravity field of polar regions and because of the non-polar orbits, a polar gaps remained in the satellite data coverage [54]. The Arctic Gravity Project [19] in the north polar region (64°to 90°N) provided a public-domain gravity grid of the Arctic gravity field in collaboration with members from different circumarctic countries exploiting the mainly airborne survey activities carried out in these regions. The ESA PolarGAP gravity field campaign carried out in the period 2015-2016 had as principal aim to use airborne gravity surveys over the southern polar region to cover the polar gap of GOCE in this area (south of 83.5°S) [51].

In geodetic airborne surveys scalar gravimetry systems are generally used, and with the aim to cover large regions, the spacing between flight lines is relatively large as well as the speed of the aircraft. Moreover to minimize the effect of turbulence on the measurement system the flight altitude is quite high, few thousands of meters.

Regarding geophysics applications, airborne gravimetry is mainly used for regional geological studies and for resource exploration. As shown in the figure below, mineral prospecting requires an accuracy of few mGal (better than 5

mGal) at spatial resolution of 1-5 *km*.

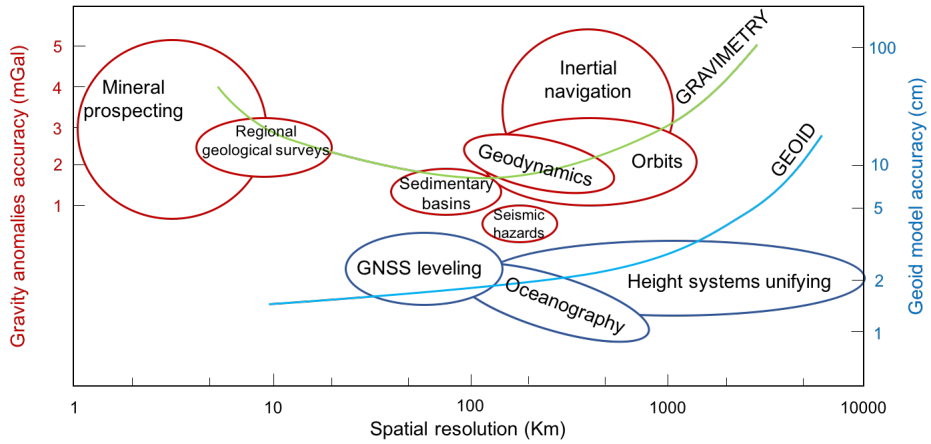

Figure 3.3: Required accuracies and resolution for airborne gravimetry applications

To obtain high accurate data at high spatial resolution, useful for resource exploration, airborne surveys are generally flown at low speeds over small areas with a flight track spacing denser than the spacing used for geodetic applications. The companies operating in this field and providing airborne surveys, typically flows with flight lines spacing of 500-1000 m at an average ground speed of about 50 ms^{-1} at an altitude of around 150 m offshore and a minimum clearance of 300 m above the topography (see CarbonNet project 2012).

Airborne gravimetry for resources exploration can be more efficient than terrestrial measurement technique but several studies are actually carried on to reduce time and costs of airborne campaigns. One investigation area is focused on the use of strapdown INS, that are cheaper than stabilized platforms and can potentially reach comparable accuracies [22]. Another field of investigation is the use of Unmanned Airborne Vehicles (UAV) already successfully applied in other research fields, like remote sensing and atmospheric sciences (see [12]). The use of UAV would mean the possibility to reduce the time of a campaign employing more than one vehicle.

Chapter 4

Pre-processing of airborne gravity data: the VIKING algorithm

---

The data collected during an aerogravimetric survey, as explained before, are not direct measurements of the gravity accelerations but they consist in a set of forces sensed by the instrumentation loaded on board that require to be properly combined to derive the interested accelerations. Even if for this type of surveys various measurements techniques are available, within this work the standard instrumentation is composed by a stabilized platform that mounts a gravimeter to sense the specific force, and a GNSS receiver to determine with high accuracy the trajectory, velocity and acceleration of the aircraft.

The current state of the art for classical airborne gravimetry, in terms of accuracy and spatial resolution, can not be easily identified since these parameters are directly related to the interested application which of course influences the survey characteristics. However, the accuracy and the spatial resolution, for a standard survey for resources exploration (with flight lines spacing of the about 1 km or below) done using stabilized platform systems and ground infrastructures for GNSS positioning, are of the order of $1 - 1.5$ $mGal$ at resolution of few km [50, 58]. The objective of the VIKING project is to improve, for this kind of applications, the accuracy below the $mGal$ level at a spatial resolution of about 1 km. For this purpose, before combining the different data, a proper

pre-processing of the observations is required. The term "pre-processing" in this project regards all the adjustments and manipulations that have to be applied to the different observations acquired in a measurement flight till their combination to obtain the gravity accelerations. The proposed innovative methodology is based on the introduction of the so called variometric approach [14] for GNSS data together with the exploitation of more than one single GNSS constellation. Furthermore it includes some algorithms implemented to prepare raw gravimeter observations for the subsequent combination with GNSS accelerations.

In this chapter, the VIKING methodology will be presented with a description of the algorithms developed and some theoretical aspects for GNSS and gravimeter data elaboration. In Section 4.1 the general observable to be used for GNSS accelerations estimation is derived starting from the classical GNSS equations. Moreover the procedure to compute the GNSS accelerations is described too. Section 4.2 regards the gravimeter data processing, focusing on the corrections that have to be taken into account to reduce errors in the derived gravity accelerations and the procedure to optimally filter the data. Finally a description on the optimal combination of GNSS and gravimeter data is given in Section 4.3.

4.1 The variometric approach for GNSS processing

The principal objective of this section is to recall the theory behind the estimation of GNSS accelerations within the variometric approach [14]. The basic idea is the definition of a new observation equation directly sensitive to the antenna acceleration. The new observable is obtained from the manipulation of the classical GNSS phase observation (Eq. 3.13) which instead is sensitive to the actual antenna position. Before introducing the equations it has to be underlined that the VIKING methodology has been expressly thought for airborne gravimetry applied to resources exploration geophysics. This means that the final target of GNSS pre-processing is the estimation of the aircraft accelerations over a region with a maximum extension of 100 x 100 km^2 and acquired close to the ground with accuracies possibly better than 1 $mGal$ at a spatial resolution of about 500 m. For a complete description of typical characteristics of such airborne acquisition the interest reader can refer to [64]. To reach this accuracy level, four main assumptions have to be done:

- an approximated trajectory $\underline{\tilde{x}}$ of the aircraft flight is known; being $\underline{x}$ the real trajectory (see Fig. 4.1), the error of the approximated track for each epoch t, $\underline{\xi}_t = \underline{x}_t - \underline{\tilde{x}}_t$, is supposed to be smaller than 10 cm;
- the aircraft is flying at an almost constant velocity of 50 ms^{-1}; this means

that, considering for example as final target an acceleration at a spatial resolution of about 500 m, the vehicle acceleration can be modeled in principle with a temporal resolution of 10 s;

- several GNSS constellations are available and used, exploiting the largest number of satellites;
- GNSS observations are cycle-slip free; this is satisfied adopting specific algorithms to detect and fix the cycle-slips in the acquired data.

About the use of multi constellations, nowadays this is more and more common in the airborne geophysical surveys, due to the increasing number of available constellations and to the modernization of GNSS receivers which can acquire signals from the different constellations.

The geometry of the GNSS problem is schematically presented in Fig. 4.1. According to the notation used in this figure the classical GNSS observation equation can be written as:

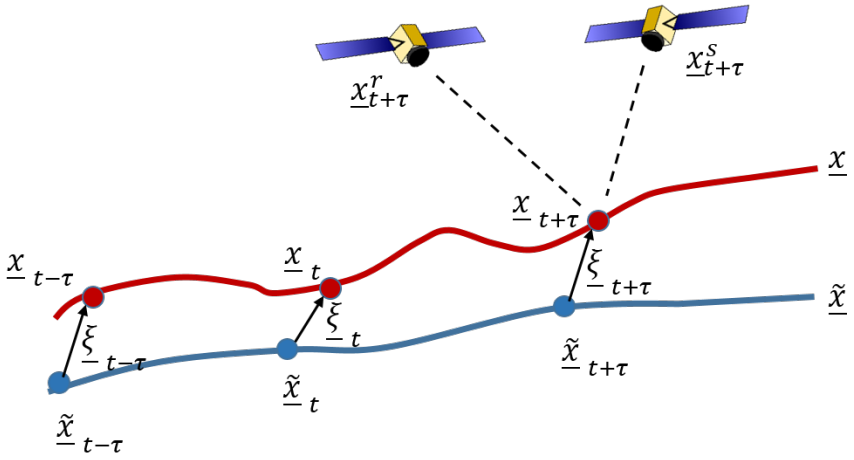

Figure 4.1: Schematic representation of the VIKING GNSS problem

$$L^s_{t+\tau} = \rho^s_{t+\tau} + \sigma^s_{t+\tau} - \sigma_{t+\tau} - N^s\lambda + T^s_{t+\tau} - I^s_{t+\tau} + \nu^s_{t+\tau} \tag{4.1}$$

where $L^s_{t+\tau}$ is the GNSS phase observation for satellite s at epoch $t+\tau$, $\rho^s_{t+\tau} = \left\|\underline{x}^s_{t+\tau} - \underline{x}_{t+\tau}\right\|$, $\sigma^s_{t+\tau}$ and $\sigma_{t+\tau}$ are the satellite and the receiver clock offsets respectively, N^s is the (integer) initial ambiguity for satellite s, λ is the wavelength for the considered GNSS signal, $T^s_{t+\tau}$ and $I^s_{t+\tau}$ are the tropospheric and

ionospheric delays and finally $\nu^s_{t+\tau}$ is the observation error due to the receiver circuitry.

Taking in consideration two different satellites (s and r) as represented in Fig. 4.1, it is possible to compute the difference between these two GNSS phase observations at the same receiver:

$$L^{sr}_{t+\tau} = L^s_{t+\tau} - L^r_{t+\tau} \tag{4.2}$$

denoting with the superscript $\cdot^{sr}$ the difference between $\cdot^s$ and $\cdot^r$. Replacing in Eq. 4.2 the general expression for the single GNSS phase observation (Eq. 4.1) the following observable is derived:

$$L^{sr}_{t+\tau} = \rho^{sr}_{t+\tau} + \sigma^{sr}_{t+\tau} - N^{sr}\lambda + T^{sr}_{t+\tau} - I^{sr}_{t+\tau} + \nu^{sr}_{t+\tau}. \tag{4.3}$$

It can be seen that this difference, as well known in GNSS literature, zeroes the receiver clock offset in Eq. 4.1 and that, since λ is the same wavelength for two satellites of a certain constellation, $N^{sr} = N^s - N^r$ remains an integer constant ambiguity.

Considering now two epochs t and $t+\tau$ (e.g. with $\tau = 5$ s which corresponds to an acceleration estimate with temporal resolution of 10 s), it can be computed another difference introducing the new observable $L^{sr}_{t+\tau,t} = L^{sr}_{t+\tau} - L^{sr}_t$, which full expression is:

$$\begin{aligned} L^{sr}_{t+\tau,t} &= \rho^{sr}_{t+\tau,t} + \sigma^{sr}_{t+\tau,t} + T^{sr}_{t+\tau,t} - I^{sr}_{t+\tau,t} + \nu^{sr}_{t+\tau,t} = \\ &= \rho^{sr}_{t+\tau,t} + \left[\left(\sigma^s_{t+\tau} - \sigma^s_t\right) - \left(\sigma^r_{t+\tau} - \sigma^r_t\right)\right] + \left[\left(T^s_{t+\tau} - T^s_t\right) - \left(T^r_{t+\tau} - T^r_t\right)\right] + \\ &- \left[\left(I^s_{t+\tau} - I^s_t\right) - \left(I^r_{t+\tau} - I^r_t\right)\right] + \left[\left(\nu^s_{t+\tau} - \nu^s_t\right) - \left(\nu^r_{t+\tau} - \nu^r_t\right)\right]. \end{aligned} \tag{4.4}$$

It can be noted in this equation that, assuming data without cycle-slips, when computing the difference between two consecutive epochs the term related to the initial ambiguity is removed. This observable is sensitive to the aircraft velocity, so to obtain the final expression relative to the acceleration another epoch has to be considered, e.g. $t - \tau$, and the observable becomes:

$$\begin{aligned} L^{sr}_{t+\tau,t} - L^{sr}_{t,t-\tau} &= \rho^{sr}_{t+\tau,t} - \rho^{sr}_{t,t-\tau} + \\ &+ \left[\left(\sigma^s_{t+\tau} - 2\sigma^s_t + \sigma^s_{t-\tau}\right) - \left(\sigma^r_{t+\tau} - 2\sigma^r_t + \sigma^r_{t-\tau}\right)\right] + \\ &+ \left[\left(T^s_{t+\tau} - 2T^s_t + T^s_{t-\tau}\right) - \left(T^r_{t+\tau} - 2T^r_t + T^r_{t-\tau}\right)\right] + \\ &- \left[\left(I^s_{t+\tau} - 2I^s_t + I^s_{t-\tau}\right) - \left(I^r_{t+\tau} - 2I^r_t + I^r_{t-\tau}\right)\right] + \\ &+ \left[\left(\nu^s_{t+\tau} - 2\nu^s_t + \nu^s_{t-\tau}\right) - \left(\nu^r_{t+\tau} - 2\nu^r_t + \nu^r_{t-\tau}\right)\right]. \end{aligned} \tag{4.5}$$

To make this quantity dimensionally homogeneous to an acceleration one can divide it by τ^2. Now let analyze each term of Eq. 4.5 to evaluate the order of magnitude of their relative error.

- $\rho^{sr}_{t+\tau,t} - \rho^{sr}_{t,t-\tau}$ is the term related to geometric distances between the receiver and satellites; it contains the unknown receiver position coordinates that, as will be explained later on, can be associated to the receiver accelerations
- $\left[\left(\sigma^s_{t+\tau} - 2\sigma^s_t + \sigma^s_{t-\tau}\right) - \left(\sigma^r_{t+\tau} - 2\sigma^r_t + \sigma^r_{t-\tau}\right)\right]$ is the term of satellites clock errors; in general the single σ^s_t can be computed in post-processing from the ephemerides with an accuracy of about 20 ps (see for instance *http://www.igs.org/products*) that, multiplied by the speed of light, corresponds to about 0.6 cm. Taking into account that the satellites clock errors are modeled within the ephemerides and that, in a time interval of 24 hours, their standard deviation is of about 30 ps, it is possible to suppose that in a time interval of 5 s this error standard deviation can be reduced at least of two order of magnitude (i.e. 0.1 ps which corresponds to about $3 \cdot 10^{-3}$ cm) [78]. As a consequence, propagating this error, the order of magnitude of the accuracy of the full term is around 0.08 mm which divided by 25 s^2 returns a final accuracy in terms of accelerations of the order of 0.3 $mGal$, admissible for the project target;
- $\left[\left(T^s_{t+\tau} - 2T^s_t + T^s_{t-\tau}\right) - \left(T^r_{t+\tau} - 2T^r_t + T^r_{t-\tau}\right)\right]$ represents the error related to the tropospheric delay, which can be modeled by means of the Saastamoinen formula [32]. Considering a cut-off angle of 15° and using this model, within a time interval of 5 s, this delay term has a standard deviation of about 0.2 mm. Now assuming for the residuals high frequencies (not modeled by Saastamoinen) a standard deviation of about 10% of the standard deviation of the model, we obtain a deviation of about 0.02 mm. In the end, by propagating the error of the whole term, the standard deviation becomes smaller than 0.1 mm, that divided by 25 s^2, results again to be smaller than 0.5 $mGal$.
- $\left[\left(I^s_{t+\tau} - 2I^s_t + I^s_{t-\tau}\right) - \left(I^r_{t+\tau} - 2I^r_t + I^r_{t-\tau}\right)\right]$ is the ionospheric error term; for baselines smaller than 1 km, if we consider the TEC spatial variability [37], this delay could be negligible. Moreover, for geophysical purposes since we suppose the aircraft flying at 50 ms^{-1} and a time step τ of 5 s the considered baselines are of about 500 m so this term could be neglected. However, since in airborne gravity surveys for resources exploration double-frequency GNSS receivers are usually available the iono-free combination [42] can be used, solving the problem.
- $\left[\left(\nu^s_{t+\tau} - 2\nu^s_t + \nu^s_{t-\tau}\right) - \left(\nu^r_{t+\tau} - 2\nu^r_t + \nu^r_{t-\tau}\right)\right]$ represents the observation error; generally the standard deviation of the observation error is $\sigma_\nu = 1$

mm so for the variance propagation the full term standard deviation will be $\sqrt{8}\sigma_\nu = 3.0\ mm$. Now assuming an observation rate of 20 Hz of 20 different satellites, in 5 s the number of independent observations is about 2000 and the total error decreases at $\frac{3.0}{\sqrt{2000}} = 0.07\ mm$, which corresponds to about 0.3 $mGal$ admissible for the final target.

Once proven that all the above terms, except for the first one, have errors in the range of few tents of a $mGal$ it is possible to proceed with the linearization of the Eq. 4.5 with respect to the unknown acceleration of the GNSS receiver. Lets recall that:

$$\rho^s_{t+\tau} = \left\| \underline{x}^s_{t+\tau} - \underline{\tilde{x}}_{t+\tau} - \underline{\xi}_{t+\tau} \right\| \tag{4.6}$$

so the term $\rho^s_{t+\tau}$ can be rewritten as:

$$\rho^s_{t+\tau} \approx \tilde{\rho}^s_{t+\tau} - \underline{\tilde{e}}^s_{t+\tau} \cdot \underline{\xi}_{t+\tau} \tag{4.7}$$

where the $\underline{\tilde{e}}^s_{t+\tau}$ corresponds to the unit vector centered at the receiver with direction toward the satellite s. If $\delta\rho^s_{t+\tau}$ is the difference $\rho^s_{t+\tau} - \tilde{\rho}^s_{t+\tau}$, considering two different epochs $t+\tau$ and t, we have:

$$\delta\rho^s_{t+\tau,t} = -\underline{\tilde{e}}^s_{t+\tau} \cdot \underline{\xi}_{t+\tau} + \underline{\tilde{e}}^s_t \cdot \underline{\xi}_t. \tag{4.8}$$

This equation, by the general identity $(ab - cd) = \frac{a+c}{2}(b-d) + (a-c)\frac{b+d}{2}$, can be rewritten as:

$$\delta\rho^s_{t+\tau,t} = -\frac{\underline{\tilde{e}}^s_{t+\tau} + \underline{\tilde{e}}^s_t}{2} \cdot \left(\underline{\xi}_{t+\tau} - \underline{\xi}_t\right) - \left(\underline{\tilde{e}}^s_{t+\tau} - \underline{\tilde{e}}^s_t\right) \cdot \frac{\underline{\xi}_{t+\tau} + \underline{\xi}_t}{2} \tag{4.9}$$

Analyzing the last term in Eq. 4.9 it can be proven that, as a consequence of the initial hypothesis, it is negligible. In fact, the order of magnitude of $\frac{\underline{\xi}_{t+\tau} + \underline{\xi}_t}{2}$ is smaller than 10 cm (for the hypothesis of known approximated trajectory), while about the term $\left(\underline{\tilde{e}}^s_{t+\tau} - \underline{\tilde{e}}^s_t\right)$ some considerations can be done as shown in the following. Given the satellite velocity of about 3.7 kms^{-1}, it is possible to derive the approximated angle between the two versors ($\underline{\tilde{e}}^s_t$ and $\underline{\tilde{e}}^s_{t+\tau}$) in 5 s, which results to be:

$$\theta = \frac{\omega}{\overline{h}_{sat}} \cdot \Delta t = \frac{3.7}{20200} \cdot 5 = 1 \cdot 10^{-3} \text{ rad} \tag{4.10}$$

being $\overline{h}_{sat}$ the mean altitude of GPS satellites. Now, the full rotation matrix $\mathbf{R} = \mathbf{R_z}\mathbf{R_y}\mathbf{R_x}$ with angles θ_1, θ_2 and θ_3, using the notation $c(\theta)$ and $s(\theta)$ for $\cos(\theta)$ and $\sin(\theta)$, results to be:

$$\mathbf{R} = \begin{bmatrix} c(\theta_3)c(\theta_1) & c(\theta_3)s(\theta_1)s(\theta_2) - s(\theta_3)c(\theta_2) & c(\theta_3)s(\theta_1)c(\theta_2) + s(\theta_3)s(\theta_2) \\ s(\theta_3)c(\theta_1) & s(\theta_3)s(\theta_1)s(\theta_2) + c(\theta_3)c(\theta_2) & s(\theta_3)s(\theta_1)c(\theta_2) - c(\theta_3)s(\theta_2) \\ s(\theta_1) & c(\theta_1)s(\theta_2) & c(\theta_1)c(\theta_2) \end{bmatrix}.$$

If we suppose that $\theta_1 = \theta_2 = \theta_3 = 1 \cdot 10^{-3}\ rad$ and that for small angles $\cos(\theta) \simeq 1 - \frac{\theta^2}{2}$ and $\sin(\theta) \simeq \theta - \frac{\theta^3}{6}$, the rotation matrix linearized, neglecting second order terms, will change in:

$$\mathbf{R} = \begin{bmatrix} 1 & -\theta & \theta \\ \theta & 1 & -\theta \\ -\theta & \theta & 1 \end{bmatrix}$$

as a consequence:

$$\left(\tilde{\underline{e}}^s_{t+\tau} - \tilde{\underline{e}}^s_t\right) = \begin{bmatrix} 1 & -\theta & \theta \\ \theta & 1 & -\theta \\ -\theta & \theta & 1 \end{bmatrix} \begin{bmatrix} e_x \\ e_y \\ e_z \end{bmatrix} - \begin{bmatrix} e_x \\ e_y \\ e_z \end{bmatrix}. \tag{4.11}$$

This proves that the term $\left(\tilde{\underline{e}}^s_{t+\tau} - \tilde{\underline{e}}^s_t\right)$ has the same order of magnitude of the angle θ, so it is smaller than 10^{-3}. Consequently the whole last term of Eq. 4.9 is smaller than 0.1 mm. This means that:

$$\delta\rho^s_{t+\tau,t} \approx -\tilde{\underline{e}}^s_{t+\frac{\tau}{2}} \cdot \left(\underline{\xi}_{t+\tau} - \underline{\xi}_t\right) \quad \text{with} \quad \tilde{\underline{e}}^s_{t+\frac{\tau}{2}} = \frac{\tilde{\underline{e}}^s_{t+\tau} + \tilde{\underline{e}}^s_t}{2}. \tag{4.12}$$

Note that $\left(\tilde{\underline{x}}_{t+\tau} - \tilde{\underline{x}}_t + \underline{\xi}_{t+\tau} - \underline{\xi}_t\right)$ is the position variation in 5 s so if divided by the time step represents the velocity of the moving vehicle while $\tilde{\underline{e}}^s_{t+\frac{\tau}{2}}$ is the mean unit vector in the time interval directed toward satellite s. Similarly introducing the other satellite r, the difference between $\delta\rho^s_{t+\tau,t}$ and $\delta\rho^r_{t+\tau,t}$ results in:

$$\begin{aligned} \delta\rho^{sr}_{t+\tau,t} &\approx -\tilde{\underline{e}}^s_{t+\frac{\tau}{2}} \cdot \left(\underline{\xi}_{t+\tau} - \underline{\xi}_t\right) + \tilde{\underline{e}}^r_{t+\frac{\tau}{2}} \cdot \left(\underline{\xi}_{t+\tau} - \underline{\xi}_t\right) = \\ &= -\left(\tilde{\underline{e}}^s_{t+\frac{\tau}{2}} + \tilde{\underline{e}}^r_{t+\frac{\tau}{2}}\right) \cdot \left(\underline{\xi}_{t+\tau} - \underline{\xi}_t\right) = \\ &= -\tilde{\underline{e}}^{sr}_{t+\frac{\tau}{2}} \cdot \left(\underline{\xi}_{t+\tau} - \underline{\xi}_t\right). \end{aligned} \tag{4.13}$$

Adding another difference in time with respect to the epochs t and $t-\tau$, we get:

$$\begin{aligned}\delta\rho^{sr}_{t+\tau,t} - \delta\rho^{sr}_{t,t-\tau} &= -\underline{\tilde{e}}^{sr}_{t+\frac{\tau}{2}} \cdot \left(\underline{\xi}_{t+\tau} - \underline{\xi}_{t}\right) + \underline{\tilde{e}}^{sr}_{t-\frac{\tau}{2}} \cdot \left(\underline{\xi}_{t} - \underline{\xi}_{t-\tau}\right) = \\ &= -\frac{\underline{\tilde{e}}^{sr}_{t+\frac{\tau}{2}} + \underline{\tilde{e}}^{sr}_{t-\frac{\tau}{2}}}{2} \cdot \left(\underline{\xi}_{t+\tau} - 2\underline{\xi}_{t} + \underline{\xi}_{t-\tau}\right) - \\ &- \left(\underline{\tilde{e}}^{sr}_{t+\frac{\tau}{2}} + \underline{\tilde{e}}^{sr}_{t-\frac{\tau}{2}}\right) \cdot \frac{\underline{\xi}_{t+\tau} - \underline{\xi}_{t-\tau}}{2}. \end{aligned} \tag{4.14}$$

Similarly to the reasoning adopted for the last term of Eq. 4.9, also the last term of Eq. 4.14 can be neglected, thus obtaining:

$$\delta\rho^{sr}_{t+\tau,t} - \delta\rho^{sr}_{t,t-\tau} = -\frac{\underline{\tilde{e}}^{sr}_{t+\frac{\tau}{2}} + \underline{\tilde{e}}^{sr}_{t-\frac{\tau}{2}}}{2} \cdot \left(\underline{\xi}_{t+\tau} - 2\underline{\xi}_{t} + \underline{\xi}_{t-\tau}\right). \tag{4.15}$$

Note that, since we are interested in the accelerations the term $\underline{\xi}_{t+\tau} - 2\underline{\xi}_{t} + \underline{\xi}_{t-\tau}$ should be divided by the time variation square, supposed to be for instance 25 s^2, according to the second assumption made at the beginning of this section. In this way this term is proportional, to the correction to be applied to the approximated acceleration (obtained from the approximated position $\underline{\tilde{x}}$) to compute the actual acceleration. The final linearized observation equation reads:

$$L^{sr}_{t+\tau,t} - L^{sr}_{t,t-\tau} = \tilde{\rho}^{sr}_{t+\tau,t} - \tilde{\rho}^{sr}_{t,t-\tau} - \frac{\underline{\tilde{e}}^{sr}_{t+\frac{\tau}{2}} + \underline{\tilde{e}}^{sr}_{t-\frac{\tau}{2}}}{2} \cdot \left(\underline{\xi}_{t+\tau} - 2\underline{\xi}_{t} + \underline{\xi}_{t-\tau}\right). \tag{4.16}$$

Looking at Eq. 4.16 to estimate the unknown values of the correction for aircraft approximated accelerations, the procedure requires:

- approximated values of the aircraft trajectory and satellite positions to compute the $\underline{\tilde{e}}^{sr}_{t\pm\frac{\tau}{2}}$ term and $\tilde{\rho}^{sr}_{t+\tau,t}$ and $\tilde{\rho}^{sr}_{t,t-\tau}$;
- GNSS observations without cycle-slips.

Regarding the first point, once computed the satellites positions from the ephemerids, the approximated aircraft trajectory can be estimated in different ways: if a ground infrastructure is available, it can be derived by using a differential approach (classical double differences) or, if the infrastructure is not available, it can be estimated by means of a classical stand-alone GNSS positioning by means of code and phase observations. More details on GNSS standard processing procedures can be found in [13]. To reduce the errors of the approximated receiver coordinates estimates, in this step the tropospheric and ionospheric effects are modeled and removed from the observations. Moreover to exploit the

various GNSS systems observations, the so called inter-system biases are estimated too. This is done by properly adding in the Least Squares adjustment an additional ancillary unknown for each constellation. [69, 71]

About the cycle-slips detection, within the VIKING methodology, it is performed by means of four different techniques, standardly used in GNSS processing [35]: a comparison between phase and code observations (CODE), a comparison between phase and Doppler shift observations (DOPPLER), an analysis of time variation of phase observations (TIME) and analysis of geometry free combination (GEO-FREE). The equations of the above observables are:

$$\text{CODE}_t = \frac{P_t^s - \lambda L_t^s - 2I_t^s}{\lambda} \tag{4.17}$$

$$\text{DOPPLER}_t = L_{t+\tau}^s - \left(L_t^s + \frac{\phi_{t+\tau}^s + \phi_t^s}{2}\tau \right) \tag{4.18}$$

$$\text{TIME}_t = L_{t+\tau}^s - 2L_t^s + L_{t-\tau}^s \tag{4.19}$$

$$\text{GEO-FREE}_t = \lambda_1 L1_t^s - \lambda_2 L2_t^s - \frac{f_1^2 - f_2^2}{f_1^2 f_2^2} I \tag{4.20}$$

where P and L are the pseudorange and carrier phase observation, I is the ionospheric delay, ϕ is the Doppler observation, λ_1 and λ_2 are the wavelengths of the two carrier phases, while f_1 and f_2 are the two corresponding frequencies. In Eq. 4.20 the last term is the ionospheric delay scaled by a factor of $\left(\frac{f_1^2 - f_2^2}{f_1^2 f_2^2}\right)$, referred to as ionospheric residual.

In case of absence of cycle-slips the first two quantities, namely $CODE_t$ and $DOPPLER_t$ are expected to be zero, while the last two are expected to be a smooth signal. On the contrary if a cycle-slip is present in the phase observations a jump appears in all the above observables. In order to detect a cycle-slip the four observables are computed for all the available epochs, after that they are ordered by their smoothness thus selecting the two methods with the smallest standard deviation. Finally a certain epoch is flagged as cycle-slip, if a jump larger than a certain threshold (e.g. 0.6 cycles), occurs in both the two selected observables. Once the potential cycle-slip is detected, by means of a Grubbs test [26], the integer number of cycles slipped is estimated and the phase observation is corrected accordingly.

Once detected and repaired the cycle slips from the observations, estimated the satellites positions and the approximated aircraft tracks, the linearized Eq. 4.16 is solved in term of the unknown accelerations corrections by means of a Least Square adjustment. Note that the well known biases and drifts typical of the variometric approach [14] can be here safely disregarded due to the subsequent application of the Wiener filter presented in the next Chapter.

4.1.1 Least Squares solution

To clarify how the Least Squares solution is applied for the estimation of GNSS accelerations, the Least Squares principle is here recalled with its basic equations and its application to VIKING algorithms for GNSS.

Let start from the general observation model that relates the n observations to the m unknowns parameters.

$$\underline{y} = \mathbf{A}\underline{x} + \underline{b} + \underline{\nu} \tag{4.21}$$

where $\underline{y}$ is the $[n \times 1]$ observations vector; $\mathbf{A}$ $[n \times m]$ represents the design matrix containing the coefficients for the unknowns, $\underline{x}$ is the $[m \times 1]$ unknown parameters vector, $\underline{b}$ is the $[n \times 1]$ known term and $\underline{\nu}$ is the $[n \times 1]$ observations error (noise and uncertainties which affect the data). This latter term is assumed to be distributed as a normal Gaussian with zero mean and covariance matrix $\mathbf{C}_{\nu\nu}$ (i.e. $\nu \sim N(0, \mathbf{C}_{\nu\nu})$) [59]. The functional model is expressed as:

$$E[\underline{y}] = \mathbf{A}\underline{x}, \quad E[\underline{\nu}] = 0 \tag{4.22}$$

while the stochastic model reads as:

$$D[\underline{y}] = \mathbf{C}_{\mathbf{yy}}, \quad D[\underline{\nu}] = \mathbf{C}_{\nu\nu} = \sigma_0^2\mathbf{Q} \tag{4.23}$$

where $E[\,\cdot\,]$ is the expectation operator and $D[\,\cdot\,]$ is the dispersion operator which describes the covariance matrix of the observations and the errors. The covariance matrix of the observations error $\mathbf{C}_{\nu\nu}$ can be expressed in function of the a priori variance σ_0^2 multiplied by the cofactor matrix $\mathbf{Q}$. The inverse of the cofactor matrix is denoted as the weight matrix

$$\mathbf{W} = \mathbf{Q}^{-1}. \tag{4.24}$$

If the observations are considered independent from one another the weight matrix becomes diagonal because all the other elements which express the correlations between observations are zeroed. The Least Squares principle states that, to determine the unknown parameters in Eq. 4.21, one has to impose the sum of the squares of the residuals to be minimum:

$$\underline{v}^T\,\mathbf{W}\underline{v} = (\underline{y} - \mathbf{A}\,\underline{\hat{x}} - \underline{b})^T\,\mathbf{W}\,(\underline{y} - \mathbf{A}\,\underline{\hat{x}} - \underline{b}) = \text{minimum}. \tag{4.25}$$

So the equation for the estimates of the unknown parameters $\underline{\hat{x}}$ is:

$$\underline{\hat{x}} = (\mathbf{A}^T \mathbf{W} \mathbf{A})^{-1} \mathbf{A}^T \mathbf{W} \left(\underline{y} - \underline{b}\right) = \mathbf{N}^{-1} \mathbf{A}^T \mathbf{W} \left(\underline{y} - \underline{b}\right) \tag{4.26}$$

where $\mathbf{N} = \mathbf{A}^T \mathbf{W} \mathbf{A}$) is the so called normal matrix. Once estimated the unknown parameters it is possible to compute the residuals

$$\underline{\hat{v}} = \underline{y} - \mathbf{A}\,\underline{\hat{x}} - \underline{b} \tag{4.27}$$

which are then used for the a posteriori variance estimation

$$\hat{\sigma_0^2} = \frac{\underline{\hat{v}}^T \mathbf{W}\, \underline{\hat{v}}}{n - m}. \tag{4.28}$$

Once known the a posteriori variance, the covariance matrices of the estimated parameters $\underline{\hat{x}}$ and the derived $\underline{\hat{y}} = A\underline{\hat{x}} + \underline{b}$ can be obtained too:

$$\mathbf{C_{\hat{x}\hat{x}}} = \hat{\sigma_0^2}\mathbf{N^{-1}}, \quad \mathbf{C_{\hat{y}\hat{y}}} = \mathbf{A}\mathbf{C_{\hat{x}\hat{x}}}\mathbf{A^T}. \tag{4.29}$$

4.2 Gravimeter processing

In this section the theoretical aspects related to the processing of the accelerations sensed by the gravimeter, before their combination with GNSS derived accelerations, are recalled. The gravimeter data require to be corrected for all the errors affecting the instrumentation on board of the aircraft; moreover, being acquired with a very high rate sampling up to 128 Hz, they are characterized by large noise which is the sum of the accelerometer errors and the high frequency signal (accelerations with frequencies higher than 0.2 Hz which are not sensed by the GNSS). This means that gravimeter data need to be filtered and downsampled without losing information on the real gravity signal.

Considering the different corrections to be applied to gravimeter data, the first one is related to the geometry of the instruments on board due to the fact that the position of the center of mass of the gravimeter is not coincident with the GNSS antenna phase center. This effect is referred to as the lever arm effect [61] and if not properly accounted for it causes the two instruments to measure accelerations at different points. In order to compute it, the coordinates of the gravimeter center of mass and GNSS antenna phase center should be known in

the aircraft reference frame (*b-frame*) to measure the precise distance between them, also called the arm. The actual three dimensional position of the arm, for each observation epoch t, can be determined by multiplying it by the rotation matrix R computed from the roll (r) and pitch (p) angles (Fig. 4.2).

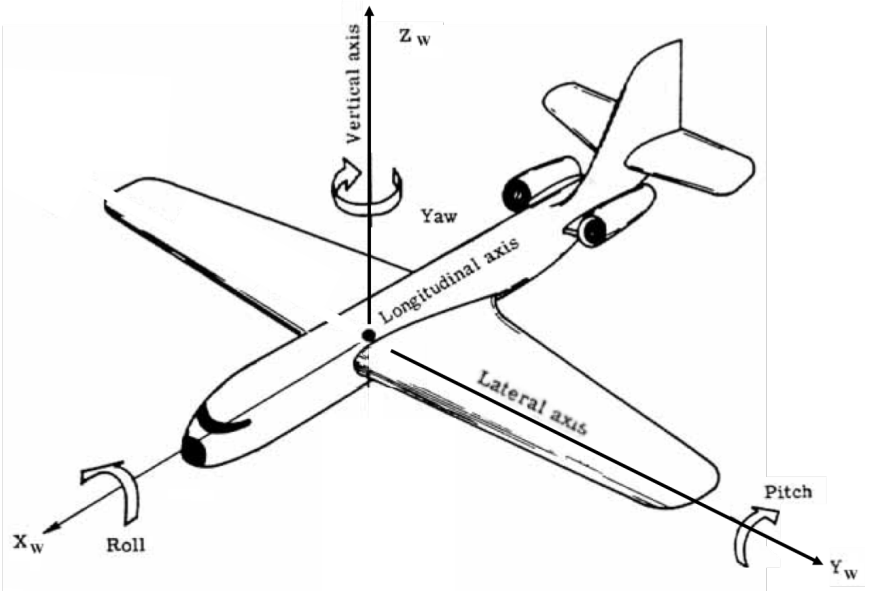

Figure 4.2: Roll, pitch and yaw rotation angles

$$\mathbf{R} = \mathbf{R_y}\mathbf{R_x} = \begin{bmatrix} cos(p) & 0 & -sin(p) \\ 0 & 1 & 0 \\ sin(p) & 0 & cos(p) \end{bmatrix} \begin{bmatrix} 1 & 0 & 0 \\ 0 & cos(r) & sin(r) \\ 0 & -sin(r) & cos(r) \end{bmatrix}.$$

Finally the lever arm term is estimated with a double differentiation in time [34] and it is removed from the gravimeter observations.

The second effect that can not be neglected when dealing with gravimeter observations is the so called Eötös effect. This correction term needs to be added to gravimeter observations to compensate for horizontal motion over the Earth's surface, which cause a change in the perceived gravitational force due to the change in centrifugal acceleration. When moving in the East direction in fact the vehicle's angular velocity is increased (in addition to the Earth's rotation) and thus the centrifugal force is increased too, resulting in a perceived reduction

of the gravitational force. To compute the Eötös effect it is necessary to know the aircraft velocities in the navigational frame (*l-frame*) and the East-West and North-South direction, v_e and v_n respectively, as well as the aircraft latitude φ and altitude h. Once known all these parameters the Eötös term can be computed adopting the following formula, derived manipulating the one proposed by [29]:

$$Eo = \frac{v_e^2}{\frac{r}{(1-e^2 sin^2(\varphi))^{\frac{1}{2}}} + h} - 2\omega v_e^2 cos(\varphi) - \frac{v_n^2}{\frac{r(1-e^2)}{(1-e^2 sin^2(\varphi))^{\frac{3}{2}}} + h} \tag{4.30}$$

where r is the Earth's radius at the equator, e^2 is the Earth's first eccentricity and ω is the Earth's angular velocity.

For airborne gravimetry applied to resources exploration purposes, these two corrections are fundamental to reach the required accuracies: the figures below (Fig. 4.3 and Fig. 4.4) show an example of the entity of these correction terms for a single flight line of an airborne survey.

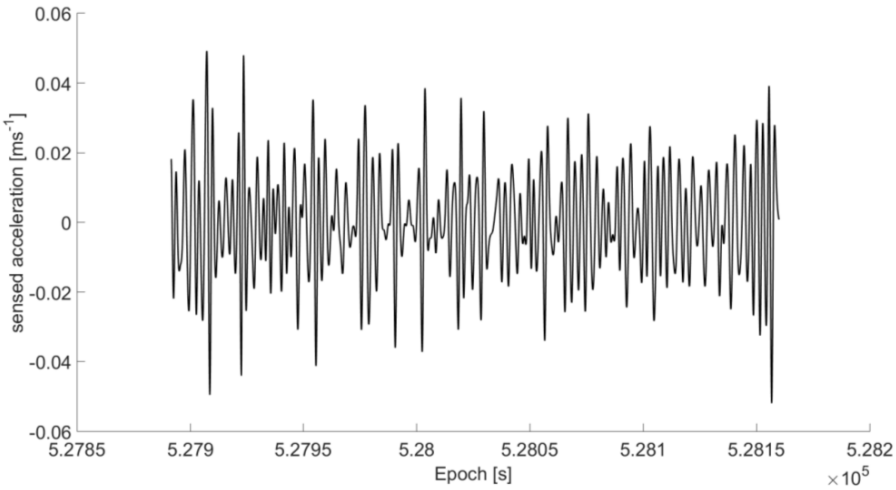

Figure 4.3: Lever arm effect for a single flight line

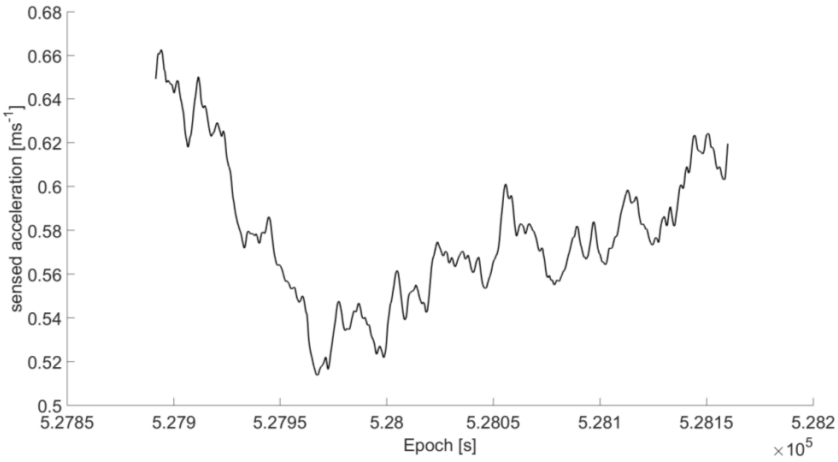

Figure 4.4: Eötvös effect for a single flight line

Once the above corrections have been applied to the gravimeter observations, another important aspect to deal with is the very different rate of acquisition for the gravimeter and the GNSS receiver. Generally the former acquires data at 128 Hz while the latter usually has an acquisition rate of 10 or 20 Hz. As a consequence the gravimeter observations are characterized by the presence of high frequency signal, due for instance to air turbulence, which are not present in the GNSS counterpart and should be therefore considered as noise. Within this project, in the VIKING solution a first operation to reduce this noise and the acquisition rate consists in applying a moving average to the gravimeter observations. The size of the moving average window has to be properly chosen in such a way to have mean values at a frequency close to the acquisition rate of GNSS receiver. The importance of this step regards the necessity to leave unchanged the average accelerations which will be subsequently used to determine the gravitational field. Supposing to have gravimeter accelerations at 128 Hz and GNSS derived accelerations at 20 Hz (as for the test airborne survey analyzed within this project), a moving average on 8 epochs could be suitable, reducing the gravimeter sampling rate at a frequency of 16 against 128 Hz. Furthermore, assuming the vehicle to move at a constant velocity of 50 ms^{-1}, it is proven that the gravitational field informations remain almost unchanged, being the spatial resolution of the averaged data of about 3.1 m. In the proposed procedure the moving average is performed exploiting the convolution theorem in the frequency

domain and once applied, the data are downsampled by a factor equal to the size of the moving average itself.

4.3 Spline interpolation and combination of GNSS and gravimeter data

The last step of the "pre-processing" section is the combination of GNSS derived accelerations and gravimeters accelerations to obtain gravity observations, objective of analysis of the next chapter. Once both dataset have been adjusted for the errors affecting the measurement units, the final operation, before combining datasets, consists in the application of a cubic spline interpolation, thus allowing the synchronization of the two different measurement systems. Cubic splines produce an interpolated function that is continuous up to the second derivative. This operation, if the number of splines adopted is properly chosen, allows to reduce the observation noise and to predict accelerations at any epoch (necessary for the combination of not synchronized datasets).

In one dimension a cubic spline can be expressed and represented as follow:

$$\varphi_3(t) = \int \varphi_1(\tau)\varphi_1(t-\tau)d\tau = \begin{cases} \frac{1}{6}(t+2)^3 & -2 \leq t < -1 \\ \frac{1}{6}[(t+2)^3 - 4(t+1)^3] & -1 \leq t < 0 \\ \frac{1}{6}[(2-t)^3 - 4(1-t)^3] & 0 \leq t < 1 \\ \frac{1}{6}(2-t)^3 & 1 \leq t < 2 \\ 0 & \text{elsewhere} \end{cases} \tag{4.31}$$

where φ_1 is the first order spline, with a triangular shape on $[-1, 1]$, expressed as:

$$\varphi_1(t) = \begin{cases} 1 - |t| & |t| < 1 \\ 0 & t > 1 \end{cases} \tag{4.32}$$

When using this type of splines, the interpolated function is obtained as a weighted sum of translated splines, centered at regularly distributed grid points t_i:

$$y(t) = \Sigma_k x_k \varphi_3 \left(\frac{t - t_k}{\Delta} \right) \tag{4.33}$$

where Δ corresponds to the grid step and x_k represents the unknown splines

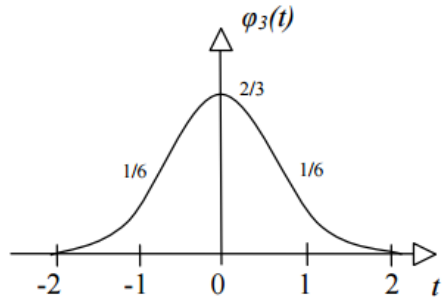

Figure 4.5: Cubic spline

coefficients. The generic expression of the interpolated function in a certain observation point $\bar{t}$ is given by:

$$y(\bar{t}) = x_{i-1}\varphi_3\left(\frac{\bar{t}-t_{i-1}}{\Delta}\right) + x_i\varphi_3\left(\frac{\bar{t}-t_i}{\Delta}\right) + x_{i+1}\varphi_3\left(\frac{\bar{t}-t_{i+1}}{\Delta}\right) + \\ + x_{i+2}\varphi_3\left(\frac{\bar{t}-t_{i+1}}{\Delta}\right) = x_{i-1}a_{i-1} + x_i a_i + x_{i+1}a_{i+1} + x_{i+2}a_{i+2}. \quad (4.34)$$

To determine the k unknown parameters the Least Squares adjustment is used so, by considering all the available observations, once filled the design matrix ($\mathbf{A}$) and the observation term $\underline{y}$, the splines parameters vector $\underline{x}$ is estimated as:

$$\underline{\hat{x}} = \mathbf{N}^{-1}\mathbf{A}^T\underline{y} \quad (4.35)$$

where $\mathbf{N}$ is the normal matrix computed as $\mathbf{N} = \mathbf{A^T Q^{-1} A}$, with $\mathbf{Q}$ the cofactor matrix.

After the synchronization of the GNSS and gravimeter acceleration observations, the "raw" gravity acceleration is correctly derived simply as the difference of the two dataset:

$$g = f_{grav,corrected} - \ddot{x}_{GNSS} = f_{grav} - f_{lever\,arm} - f_{Eötvös} - \ddot{x}_{GNSS}. \quad (4.36)$$

Chapter 5

Processing of airborne gravity data

The gravity accelerations derived from airborne gravimetric observations are still dominated by noise gathered during the acquisition process, e.g. because of the vehicle vibrations and the atmospheric turbulence. For this reason, the application of a proper procedure is necessary to analyze and elaborate the data in terms of grids or sparse points of gravity anomalies or disturbances. The main problem related to airborne gravity data processing is the extremely high noise-to-signal ratio, e.g. higher than 1000, that has to be properly reduced applying a procedure which can disentangle the noise from the actual gravity signal. Traditionally the procedure used for processing gravity accelerations is a remove-compute-restore procedure that permits to obtain, starting from the sparse observations, predicted grids or sparse points over a certain region. The methodology developed within this work, and presented in this chapter, is a remove-compute-restore -like procedure that, applying a proper filter, allows to first recover the valuable signal from the "raw" gravity accelerations and then to grid these data or extrapolate them on a set of sparse points [57]. This procedure include a Wiener filter and a Least Squares Collocation adjustment. Note that, depending on the final result of this processing, namely a grid or a set of sparse points of predicted gravity disturbances, the Least Squares collocation is equivalent to a gridding or a filtering operation respectively. The proposed methodology is basically an adaptation of the Space-Wise approach developed by Politecnico di Milano to process the data coming from the ESA satellite grav-

ity mission GOCE. The GOCE Space-Wise approach is based on gridding by Least Squares Collocation locally adapting the signal spatial correlation and considering the noise-time correlation of the on-board gravimeter. The aim of this approach is to better recover the local content of GOCE data at the cost of a lower level of global regularization [53]. An important issue related to the Space-Wise approach, adapted to airborne gravimetry processing, is the knowledge of the observation error which is extremely different in the two scopes. For the application to satellite gravimetric GOCE data, as a consequence of the detailed planning of the mission, the design of the entire satellite and the deep testing conducted on all the instrumentations, the stochastic properties of the observation error are considered a-priori well known [67](at least in terms of spectral characteristics). In the case of airborne gravimetry instead the situation is quite different: considering the complexity of the acquisition environment, it is not possible to have an a-priori knowledge of this error, that consequently requires an additional procedure to retrieve it from the observations themselves.

In this chapter, the procedure developed to filter and grid the gravity raw accelerations is presented. First of all, in Section 5.1 the complete processing scheme is shown and described in details. Then, Section 5.2 is dedicated to the Wiener filter while Section 5.4 is dedicated to the Least Squares Collocation adjustment finalized to the final filtering or gridding of the gravity data. Moreover the methodology developed for the evaluation of the observation error stochastic properties is presented too in Section 5.3.

5.1 Remove-compute-restore procedure

To predict grids of gravity anomalies or disturbances starting from the raw gravity accelerations, derived from airborne measurements, two main problems have to be solved. The first problem is related to the correct separation of the low frequencies signal from the observation colored noise; the second one regards the application of a proper filter to disentangle the high frequencies noise from the actual gravity signal. It is worth to be mentioned that the observation colored noise is characterized by low frequencies due to drifts of the instrumental measurement system and by high frequencies associated to the aircraft vibrations, atmospheric turbulence, etc. The former problem, namely the removal of the low frequencies signal, can be solved nowadays by exploiting Global Gravity Models (GGMs). To retrieve the low frequencies of the local gravity field in fact global models derived from satellite gravimetry/gradiometry (e.g. GRACE and GOCE data) can be used, as well as models obtained from the integration of satellite data with radar altimetry and surface measurements. The latter problem, namely the separation of high frequencies noise from the actual signal, is solved choosing the proper filter to be applied.

By merging GGM and local airborne data the combined gravity field signal is characterized, for the low frequencies, basically by the information of GGM and for the medium and high frequencies, by information coming from the filtered airborne signal itself.

The most commonly adopted and applied approach to airborne gravity observations is the remove-compute-restore technique [62] which can be summarized as follow. In the remove step, a low frequency signal, predicted from GGMs, and an high frequency one, obtained from the computation of the gravitational effect of topography, are removed from the observations; the observations are then filtered to separate the signal from the noise. In the compute step, the filtered gravity accelerations are converted in grids or sparse points of gravity anomalies/disturbances using for example the Least Squares Collocation. Finally, after having carried out the compute step, the long-wavelength and short-wavelength signals removed at the beginning are restored back.

The implemented procedure, presented within this work, is basically a remove-compute-restore procedure and the proposed processing scheme is shown in Fig. 5.1 and outlined in the following.

The first step consists in creating a reference signal, δg_{ref}, along the aircraft trajectory; it is generated from existing GGMs adding to it a Residual Terrain Correction (RTC):

$$\delta g_{ref} = \delta g_{GGM} + \delta g_{RTC}. \tag{5.1}$$

The first term on the right, namely δg_{GGM}, results from a spherical harmonic synthesis of the GGM up to its maximum degree/order L_{max}. This operation consists in using the coefficients $C_{\ell m}$ and $S_{\ell m}$, given by the GGM, to compute the desired functional of the gravitational potential. In the case of gravity disturbances the following expression is used:

$$\delta g(\varphi,\lambda,r) = -\frac{\partial T}{\partial r} = \frac{GM}{r^2}\sum_{m=0}^{L_{max}}\Bigg[cos(m\lambda)\sum_{\ell=L_{min}}^{L_{max}}(\ell+1)\left(\frac{a}{r}\right)^{\ell}C_{\ell m}P_{\ell m}sin(\varphi)+ \\ + sin(m\lambda)\sum_{\ell=L_{min}}^{L_{max}}(\ell+1)\left(\frac{a}{r}\right)^{\ell}S_{\ell m}P_{\ell m}sin(\varphi)\Bigg]. \tag{5.2}$$

The second term of Eq. 5.1, namely δg_{RTC}, is the result of the difference between two terrain corrections: the first one computed using a high resolution Digital Terrain Model (DTM) and the second one computed with a smoother DTM obtained applying a moving average window to the original refined terrain

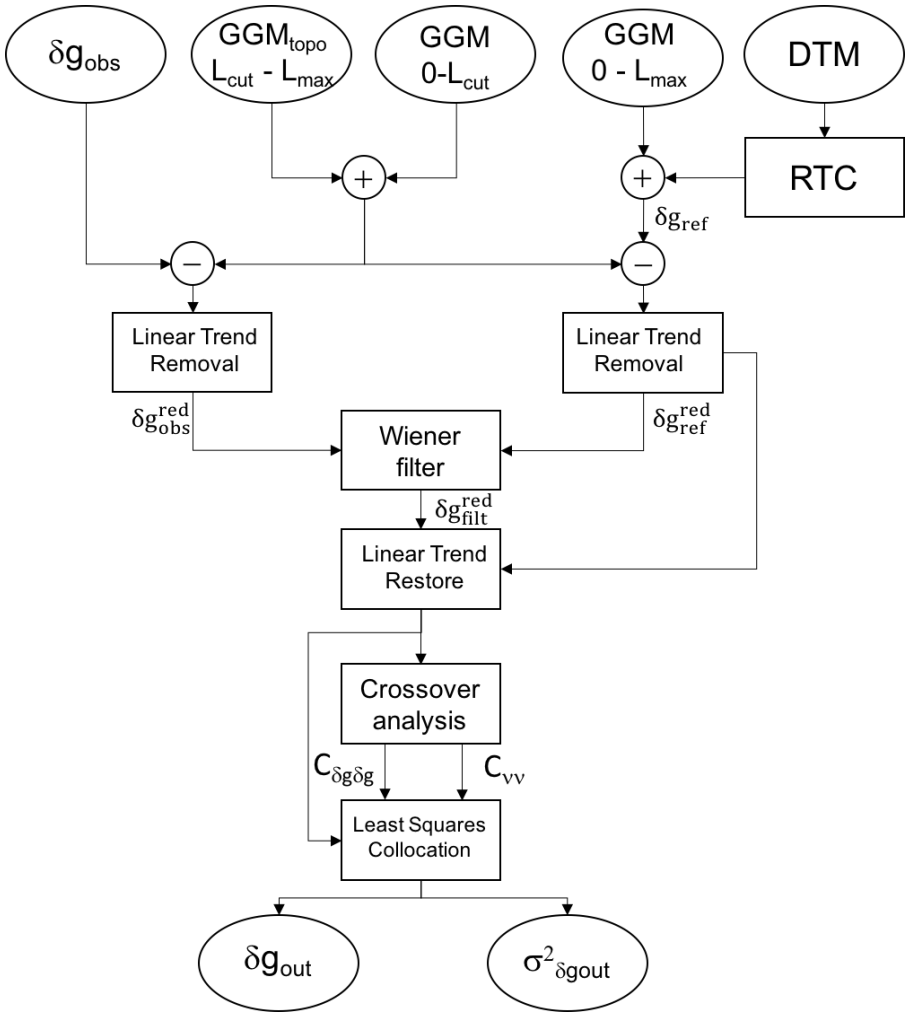

Figure 5.1: Flow chart of the procedure implemented to filter and grid raw aero-gravimetric data

model. The spatial resolution of the window depends on L_{max}, as reported in [40]:

$$\lambda = \frac{40.000 \text{ km}}{L_{max} + 0.5}. \tag{5.3}$$

The terrain correction, that consists in computing the vertical attraction due to topographic masses, within the proposed procedure has been computed using a hybrid algorithm that exploits a combined Fast Fourier Transform - prisms approach and works in spherical approximation [56].

Actually the term coming from GGM in Eq. 5.1 is known to contain information on the Earth's gravitational field only up to a maximum wavelength, that can be roughly estimated by means of Eq. 5.3. Consequently the meaning of Eq. 5.1 is to compute the best δg model on the flight tracks (before exploiting the airborne observations themselves) by completing the effect of the GGM with the one of the residual topography. The reason why we use a "residual" topography for the terrain effects, is that the low frequency of the terrain gravimetric signal is already incorporated into the global model GGM (see the discussion in [31]). Note also that in δg_{ref} the most important missing information is basically the one related to the density variation in the residual topography: in fact, while GGM contains real gravity observations, the term δg_{RTC} is the effect of the residual topography usually computed with a standard density of 2670 g/m^3.

Once the reference signal has been created, the following step is the remove one. It consists in subtracting from both the observed and the reference signals, δg_{obs} and δg_{ref} respectively, the contribution of a global model for the low frequencies and of a global model of terrain correction for the medium-high frequencies. The contribution for the low frequencies is estimated from the same global model used to create the reference signal with a spherical harmonic synthesis up to a certain intermediate degree L_{cut} (e.g. 210 or 360). The contribution of the topography instead is derived from a spherical harmonic synthesis of a global gravity model related to the topography (e.g. dV_ell_ret2012) from the same L_{cut} to the maximum degree of the model L_{max}. These kind of models related to the topography are basically a spherical harmonic representation of the Earth's topographic gravitational potential and consent to estimate the terrain correction term due to the Earth's mass distribution considered by the model. The choice of L_{cut} should be carefully performed since this degree is basically used to define the limit between low frequencies, where for the final estimates only the GGM data are adopted, and medium-high frequencies, in which the airborne observations count more than GGM. Moreover within the remove step, if required, a linear trend for each single flight line, estimated from the reference signal, is also removed. This last operation is required considering that in general the inertial observations are contaminated by drifts and biases. The above procedure leaves the reduced observations δg_{obs}^{red} and the reduced reference signal δg_{ref}^{red} with zero mean and with a smaller amplitude and spatial correlation with respect to the original signals.

The third step is the filtering of δg_{obs}^{red} by means of the application of a Wiener filter along each single flight track. As will be detailed in the next section the

Wiener filter filters the reduced raw gravity observations according to the power spectrum expected from the reduced reference model. After the data have been filtered and the colored noise has been separated from the observations, the linear trend removed in the previous step is added back thus obtaining regularly sampled tracks of the filtered reduced gravity disturbances δg_{fil}^{red}.

Now, before the compute step in which the Least Squares Collocation is used to derive from δg_{fil}^{red} the gravity disturbances in correspondence of the interested grid nodes, the covariance functions of both the noise and the signal require to be estimated. Regarding the noise, an analysis of the residuals at the crossovers, i.e. by definition the intersection points between two different aircraft tracks, is performed. The analysis of the residuals of δg_{fil}^{red} at these points can provide an empirical estimate of the noise stochastic properties along the aircraft trajectory. The signal covariance function is instead empirically estimated from the observations, so, differently from the error covariance which is an along-track one, it is a spatial one that is modeled as a linear combination of a set of Bessel functions of the first order and zero degree [76].

A grid or a set of sparse points of δg_{fil}^{red} and their corresponding error are generated by a Least Squares Collocation solution, namely in the compute step and in conclusion, within the restore step, the signal removed at the beginning of the procedure are restored back.

The description of the Wiener filter, the crossovers analysis as well as the signal covariance estimation and the Least Squares Collocation solution will be further described in the following sections of this chapter.

5.2 The Wiener filter

As stated in the previous section the first operation of the whole processing procedure is building a reference signal δg_{ref}, without using airborne data, that has to be as close as possible to the actual gravity field. This signal can be generated by using a high-degree GGM (e.g. EIGEN-6C4 or GECO) and adding to it a residual terrain correction, to fill the missing high frequencies that lack in these global models. The importance of creating this δg_{ref} is due to the fact that the recently developed GGMs in principle exploit the gravity data coming from the ultimate gravimetric satellite missions (i.e. GRACE and GOCE) and this means that their low frequencies are expected to be more reliable or at least better sampled than the ones derived from airborne measurements. For this reason, the δg_{ref} is practically used to retrieve the low frequencies of the filtered signal but, as described further on this chapter, it can be used also to estimate the filtered signal stochastic properties.

After that, the first operation is the remove step which consists in reducing both observations and reference signal for the low and medium-high frequencies

by synthesizing a GGM and a GGM related to the topography. The choice of the proper degree L_{cut}, that separates the low frequencies from the medium-high ones, is a critical issue that can be solved in two ways. In the first case, it can be empirically fixed on the basis of the formal error of the GGM (so by selecting it in such a way that the cumulative error of the model is smaller than a given threshold); in the second one, it can be defined as a function of the dimension of the investigated area (e.g. supposing to have an area of 100 x 100 km^2, inverting Eq. 5.3, L_{max} results to be 400). The reduction of the observed signal consents to obtain a signal that, once subtracted the low frequencies from the reference GGM, is independent from the gravity measurements at the calibration point (generally located at the departure airport). The reference signal instead, after the remove operations, is characterized by zero low frequencies and reduced medium-high frequencies.

To filter the reduced observations δg_{obs}^{red} a track-by-track Wiener filter in the frequency domain can be applied. This is a filter generally adopted in signal processing that produces an estimate of the desired random process by the linear time-invariant filtering of an observed process affected by noise, under the assumption of knowing the spectra of both stationary signal and noise. For example, the observed signal can consist of an unknown signal of interest corrupted by additive noise. This filter is based on a statistical approach, since it used the Minimum Mean Square Error (MMSE) estimator. The principal assumption for the application of the Wiener filter is that the signal and the additive noise are stationary linear stochastic processes with known spectral characteristics or known autocorrelation and cross-correlation. Given a general system:

$$y(t) = x(t) + \nu(t) \tag{5.4}$$

where $x(t)$ is the original signal (unknown) at a certain epoch t, $\nu(t)$ is the additive noise (unknown), independent of $x(t)$, and $y(t)$ is the observed signal. The objective is to find a function $g(t)$ that allows to estimate $x(t)$ by the following constitutive formula:

$$\hat{x}(t) = (g * y)(t). \tag{5.5}$$

In Eq. 5.5, $\hat{x}$ represents the estimate of $x(t)$ that minimizes the mean square error. Moving to the frequency domain, the filter $G(f)$ which is the Fourier Transform of g at frequency f, can be easily described as:

$$G(f) = \frac{S(f)}{S(f) + N(f)} \tag{5.6}$$

where $S(f)$ and $N(f)$ represent the mean power spectral densities of the original signal $x(t)$ and of the additional noise $n(t)$ respectively. In the frequency domain the filtering operation results in:

$$\hat{X}(f) = G(f)Y(f) \tag{5.7}$$

with $\hat{X}(f)$ and $Y(f)$ the Fourier Transform of $\hat{x}(t)$ and $y(t)$ respectively. The final filtered signal $\hat{x}(t)$ is obtained by simply performing the inverse Fourier Transform on $\hat{X}(f)$. Rewriting Eq. 5.6 in the following way, the performance of the Wiener filter becomes apparent:

$$G(f) = \frac{1}{1 + \frac{N(f)}{S(f)}} = \frac{1}{1 + \frac{1}{SNR(f)}}. \tag{5.8}$$

Here, $SNR(f) = \frac{S(f)}{N(f)}$ is the signal-to-noise ratio. At the frequencies in which the noise increases, the signal-to-noise ratio decreases, so the filter $G(f)$ decreases too. This means that the Wiener filter attenuates frequencies depending on their signal-to-noise ratio.

A simplification of the Wiener Filter formula runs as follows. As said before, the Wiener filter is used to produce an estimate of the original unknown noisy signal that minimizes the mean square error, which may be expressed as:

$$\epsilon(f) = \mathbb{E}|X(f) - \hat{X}(f)|^2 \tag{5.9}$$

where $\mathbb{E}$ is the expectation operator. Substituting in Eq. 5.9 the expression for $\hat{X}(f)$ we get:

$$\begin{aligned} \epsilon(f) &= \mathbb{E}|X(f) - G(f)Y(f)|^2 \\ &= \mathbb{E}|X(f) - G(f)\left[X(f) + V(f)\right]|^2 \\ &= \mathbb{E}|\left[1 - G(f)\right]X(f) + G(f)V(f)|^2 \end{aligned} \tag{5.10}$$

with $V(f)$ the Fourier Transform of the observation noise $\nu(f)$. If we expand the square, we obtain:

$$\begin{aligned} \epsilon(f) = &\left[1 - G(f)\right]\left[1 - G(f)\right]^* \mathbb{E}|X(f)|^2 + \\ &- \left[1 - G(f)\right]G^*(f)\mathbb{E}\{X(f)V^*(f)\} + \\ &- G(f)\left[1 - G(f)\right]^* \mathbb{E}\{V(f)X^*(f)\} + \\ &+ G(f)G^*(f)\mathbb{E}|V(f)|^2. \end{aligned} \tag{5.11}$$

Recalling the assumption that the noise is independent of the signal, we have:

$$\mathbb{E}\{X(f)V^*(f)\} = \mathbb{E}\{V(f)X^*(f)\} = 0 \tag{5.12}$$

and defining the power spectral densities as follows:

$$S(f) = \mathbb{E}|X(f)|^2 \tag{5.13}$$

$$N(f) = \mathbb{E}|V(f)|^2 \tag{5.14}$$

Eq. 5.11 becomes:

$$\epsilon(f) = [1 - G(f)]\,[1 - G(f)]^*\,S(f) + G(f)G^*(f)N(f). \tag{5.15}$$

To find the minimum error value, the derivative of $\epsilon(f)$ with respect to $G(f)$ has to be computed and set equal to zero:

$$\frac{\mathrm{d}\epsilon(f)}{\mathrm{d}G(f)} = G^*(f)N(f) - [1 - G(f)]^*\,S(f) = 0; \tag{5.16}$$

this final equality can be rearranged to give the Wiener filter.

In conclusion, for our purposes the filter G is:

$$G = \frac{S_{\delta g}}{S_{\delta g} + S_\nu} \tag{5.17}$$

with $S_{\delta g}$ and S_ν the power spectral densities of the reduced signal and the observation noise, respectively. The former is computed from the reference signal δg^{red}_{ref} applying the Fourier transform in the following way:

$$S_{\delta g} = \mid \mathrm{FFT}(\delta g^{red}_{ref}) \mid^2 . \tag{5.18}$$

The latter is derived from the difference between the spectral density of the observed signal δg^{red}_{obs} and the spectral density of the reference δg^{red}_{ref}:

$$S_\nu = \mid \mathrm{FFT}(\delta g^{red}_{obs}) \mid^2 - S_{\delta g}. \tag{5.19}$$

In practice, considering that the reduced reference signal has zero low frequencies, after the application of the Wiener filter we obtain a filtered observed signal that has these low frequencies replaced by the GGM ones. Note that within this step which largely depends on the δg_{ref} model, it is better to underestimate S_ν in such a way to be sure that no signal is erroneously filtered and letting the Least Squares Collocation step to refine the Wiener filter.

In conclusion, after the filtering operation, the linear trend previously removed is restored back. The output of this part of the procedure results in a set of regularly sampled tracks of reduced and filtered gravity disturbances δg_{fil}^{red}.

5.3 The crossover analysis

The characterization of the noise affecting airborne gravity observations, in terms of its stochastic properties, is an important issue to be solved. Within the processing procedure here proposed this problem has been solved by using the crossover analysis. In classical airborne gravity data processing, this method is usually adopted but for different scopes: in particular it is simply used to evaluate the quality of the filtered data [3] or it is used to retrieve the low frequencies of the gravitational field on the basis of the crossovers [10]. In this work the crossover analysis is adopted to empirically retrieve the along-track observations error covariance function.

As seen in the Wiener filter section, the result of the along-track filtering procedure is a dataset in which the signal to noise ratio is greatly increased thanks to the exploitation of external information (from the reference gravity signal). However a further refinement based on the airborne gravity observations is desirable, especially if S_ν has been underestimated. To do so, a proper knowledge of the along-track error covariance is fundamental.

In an airborne gravimetric survey generally there are two main flight directions, perpendicular with each other, that allows to divide the flight lines in two different categories: namely called traverse and control lines. By definition the crossover is the point at the intersection between a traverse and a control line (see Fig. 5.2).

To apply the crossover analysis the first thing to do is to model each aircraft track as a straight line, estimating its parameters by means of a Least Squares adjustment. This modeling step is necessary to identify the intersection point between the two considered tracks. Then the gravity field is evaluated in correspondence of the intersections of traverse and control lines, computing separately the gravity field from each single line. To predict the gravity field on the modeled line a Lagrangian interpolation is applied [15]. Basically the interpolating function results in the Lagrange polynomial $P(x)$ of degree $\leq (n-1)$ that passes through the n observation points. It is a linear combination of Lagrange basis

polynomials $P_i(x)$ and it is given by:

$$P(x) = \sum_{i=0}^{n} y_i P_i(x) \tag{5.20}$$

where $P_i(x)$ is:

$$P_i(x) = \prod_{k=1 \ k \neq i}^{n} \frac{x - x_k}{x_i - x_k}. \tag{5.21}$$

After the interpolation, the gravity field values on the modeled lines are predicted at the intersection points. Considering the dynamic environment in which measurements are done, it is possible that the two flight lines at their intersection are characterized by different heights. To overcome this problem and to properly evaluate the residual at the crossovers, the gravity values derived from the two lines at their intersections are moved along the vertical direction. This step is performed by linearizing the problem and computing the second radial derivative of the gravity field from the reference model (see Fig. 5.2).

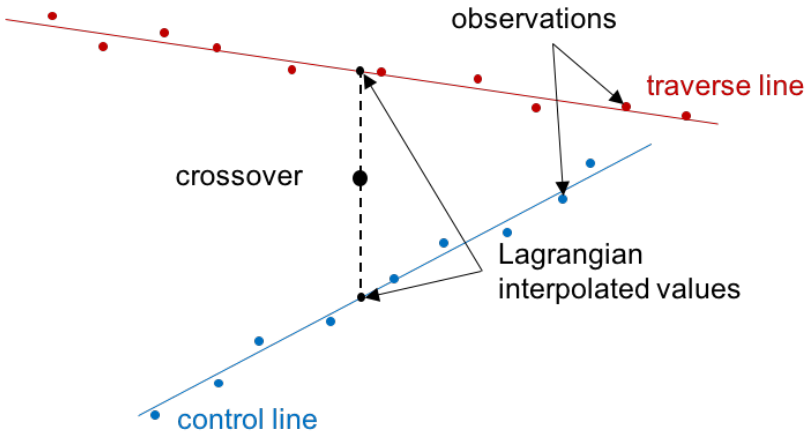

Figure 5.2: Geometry of the crossover analysis

Note that to derive the residuals at the crossover, the gravity field data are shifted in both the horizontal and vertical directions. However these "movements" produce in general a limited effect. In fact, analyzing the data of a real acquisition

(i.e. the dataset used in the Numerical Tests chapter) the maximum along-track shift can be in the worst case of 250 meters, while in the vertical direction it is of about 1 m, in both cases these differences are negligible especially when dealing with the reduced signal.

Once evaluated the residuals at the crossovers, they can be associated to the error of the filtered gravity disturbances at the same observed point from different tracks. So, taking each control line the whole set of its estimated errors can be used to compute the empirical along-track error covariances. If the along-track error is stationary (i.e. if we can suppose that its stochastic properties does not change in time and therefore are the same for all the survey tracks), which is a realistic hypothesis to be applied to an airborne gravimetric survey, it is possible to average the error covariances of all the control lines to obtain the final estimate of the empirical along-track error covariance function. This operation guarantees the estimate of a robust error covariance, property that can not be valid for a single flight line, due to the limited number of covariance samples retrievable, in particular for long wavelengths. This empirical error covariance is then interpolated by means of a proper theoretical covariance function and the covariance matrix $C_{\nu\nu}(\psi)$ (with ψ representing the spherical distance along the aircraft track) is generated for the subsequent Least Squares Collocation. The covariance modeling algorithms adopted within this processing method are presented in the following section.

The importance of the crossover analysis is due to the fact that it does not only permit to derive the empirical covariance of the observations error but it also consents, as stated before, to evaluate the goodness of the Wiener filtering described in the previous section.

5.4 Least Squares Collocation

In order to compute the final gravity disturbances δg on a grid or on a set of sparse points, besides the empirical covariance of the observation error, also the observed signal empirical covariance requires to be evaluated.

To retrieve this empirical covariance two possible strategies can be followed. The first possibility consists in retrieve it from the original reference global model. In details, a grid of reference gravity disturbances δg_{ref} can be generated from the global model, and, once reduced, it can be used to create the empirical covariance function. The second strategy consists in estimating it from the airborne filtered reduced data only. The principal difference between these two approaches is that the second approach, differently from the first one, is completely independent from the reference gravity model and depends only from the observed airborne data. However it is important to note also that, using the first strategy (i.e. the grid derived from the reference signal), a wider set of data with respect to

the second approach are considered for the estimation of the covariance function. This allows a better estimate close (with respect to the correlation length of the reduced signal covariance) to the survey boundaries since not only the data in correspondence of the flight tracks are used but also all those data within the gridded area.

For the proposed methodology, the second strategy has been adopted with the aim to define a procedure not strongly dependent from external data. However within this chapter, both strategies have been presented in details in the following subsections. To model both signal and observation error covariance functions various well-known models (i.e. Gaussian, exponential models or a linear combination of Bessel functions with positive coefficients) can be adopted. In particular, the linear combination of Bessel functions of the first order is well suited to describe the gravity covariance due to the fact that it can properly describes the typical oscillations that characterize the empirical gravity field covariance.

Note that the separation between signal and noise is performed basically here within the covariance estimation. In details it is performed by supposing that the error is correlated only along-track (i.e. noises of two different tracks are uncorrelated which is a well satisfied hypothesis) and the signal is of course correlated isotropically in a given area, which is again a well satisfied hypothesis (see Fig. 5.3).

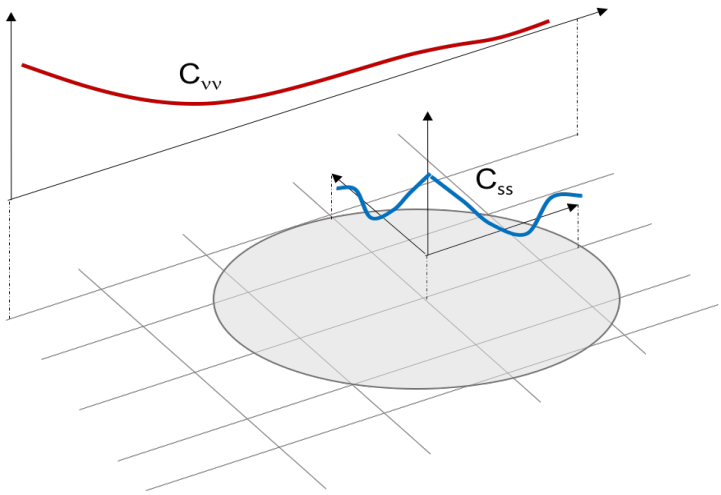

Figure 5.3: Signal and noise empirical covariances: the signal covariance (blue) is supposed correlated isotropically in a given area; the noise covariance (red) is assumed correlated only along-track

5.4.1 Empirical covariance estimation from grid

In the first strategy presented to estimate the signal empirical covariance the reference reduced grid of δg_{ref}^{red} is used. Then, this empirical covariance is fit with a set of n Bessel functions of the first order and zero degree: in details, it is built as a linear combination (with positive coefficients) of these Bessel functions. The fitting step is performed automatically in the frequency domain exploiting the relation between the 2D power spectral densities and Bessel functions, as shown in the following.

It has to be stated that in this approach we are passing from a spherical to a Cartesian approximation. Given the limited amplitude of the processing area this is considered as an acceptable approximation.

Let suppose to have a grid of reduced gravity disturbances $\delta g_{ref}^{red}(\underline{x})$ (that in the following will be denoted with $\delta g(\underline{x})$ to simplify the notation), characterized by a zero mean and with a homogeneous and isotropic behavior. In here $\underline{x}$ is a vector representing the two planar coordinates of the grid point. The first operation is the computation of its Fast Fourier Transform (FFT), denoted as $FFT(\delta g(\underline{p}))$, with $\underline{p}$ the wave number vector with components along the directions defined by the ($\underline{x}$) vector. Considering N bins, for each single i-th bin it is possible to compute the following average:

$$S_i(p) = \sum_{\underline{p} \epsilon \Omega_{p_i}} \frac{|FFT(\delta g(\underline{p}))|}{n} \tag{5.22}$$

where $p = |\underline{p}|$ represents the number of values included within the i-bin and Ω_{p_i} is defined as follow:

$$\Omega_{p_i} = \overline{p}_i \leq p \leq \overline{p}_i + \Delta p. \tag{5.23}$$

In Eq. 5.23 $\overline{p}_i$ represents a set of values ranging from 0 to the maximum p with an increment given by $\frac{\max|\underline{p}|}{N-1}$. The $S_i(p)$ function is basically a step function that depends only on the radial coordinates p in the plane $\underline{p}$. This averaging operation consents to move from the 2-D spectrum to the 1-D power spectral density. Being interested in a covariance function, which is, in case of an homogeneous and isotropic field, only a function on distances r between points, we note that it (namely $C(r)$) can be derived from the inverse Fourier Transform of $S_i(p)$.

Recalling the relation between the two-dimensional Fourier Transform, symmetrical with respect to the radial direction, and the Hankel Transform ([49]), we get:

$$S(p) = \int_0^{+\infty} \overline{J}_0(pr) C(r) r \mathrm{d}r \tag{5.24}$$

where $\overline{J}_0$ is related to the Bessel function of first order and 0 degree by the following expression:

$$\overline{J}_0(pr) = 2\pi J_0(2\pi pr). \tag{5.25}$$

Consequently $C(r)$ can be obtained by performing the inverse Hankel Transform [49] of Eq. 5.24:

$$C(r) = \int_0^{+\infty} \overline{J}_0(pr) S(p) p \mathrm{d}p. \tag{5.26}$$

Recalling also the following formula, proposed in [76]:

$$\int_0^{+\infty} J_0(ar) \frac{J_1(br)}{r} r \mathrm{d}r = \begin{cases} 0 & a > b \\ \frac{1}{b} & a < b \end{cases} \tag{5.27}$$

if we consider $a = 2\pi p$, $b = 2\pi \overline{p}$, $\overline{J}_0(pr) = 2\pi J_0(pr)$ and $\overline{J}_1(pr) = 2\pi J_1(pr)$ we obtain:

$$\frac{\overline{p}}{2\pi} \int_0^{+\infty} \overline{J}_0(pr) \frac{\overline{J}_1(pr)}{r} r \mathrm{d}r = \begin{cases} 0 & p > \overline{p} \\ 1 & p < \overline{p} \end{cases} \tag{5.28}$$

Combining Eq. 5.26 and Eq. 5.28 it is possible to obtain the following expression:

$$C(r) = \sum_{i=0}^{n} S_i \left[\frac{(i+1)\Delta p}{2\pi} \frac{\overline{J}_1((i+1) + \Delta r)}{r} - \frac{i\Delta p}{2\pi} \frac{\overline{J}_1(i\Delta r)}{r} \right]. \tag{5.29}$$

Eq. 5.29 allows to estimate a covariance function corresponding to a power spectrum described in terms of linear combination of step functions as a linear combination of n Bessel functions of the first order.

5.4.2 Empirical covariance estimation from along-track data

The second strategy to model the signal covariance function consists in empirically computing it from the along-track filtered reduced signal, and subsequently modeling it with a linear combination (with positive coefficients) of Bessel functions. The coefficients of this linear combination are estimated by means of a non-negative Least Squares Adjustment.

The problem of Non Negative Least Squares (NNLS) is basically a Least Squares problem with an addition constrain, i.e. the coefficients are not allowed to become negative. It can be formulated as follow:

$$\text{Minimize } \|\mathbf{A}\underline{x} - \underline{y}\| \text{ subject to } \underline{x} \geq 0. \tag{5.30}$$

The algorithm used to solve this problem within our methodology was formulated by [41] and can be summarized as follows:

- The input variables are: the matrix $\mathbf{A}$ of dimension $m \times n$, the vector $\underline{y}$ of dimension m and a tolerance value ϵ to stop of the iterative procedure;
- The first step is the initialization of the two sets in which two indexes will be defined and modified: P and R.

$$P = \emptyset \tag{5.31}$$

$$R = \{1, 2, \cdots, n\} \tag{5.32}$$

  Moreover the vector $\underline{x}$ is initialized to zero and the vector of the residuals $\underline{w}$ is computed in the following way:

$$\underline{w} = \mathbf{A}^T(\underline{y} - \mathbf{A}\underline{x}). \tag{5.33}$$

- After the initialization, there is a main loop that is stopped only if $R = \emptyset$ and the maximum of $\underline{w}$ is greater than the tolerance ϵ. Within this loop, every index j in R (being j the index of $\max(\underline{w})$), is first removed from R and added to P. Then, being $\mathbf{A}^P$ the $\mathbf{A}$ matrix restricted to the variables of P, $\underline{s}^P$ and $\underline{s}^R$ can be estimated as:

$$\underline{s}^P = ((\mathbf{A}^P)^T\mathbf{A}^P)^{-1}(\mathbf{A}^P)^T\underline{y} \tag{5.34}$$

$$\underline{s}^R = 0 \tag{5.35}$$

  with $\underline{s}$ the vector of same length as $\underline{x}$, $\underline{s}^P$ the sub-vector with indexes from P, and $\underline{s}^R$ the sub-vector with indexes from R.

- at this point, another loop inside the previous one starts and continues while $\min(\underline{s}^P) \leq 0$: calling α, $\alpha = \min \frac{x_i}{x_i + s_i}$, for i in P where $s_i \leq 0$; $\underline{x}$ can be set equal to

$$\underline{x} = \underline{x} + \alpha(\underline{s} - \underline{x}). \tag{5.36}$$

  Now all the indexes in P such that $x_j = 0$ are moved to R and $\underline{s}^P$ and $\underline{s}^R$ are evaluated again using Eqs. 5.34 and 5.35.

- Once exited from both the internal and the external loops, the solutions for $\underline{x}$ and $\underline{w}$ are:

$$\underline{x} = \underline{s} \tag{5.37}$$

$$\underline{w} = \mathbf{A}^T(\underline{y} - \mathbf{A}\underline{x}). \tag{5.38}$$

5.4.3 Collocation solution

After that the covariance functions have been modeled, they can be used to built the covariance matrices required for the Least Squares Collocation solution. At this point of the computation so the available data are: a set of along-track filtered and reduced observations δg_{fil}^{red}, the covariance model of this signal and the covariance model of the observation noise. It is important to underline that the data (δg_{fil}^{red}) are independent line by line and characterized by a stationary noise with stochastic properties retrieved from the crossovers analysis. Note that the spatial correlation of the gravity signal is due only to the gravity field.

To predict the gravity signal on a regular planar grid from the "observed" quantities the collocation, which is a stochastic method for the interpolation, is adopted. For geophysical purposes regular grids are generally preferred because some computations can be efficiently performed in the frequency domain. The Least Squares collocation approach, which is a mathematical tool developed by T. Krarup and H. Moritz [39] [45], evolved from statistical methods to interpolate gravity anomalies, but has been shown to have wider applications within physical geodesy. The aim of collocation is to predict the interested signal where measurements have not been made.

Let us suppose to consider an observed signal $\underline{y}$ (of dimension $n \times 1$) or a random field (i.e. in our case the gravity disturbances). Since we are dealing with a reduced field and with observations acquired for resources exploration (i.e. field at an almost constant altitude as low as possible), the problem is basically a simplified problem. In particular we can suppose that the observations

have been acquired at the same altitude and also that we want to estimate a grid at the same altitude too. A consequence of this assumption is that in this way it is possible to neglect the use of Poisson kernel to propagate gravity in vertical direction and we can work with a simplified observation equation, which can be expressed as:

$$\underline{y} = \underline{x} + \underline{\nu} \tag{5.39}$$

where $\underline{x}$ represents the actual signal and $\underline{\nu}$ is the observation noise. The stochastic properties of the actual signal $\underline{x}$ are:

$$\mathbb{E}\{\underline{x}\} = 0 \tag{5.40}$$

$$C_{xx} = \mathbb{E}\{\underline{x}\ \underline{x}^T\}; \tag{5.41}$$

while the statistics of the noise vector $\underline{\nu}$ are:

$$\mathbb{E}\{\underline{\nu}\} = 0 \tag{5.42}$$

$$C_{\nu\nu} = \mathbb{E}\{\underline{\nu}\ \underline{\nu}^T\}. \tag{5.43}$$

Moreover the following assumption is made:

$$\mathbf{E}\{\underline{y}\ \underline{\nu}\} = 0 \tag{5.44}$$

so the random field and the noise are linearly independent, as well as any admissible functional of the field.

The objective of the gridding step is to predict $\hat{\underline{y}}$ on a regular grid (of dimension $m = r \times c$) at a constant altitude. Within our case, we don't need a change of functional to predict $\hat{\underline{y}}$ since our scope is to predict gravity disturbances on a grid, starting from the observed gravity disturbances values.

To solve this problem we use the Wiener-Kolmogorov Best Linear Unbiased Predictor principle (BLUP), that is generally used for the prediction of random effects. BLUP was derived by Charles Roy Henderson in 1950 [24] and he described it as being "joint maximum likelihood estimates". Basically, the BLUP estimates of the realized values of the random variables u are linear in the sense that they are linear functions of the data, y; unbiased in the sense that the average value of the estimate is equal to the average value of the quantity being estimated; best in the sense that they have minimum mean squared error within the class of linear unbiased estimators; and predictors to distinguish them from

estimators of fixed effects [52]. We shortly report the derivation of this fundamental estimator. The BLUP principle can be summarize as follows:

$$\begin{aligned} \text{Linear} \quad & \hat{\underline{y}} = \underline{\lambda}^T \underline{y} = (\underline{\lambda}^T \underline{x} + \underline{\lambda}^T \underline{\nu}) \\ \text{Unbiased} \quad & \mathbb{E}\{\hat{\underline{y}}\} = \underline{\lambda}^T \mathbb{E}\{\underline{y}\} = \underline{\lambda}^T \mathbb{E}\{\underline{x}\} + \underline{\lambda}^T \mathbb{E}\{\underline{\nu}\} = 0 \\ \text{Best} \quad & \underline{\lambda} = \text{argmin } \varepsilon^2(\underline{\lambda}) \end{aligned}$$

where $\varepsilon^2(\underline{\lambda})$ can be expressed as:

$$\varepsilon^2(\underline{\lambda}) = \mathbb{E}\{\underline{y} - \hat{\underline{y}}\}^2 = \mathbb{E}\{\underline{y} - \underline{\lambda}^T \underline{x} - \underline{\lambda}^T \underline{\nu}\}^2. \tag{5.45}$$

Solving the square in Eq. 5.45 and considering the assumptions expressed at the beginning of this section, the $\varepsilon^2(\underline{\lambda})$ can be written in the following way:

$$\varepsilon^2(\underline{\lambda}) = \mathbb{E}\{\underline{y}\}^2 + \mathbb{E}\{\underline{\lambda}^T \underline{x}\}^2 + \mathbb{E}\{\underline{\lambda}^T \underline{\nu}\}^2 - 2\mathbb{E}\{\underline{\lambda}^T \underline{x}\ \underline{y}\}. \tag{5.46}$$

Now each single term of Eq. 5.46 can be analyzed separately as summarized below:

- $\mathbb{E}\{y\}^2$ represents the variance of the observed field:

$$\mathbb{E}\{y\}^2 = \sigma_y^2 \tag{5.47}$$

- $\mathbb{E}\{\underline{\lambda}^T \underline{x}\}^2$ and $\mathbb{E}\{\underline{\lambda}^T \underline{\nu}\}^2$ for the variance propagation law can be expressed as follow:

$$\mathbb{E}\{\underline{\lambda}^T \underline{x}\}^2 = \mathbb{E}\{(\underline{\lambda}^T \underline{x})(\underline{\lambda}^T \underline{x})\} = \underline{\lambda}^T \mathbf{C_{xx}} \underline{\lambda} \tag{5.48}$$

$$\mathbb{E}\{\underline{\lambda}^T \underline{\nu}\}^2 = \mathbb{E}\{(\underline{\lambda}^T \underline{\nu})(\underline{\lambda}^T \underline{\nu})\} = \underline{\lambda}^T \mathbf{C}_{\nu\nu} \underline{\lambda} \tag{5.49}$$

  with $\mathbf{C_{xx}}$ and $\mathbf{C}_{\nu\nu}$ the covariance matrix of the actual signal and of the noise, respectively;

- the double product term $-2\mathbb{E}\{\underline{\lambda}^T \underline{x}\ \underline{y}\}$ becames:

$$-2\mathbb{E}\{\underline{\lambda}^T \underline{x}\ \underline{y}\} = -2\underline{\lambda}^T \mathbf{C_{xy}} \tag{5.50}$$

  with $\mathbf{C_{xy}}$ the cross-covariance matrix between the $\underline{y}$ and $\underline{x}$ vectors of dimension $(m \times n)$.

So now the Eq. 5.46 can be rewritten as:

$$\varepsilon^2(\underline{\lambda}) = \sigma_y^2 + \underline{\lambda}^T \mathbf{C_{xx}} \underline{\lambda} + \underline{\lambda}^T \mathbf{C}_{\nu\nu} \underline{\lambda} - 2\underline{\lambda}^T C_{xy}. \tag{5.51}$$

The *argmin* of this equation can be simply found computing the first derivative with respect to λ, that results to be:

$$(\mathbf{C_{xx}} + \mathbf{C}_{\nu\nu})^{-1} \underline{\lambda} - \mathbf{C_{xy}} = 0; \tag{5.52}$$

once derived $\underline{\lambda}$ from Eq. 5.52, the final predicted gravity disturbances can be computed as:

$$\underline{\hat{y}} = \mathbf{C_{yx}} (\mathbf{C_{xx}} + \mathbf{C}_{\nu\nu})^{-1} \underline{y}. \tag{5.53}$$

The corresponding squared error can be derived in the following way, by applying again the variance propagation law:

$$\varepsilon^2(\underline{\lambda}) = \mathbb{E}\{\underline{y} - \underline{\hat{y}}\}^2 = \mathbf{C_{yx}} (\mathbf{C_{xx}} + \mathbf{C}_{\nu\nu})^{-1} \mathbf{C_{yx}}^T. \tag{5.54}$$

In conclusion, once estimated the final grid of gravity disturbances, in order to obtain the complete signal, all the frequencies removed before the Least Square Collocation adjustment can be restored back.

Chapter 6

Developed software suite for aerogravimetry

The implementation of a complete software for airborne gravity data processing, within this research project, was the principal topic to deal with. In fact, besides the definition of an innovative processing methodology for aerogravimetry, the software development, with the integration of the presented algorithms, occupied a major part of the whole project.

To do so, basically each phase of the proposed procedure has been implemented within a module, which can be run independently from all the other ones. This organization is justified by the fact that our purpose was the development of a flexible solution, in which the user has the possibility to analyze the actual results obtained within each step, for a deepen comprehension of the whole processing. Each single module has been firstly realized in a prototype version in Matlab language and then it has been converted in parallel C language. The Matlab language, or more in general, the Matlab programming environment has the advantage to be especially thought for mathematical operations on matrices and vectors; moreover, it is optimized for interaction with graphical outputs (see *https://www.mathworks.com/help/matlab/index.html*) thus facilitating the refinement of the various algorithms. However, being a proprietary programming language, we decided to move toward C programming language to remove the constrain of a software strictly related to an environment which requires a license and to improve the performances in terms of computational times of the final software.

This chapter has been thought to introduce the general features of the realized software. First of all, Section 6.1 is meant to introduce the state of the art of the available software for airborne gravimetry data processing. Section 6.2 presents the architecture of our solution and the following Sections from 6.3 to 6.9 are dedicated to the characteristics and functionalities of each single implemented module.

6.1 State of the art

The modeling of gravity field at regional and local scale for geophysical applications, such as resources exploration, is nowadays generally performed by means of proprietary software provided by those companies that do the aerogravimetric surveys. Within this field of application, the standard airborne gravity data delivered to the users are in general not only the "raw" acquired data, but the products resulting from a processing made by means of proprietary software. These products are always given with the relative report describing the main features of the processing procedure adopted, however a detailed definition of the algorithms implemented is usually unknown.

One of the leading companies in resources exploration, i.e. Sanders Geophysics Ltd, has developed for airborne gravity data an ad hoc system, called AirGrav. This system is based on a combination of inertial technology and Differential GPS (DGPS) mounted on a stabilized platform. Apart from the instrumentation, they developed also a specialized software for processing their acquired airborne gravity data. This proprietary software is capable of deriving grids of free-air gravity as well as Bouguer gravity with formal accuracies around 0.5 $mGal$ or below, depending on survey parameters, such as line spacing and aircraft speed, as well as the details of the specific filter used [58]. However, as stated before, being a proprietary software, a detailed definition of the algorithms implemented is unknown and the formal accuracies reported can not be easily verified.

About scientific software, developed by research institutes and commonly adopted for gravity data processing, one of the most known is probably GRAVSOFT. This software is basically a suite of Fortran programs with a Python interface for regional and local gravity field modeling, e.g. geoid determination, determination of the deflections of the vertical and recovery of gravity anomalies from satellite altimetry [25]. It has been developed since the early 1970's from various research institutes such as Geodetic Institute, National Survey and Cadastre of Denmark and the Geophysical Institute (now Geophysics Dept. of the Niels Bohr Institute) at University of Copenhagen. The GRAVSOFT package consents to do basic operations of physical geodesy (i.e. spherical harmonics, interpolation and gridding, terrain prism integration, Fourier methods and least-squares collocation), and do basic arithmetic and handling of data files, either in

point formats or grids (i.e. selection and reformatting of data, filtering of along-track data). Within the present research some of the implemented modules, such as the terrain correction one, have been tested comparing the final accuracies with respect to those obtained from GRAVSOFT.

Other programs available from the scientific community are GRADJ and the open-source Python toolkit "Fatiando a Terra" which have not been investigated within the present work since the former is not applicable to airborne gravimetry but is used only for static gravimetry and the latter only contains some useful tools for modeling and geophysical data analysis but not a complete set of modules for the whole aerogravimetry processing procedure [74].

About the spherical harmonics, this particular kind of functions are used for a great variety of applications in geodesy and geophysics so different software are available for generating and manipulating them. One of these software is SHTOOLS which is an archive of Fortran 95 and Python software that can be used to perform spherical harmonic transforms and reconstructions, rotations of data expressed in spherical harmonics, and multi taper spectral analysis on the sphere. Another tool for spherical harmonics synthesis, that is worth to be mentioned, is the one provided by the International Center for Global Gravity Field Models (ICGEM) which is one of five services coordinated by the International Gravity Field Service (IGFS) of the International Association of Geodesy (IAG). The ICGEM wesite (*http://icgem.gfz-potsdam.de/calc*) in fact, provides a web-based service for calculating different functionals of the gravity field models using spherical harmonics synthesis [4].

Regarding the terrain correction topic, which is the computation of the vertical attraction due to topographic masses, it is nowadays still a research topic. It represents an important step in geodetic and geophyisical applications: it is required in high precision geoid estimation by means of the remove-restore technique and it is used to isolate the gravitational effect of anomalous masses in geophysical exploration. Because of the increasing resolution of recently developed digital terrain models, the increasing number of available observations and the increasing accuracies of gravity data, various software have been developed in recent years to face this major issue. For instance "Tesseroids" is an open-source software, that consists in a set of command-line programs to perform the forward modeling of gravitational field in spherical coordinates [73]. It is implemented in the C programming language and uses tesseroids (spherical prisms) for the discretization of the subsurface mass distribution. To calculate the gravitational fields of tesseroids the Gauss-Legendre Quadrature formula is used to evaluate them numerically. Another software is the one developed by [23] which uses for the representation of topographic masses prisms with a polygonal base, in particular triangles, dividing each grid cell into two parts (see Fig. 6.1). However, apart from these programs that have been used to validate our terrain correction

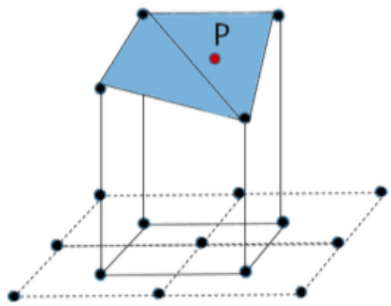

Figure 6.1: Triangular polyhedrons for the representation of topographic masses

module, various software are available to compute the gravitational terrain effect using both numerical and analytical solutions as reported in [56].

6.2 Software architecture

To be able to develop a suitable software for airborne gravimetry, especially thought for resources exploration applications, a fundamental step has been the identification of the main input/output of interest, not only in term of the whole procedure but also within each step. In particular, for designing the software architecture, the characteristics of all the data need to be clearly defined: from the data file format to the file formatting and their expected dimensions. From the consideration of all these aspects it has been possible to define firstly a prototype version in Matlab programming language and then an optimized version of the whole code in C programming language.

Due to the complexity of the processing procedure which can be set in different way, i.e. some parameters can assume different values, depending generally on the input data or the output requirements, the software system has been developed as a suite of independent elements/modules. Moreover, considering the dimension of input data and analyzing the consequent computational times, it has been decided to optimize some parts of the software with the adoption of ad hoc libraries to parallelize the processes. A schematic representation of the developed software architecture is shown in Fig. 6.2.

In terms of high level structures of the software system, it can be noticed that the whole processing procedure has been organized depending on six main theoretical topics:

- the GNSS variometric module
- the gravimeter processing module
- the harmonic synthesis module
- the terrain correction module
- the filtering module
- the gridding module

Some of these modules have been in turn organized in other sub-modules, presented in more details in the following sections. It can be noticed that some processes have been implemented simply combining other modules, e.g. the remove and restore modules are essentially a combination of the spherical harmonic module and the terrain correction one.

As shown in Fig. 6.2, the global structure of the software is composed of a three parts. The first part is dedicated to the phase we identified as the preprocessing of airborne gravity observations, in which the raw acquired GNSS and gravimeter data are manipulated to estimate the raw observed gravity disturbances. The accelerations from GNSS, output of the GNSS variometric module, and the acceleration sensed from the gravimeter, output of the gravimeter processing module, are summed up to obtain the gravity disturbances. The second part is the one focused on the harmonic synthesis of global gravity models and the terrain correction evaluation. From the GGM coefficients is possible to synthesize, on grids or sparse points, the gravity disturbances. At this output the terrain correction is added to improve the information about the high frequencies of the gravity signal. It can be noticed that this part, without the addition of airborne gravity data can be as well used to predict gravity disturbances, obviously with a reduced resolution and accuracy depending on the GGM chosen. The third part regards all the procedure, we called processing of airborne gravity disturbances. It includes all the steps, described in Chapter 5, of the remove-compute-restore method. In this phase the observed gravity disturbances are basically reduced, filtered (to remove the observation noise), gridded using LSC and finally restored, obtaining the final predicted grids or sparse points of gravity disturbances with their corresponding prediction errors.

6.3 GNSS variometric module

The GNSS variometric module implements the algorithms presented in Chapter 4 related to the GNSS observations. It works line by line, processing the GNSS observations of single aircraft track. This is possible since the raw acquired

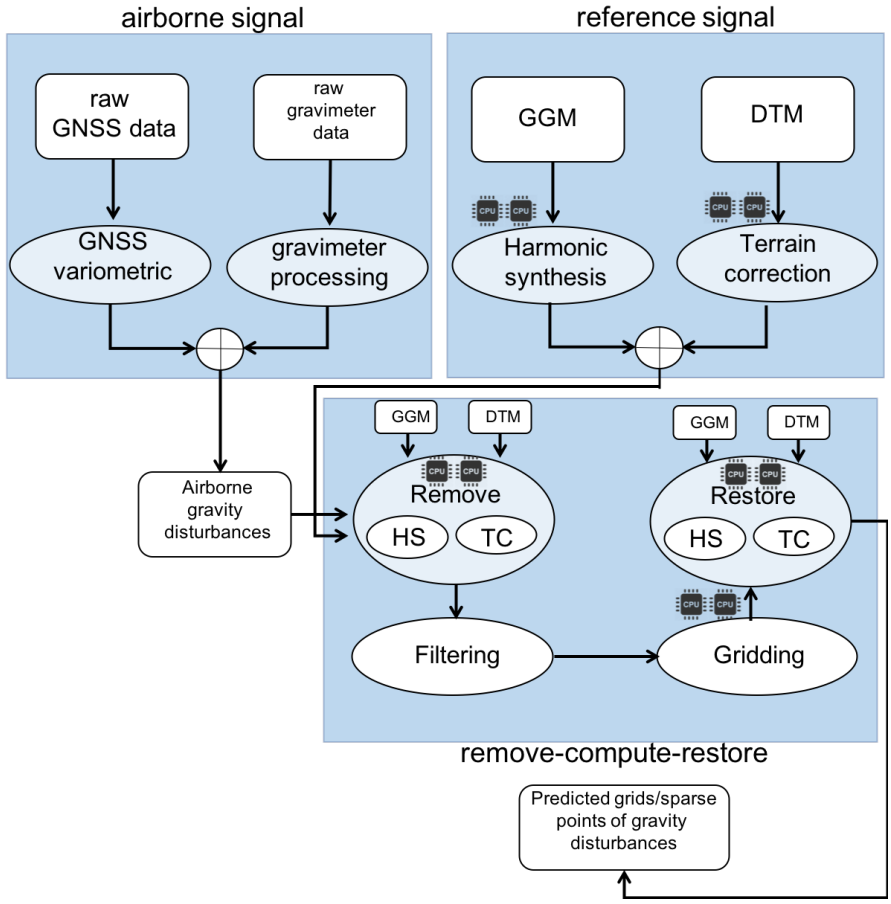

Figure 6.2: Developed software architecture

data provided by the company who made the survey, generally include also an information about the flight lines (identified by an unique index). The start and end points of a flight line do not include the trajectory curvatures.

In this module an automatic procedure to search and recognize the interest RINEX observation file has been implemented, as well as a procedure to automatically download the RINEX navigational files (if not available in the data folder). Once identified and loaded the file containing the observations related to the interested epochs (start and end epochs of the considered flight line), the pre-processing of GNSS data starts: firstly, the cycle slips affecting the GNSS

observations are detected and fixed and the satellite positions as well as the approximated receiver position are estimated. Then, the available satellites for each epoch are identified and used to compute the accelerations using LS. In conclusion a final downsampling by means of spline functions is performed to optimally combine these accelerations with the one derived from the gravimeter processing. A schematic representation is shown in Fig. 6.3.

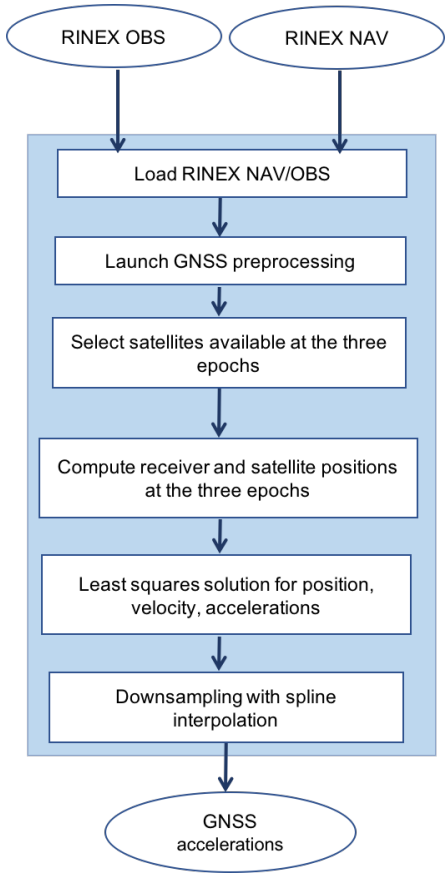

Figure 6.3: Schematic representation of the GNSS module

One of the principal issue to be addressed within this module was the definition of a procedure to manipulate in an efficient way the big RINEX data of an aerogravimetric flight. Considering that for a two days survey, about 10 RINEX observation files are needed (each one of few GB), it is clear that an optimal

way to import the relevant data was mandatory. The proposed method consents two options, depending on the hardware machine characteristics on which the software is running. The first procedure, adopted if on the working PC it is not possible to import the whole RINEX file, consists basically in cutting the original RINEX file only on the interested observation epochs, generating in this way a RINEX file of few hundreds of MB, that can be easily manipulated and imported in almost all PC. The second method consists in importing in memory all at once the full RINEX. In this way the direct access to the interested observations is quite fast and in terms of computational times there are also great advantages since it is not necessary anymore to read various time the same RINEX file (which can contains the epochs of different tracks) and to cut it to write every time a new file.

6.4 Gravimeter processing module

The gravimeter processing module regards the manipulation of gravimeter raw observations. The schematic representation of this module is presented in Fig. 6.4.

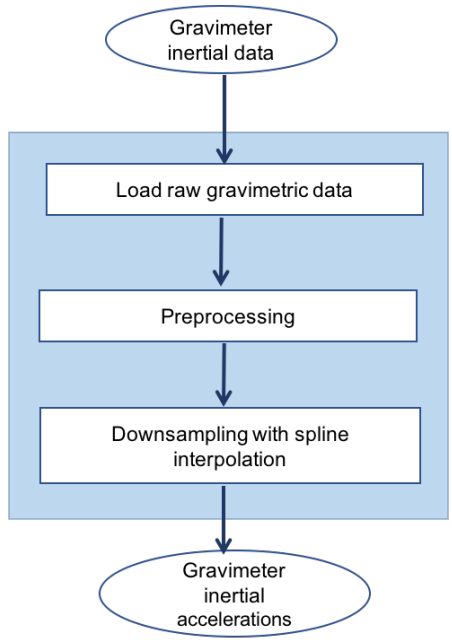

Figure 6.4: Schematic representation of the gravimeter processing module

An automatic procedure also for this step has been define to import the interesting observation file by means of the interpretation of the input file name. Once loaded the observation data, the core part of this module is the computation of the Eötvös and Lever arm effects, necessary to correct the inertial input data. Moreover, since the sampling rate of GNSS and gravimeter observations are generally extremely different (from $10 - 20\ Hz$ for GNSS data to 128 Hz for gravimeter data), a downsampling is required to reduce the gravimeter data to a sampling rate similar to the one of the GNSS. This is done by means of spline interpolation.

6.5 Spherical harmonic module

The spherical harmonic module is a toolbox that can be used to compute different functionals of the anomalous potential T, namely derivatives up to order 2 can be synthesized. To run it, a setup file is required, in which all the input data are reported as well as all the parameters that serves to specify the kind of input and output (grid or sparse points), the functional to be computed or the general parameter for the ellipsoid and the spherical harmonic model. The various functionals of the anomalous potential that can be computed are reported in Table 6.1, where the subscripts θ, λ and r stands for the colatitude $\theta = 90 - \varphi$, longitude and radius respectively; the subscripts e, n, u instead stands for East, Nord, Up. Note that the Up direction coincides with the radial one.

Due to the possibility to compute various functionals of the anomalous potential with the same combination of order/type parameters, it was possible to optimize the computational times by parallelizing the synthesis of different functionals.

Order	Type	Outputs
0	0	T
0	2	N
1	0	T_θ - T_λ - T_r
1	1	T_e - T_n - T_u
1	2	δg
2	0	$T_{\lambda\lambda}$ - $T_{\lambda\theta}$ - $T_{\lambda r}$ - $T_{\theta\theta}$ - $T_{\theta r}$ - T_{rr}
2	1	T_{ee} - T_{en} - T_{eu} - T_{nn} - T_{nu} - T_{uu}
2	3	T_{rr}
3	3	T_{rrr}

Table 6.1: Output reference table of the spherical harmonic module

6.6 Terrain correction module

The Terrain correction module is used to compute the gravity terrain effect. This module has been developed in order to guarantee high accuracy and fast computational times and it is based on a combination of classical prisms modeling and FFT techniques. It allows the user to compute not only the gravity effect of topography and bathymetric masses but also those due to sedimentary layers or to the Earth's crust-mantle discontinuity (the so called Moho). The basic version of this module works in planar approximation [56]. However an improved version in spherical approximation and with a multiresolution approach has already been developed.

To compute the gravity effect, basically the computation is split between a planar and a spherical correction term. The former is evaluated by means of the hybrid algorithm (prisms+FFT), the latter is numerically computed, discretizing the integral related to the corresponding correction term. The idea of a combined algorithm for the planar term derived on the one hand from the consideration that pure prisms, for high resolution DTMs (nowadays wide spread), can be very time consuming and not efficient. On the other hand, from the fact that the pure FFT methods generally present, for points close to the DTM surface, reduced accuracy and a non convergence of convolution integrals. Within the implemented terrain correction module, various settings have been defined to allow the user to change the dimension of the inner domain (in which the pure prisms are adopted), depending on accuracy and computational times required. Since FFT method works on grids it appears clear that if the inner domain is small, the computation is extremely fast, loosing in accuracy; on the contrary, more bigger is the inner domain and more accurate (but slow) will be the computation.

The planar term of the gravity effect of bathymetric, sedimentary and mantle masses is computed with the same procedure, described in the following, suitably changing the density constants. In case of bathymetry, considering the schematic representation of Fig. 6.5, we can consider that the effect of the water (the body B_w) can be expressed as:

$$\delta(\rho_w|B_w) = \delta(\rho_w|B_0) - \delta(\rho_w|B_r) \tag{6.1}$$

with ρ_w the water density, B_0 the prism obtained from the union of B_r and B_w. So the planar terrain correction for all those masses, excluded topography, can be evaluated computing the effect of the big prism B_0 and removing to it the effect of the body B_r computed at height $H = H_0 + \overline{H}$. For sediments, this algorithm have to be applied twice, once for the lower and once for the upper surface of sediments.

The multiresolution approach consents to enlarge the region in which the

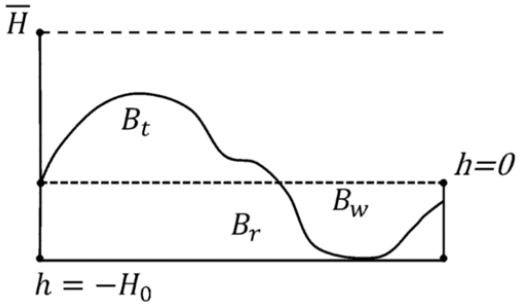

Figure 6.5: Bathymetry representation for terrain correction computation

terrain correction is computed without heavily influence the computational times. With this approach in fact, the terrain correction is first evaluated for the high resolution DTM and then it is computed for an outer domain, created from the original DTM applying a moving average to smooth, which has zeros in correspondence of the original high resolution terrain model. The two effects are in conclusion summed up.

As for the spherical harmonic module, a setup file contains all the informations about input files and parameters to be set before launch the computation. The schematic representation of the processing procedure is shown in Fig. 6.6. The processing scheme shows the standard operation performed for each single type of mass (i.e. topography, bathymetric, sedimentary and mantle masses) and in the end the various contributions are simply summed up to obtain the complete terrain correction.

6.7 Filtering module

The filtering module consents to filter the observed gravity disturbances and to remove almost all the observation noise, improving drastically the S/N ratio. The schematic representation of the filtering module is reported in Fig. 6.7. For the application of the Wiener filter along track the first step is the creation of a reference signal, given by the sum of the gravity disturbances derived from GGM and from a residual terrain correction. So this first step basically consists in exploiting the spherical harmonic module and the terrain correction one. This last one in particular is actually used twice to compute the residual terrain correction. The following step is the reduction of this reference signal, with the removal of the same frequencies removed from the observed signal with the remove/restore module.

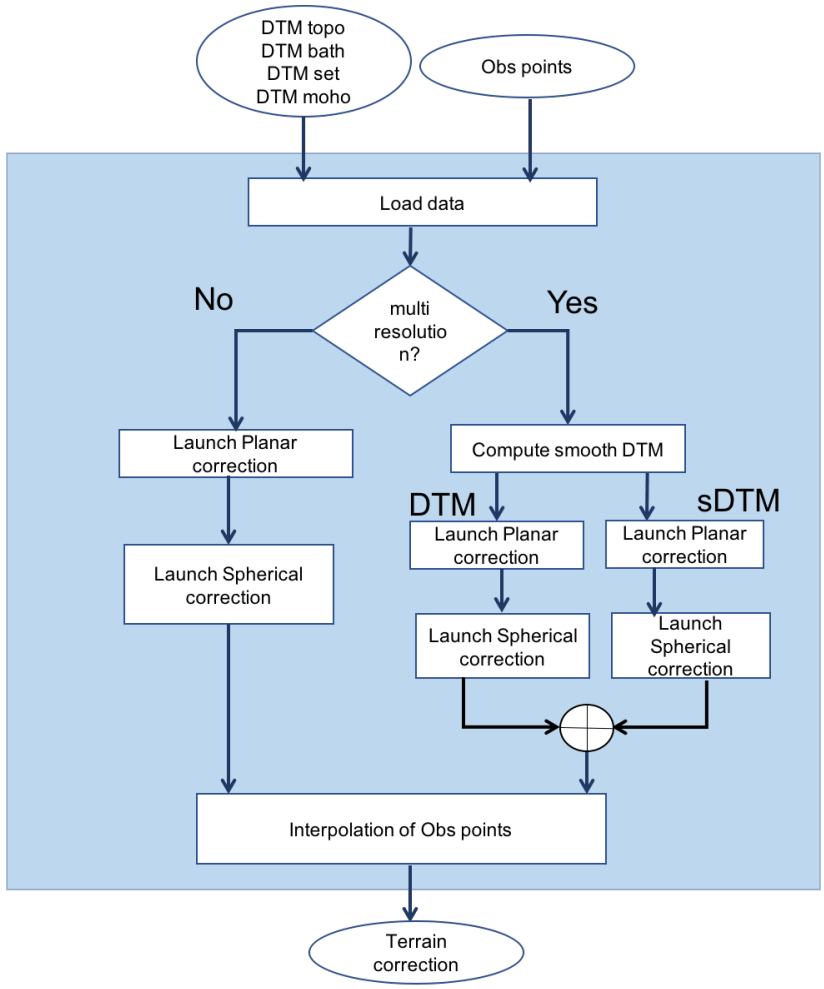

Figure 6.6: Schematic representation of the Terrain correction module

Now, working with reduced signals, the power spectral densities are computed and finally used to generate the filter which has to be applied. The filtering operation is performed along each single flight track so the filter is clearly regenerated every time a new track begins.

The filtering module too requires a setup file in input and returns in output the filtered gravity signal.

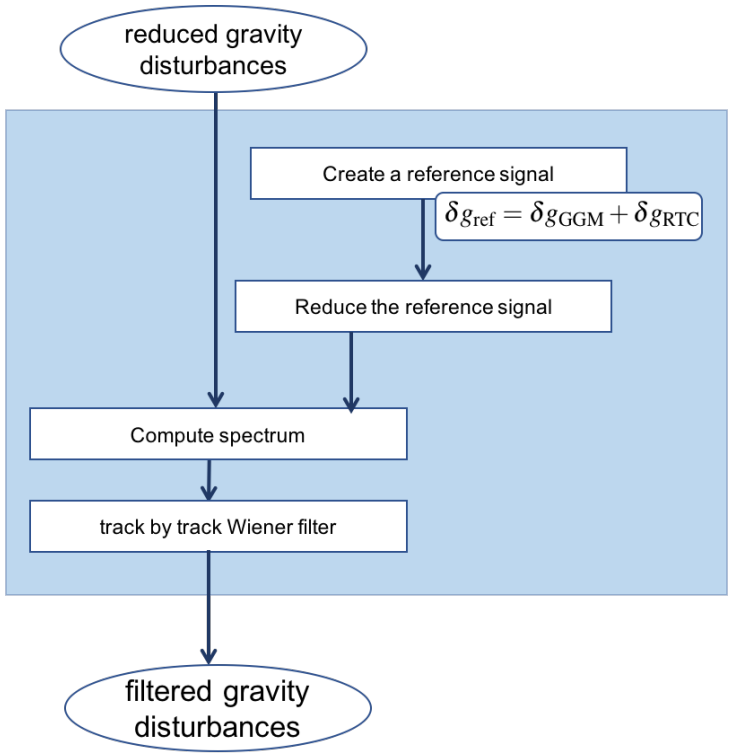

Figure 6.7: Schematic representation of the filtering module

6.7.1 Advanced filtering module

The advanced filtering module is the module for the crossover analysis. This is used to evaluate the stochastic characteristics of the observation error. It is a command line toolbox, that given in input the filtered signal, returns the empirical covariance function of the observation error. To perform the crossovers analysis, as shown in Fig. 6.8, the first step consists in interpolating the flight lines as straight lines. Then an automatic procedure has been implemented to identify and distinguish the two different kinds of flight track (control and tie lines). This operation is necessary for the identification of the crossover points. Once obtained all the crossovers the residuals of gravity disturbances are evaluated and they are used to empirically compute the error covariance along track. Since different tracks have slightly different empirical covariance functions, they are averaged to obtain the final empirical covariance function of the observation error.

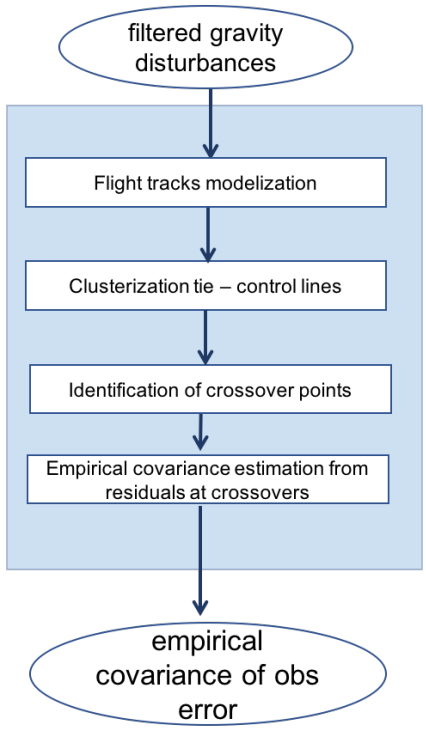

Figure 6.8: Schematic representation of the advanced filtering module

To perform the theoretical covariance function robust estimate another toolbox developed and included in the utilities group of toolboxes (described in the last section of this chapter) has been used.

6.8 Gridding module

The gridding module finally perform the LSC solution. To do so the covariance matrices of both the signal and the observation error are first derived and then used for the estimate. They are computed once known the theoretical covariance functions of both the signal and the observation error. This step is performed by means of a toolbox developed and included in the group of utilities summarized in the next section. Once computed the covariance matrices, applying the formulas reported in Chapter 5, the prediction of grids (or sparse points) with their corresponding errors are estimated and returned as output of the module.

This module can be run with a proper setup file in which are stored all the useful information for a correct computation.

6.9 Utilities

A part from all the modules presented, it has to be mentioned that a set of utilities toolboxes has been implemented too. These tools are all command line tools, easy to use. In particular:

- the *mapping toolbox* to convert data (grids or sparse points) from geodetic coordinates to local Cartesian coordinates and vice versa;
- the *smoothing toolbox* to manipulate and smooth DTMs applying a moving average;
- the *converter from grids to sparse points*, since depending on the applications data can be required in sparse points format instead of grids;
- the *remove and restore toolbox* which can be used to perform both the removal of know signals from the observed gravity disturbances and the restore of these signals once completed the prediction/gridding; it is basically a combination of the spherical harmonic synthesis module, used to synthesize the GGM and derive the low frequencies of the gravity signal, and the terrain correction module, to evaluate the medium high frequencies due to topographic masses.
- a *toolbox to perform a linear combination of grids*;
- the *empirical covariance toolbox* that can be used to estimate the empirical covariance function of a generic signal;
- the *theoretical covariance toolbox* which consents to the user to model the empirical covariance function of generic signal, choosing among three different models; depending on the input parameter set by the user it is possible to model the empirical covariance function with a classical exponential model, a Gaussian model or a linear combination of Bessel function of first order.

Chapter 7

The VIKING approach applied to real aerogravimetric data

In order to evaluate the performances of the whole VIKING software various numerical tests have been performed. In this chapter the results obtained from the processing of data coming from a real airborne gravity survey will be presented. The dataset used, has been acquired in 2014-2015 by one of the major operator providing airborne geophysical surveys for petroleum and mineral exploration, under commitment of Eni S.p.A.. For this reason, to preserve confidentiality, all the plots shown within this chapter do not present any information about the actual coordinates of surveyed area. However it is important to underline that the results presented have not been modified, representing the actual output of the VIKING processing procedure.

The tests performed are focused on the analysis of the optimal choice of some parameters involved in the computation of the final predicted values of gravity disturbances. Moreover they are aimed to evaluate the whole precessing procedure in terms of accuracy and computational times.

In Section 7.1, a brief description of the survey will be reported as well as its principal characteristics. An analysis of the optimal time interval to be chosen to compute the double differences in time from GNSS data (to derive the accelerations) will be presented in Section 7.2. Furthermore, the advantages of

a multi-constellation approach as well as some consideration on the effect of the choice of the L_{cut} parameter on the estimate of the final predicted gravity disturbances will be reported in Sections 7.3 and 7.4 respectively. In Section 7.5 instead the effect of various downsampling factors on the final collocation estimate will be analized.

At the end of the chapter, in Section 7.6, each step of the VIKING procedure will be described and the final predicted gravity disturbances with their associated prediction error will be shown.

7.1 Survey specifications

The real airborne gravity survey used to test the VIKING software has been conducted by one of the major operator providing airborne geophysical surveys between 2014-2015. As typical for airborne acquisitions for oil and gas exploration, the survey covered an area of about $1^\circ \times 1^\circ$, corresponding to about 100×100 km^2. The investigated area is entirely offshore however the coastal region immediately in proximity of the survey block had to be considered when processing the acquired data.

For the airborne navigation system, the operator used a multi-frequency GNSS receiver that recorded GNSS positional data at 20 Hz.

The inertial measurement system used is characterized by an inertial platform, which remain fixed in inertial space, independently from the manoeuvres of the aircraft, allowing precise correction of the effects of the vehicle movements. Inertial accelerations are recorded at 128 Hz.

The whole aerogravimetric survey required a total of 9 flights to complete around 5000 line km (of a complete duration of about 30 hours). During this survey 93 flight lines were flown, divided in 84 traverse lines and 11 control lines. The former type have a line spacing of about 1.500 m. The latter are spaced about 7000 m. The flight trajectory, planned taking into account the expected terrain and the performance of the aircraft at the altitudes to be encountered, was flown at averaged flying speed of about 50 ms^{-1} at averaged altitude of 150 m above sea level. The planned survey lines are illustrated in Fig. 7.1.

The GNSS data acquired during the 9 flights consist in 10 RINEX observation files (around 20 GB of ASCII file) and their corresponding RINEX navigational files. The gravimeter data consist in 9 ASCII files (each one of about 500 kB).

A local gravity value was established at the nearest airport and all flights were referenced to that value. The measuring system was calibrated to the departure point, determining its offset with respect the closest known gravity point of the area. An alignment of the system was performed prior to every flight. This offset was used also to verify the operation of the system before and after each flight.

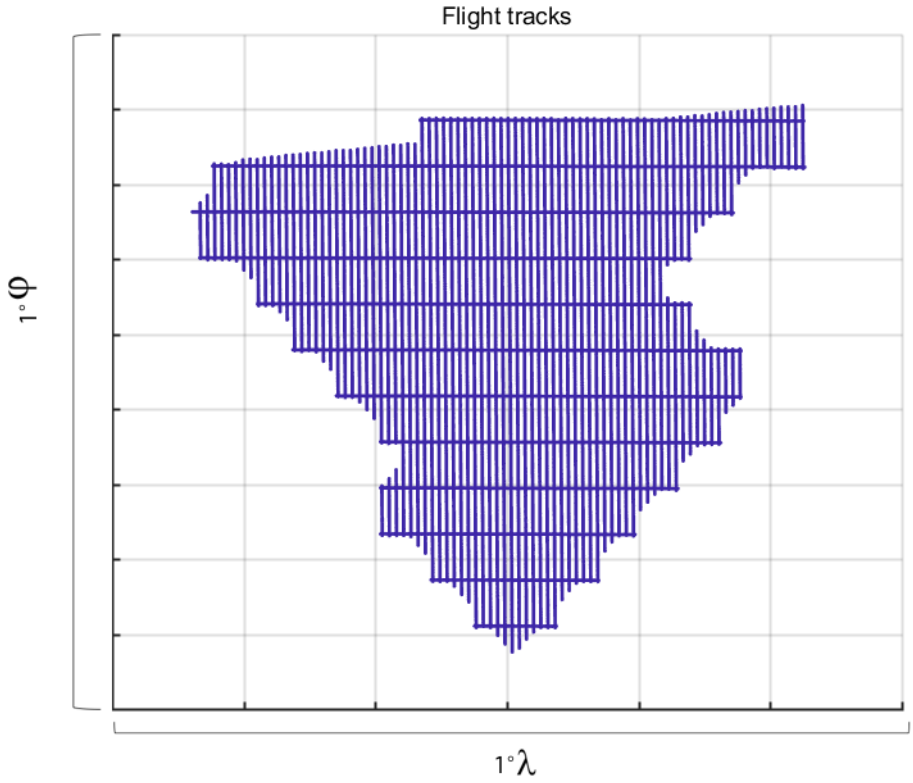

Figure 7.1: Flight lines map

7.2 Test on the optimal time step for GNSS acceleration estimation

The raw GNSS data (RINEX observation and navigational files) have been processed with the GNSS variometric module to derive the GNSS accelerations by means of the application of the variometric method. As presented in the previous chapters the GNSS accelerations are essentially derived from a double differentiation in time between consecutive epochs. The time step τ, defined in Sec 4.1, to be chosen for the selection of three epochs, has been here investigated. This parameter in fact, has to be carefully chosen, taking into account the aircraft flight speed, the GNSS data sampling rate and the desired spatial resolution. In order

to calibrate this parameter we considered 1 hour observations of a ground station close to the surveyed area. Since the station does not move, Eq. 3.3 simply reads:

$$\underline{f} = -\underline{g} \tag{7.1}$$

which of course implys $\underline{\ddot{x}} = 0$. In other words the use of a ground station basically consents to directly estimate the error associated to the GNSS derived accelerations.

Different GNSS accelerations have been estimated varying the time step parameter and the power spectra of the derived accelerations (in the z-direction) have been analyzed. The Fig. 7.2 shows the power spectra of the GNSS accelerations (in the z-direction) derived using different τ. The x-axis corresponds to wavelengths in km and the legend reports the spatial resolution, chosen a certain time step, considered an averaged flight speed of 50 ms^{-1} and a sampling rate for GNSS observations of 20 Hz. For example, a time step τ equal to 5 epochs corresponds to a spatial resolution of:

$$\text{spatial resolution} = \frac{5}{20}\ \text{s} \cdot 50\ \frac{\text{m}}{\text{s}} = 12.5\ \text{m}. \tag{7.2}$$

Considering that for the low frequencies, i.e. for the wavelengths longer than those implicitly defined by L_{cut} (e.g. wavelengths $\geq 80\ km$), the gravity signal is essentially replaced by the Wiener filter with information derived from the GGM, these wavelengths have not been taken into account in the following analysis. For the medium-high frequencies, Fig. 7.2 demonstrates that a time step interval of 20 epochs, which corresponds to 1 s (i.e. a spatial distance of 50 m), performs better than other values. The lowest spectra, corresponding to a time step of 500 and 5000 epochs (i.e. 25 and 250 s or 375 and 12500 m in terms of spatial resolution), in fact do not guarantee the assumptions made for the application of the variometric algorithm and moreover, reduce at high frequencies, the amplitude of the power spectra of the signal too. For wavelengths greater than 30 km, the 20 epochs time step ($\sim 50\ m$) is the lowest one, performing better than all the others steps. Note that actually the contribution in high frequencies is quite similar for time steps varying from 20 to 100 epochs (i.e. 1 to 5 s or 100 m to 500 m), however, in order to maximize the high frequency content of the signal, the first value was chosen as the most suitable one.

It should be observed that these spectra (functions of τ), depicted in Fig. 7.2, behave in this way because from the one hand, the increasing of τ will basically improve the accuracy (it can be seen from Eq. 4.16 that $\ddot{x} \simeq \frac{\Delta\varphi}{\Delta\tau^2}$) but on the other hand, it will lead all the assumptions done in deriving Eq. 4.16, to be not verified anymore (for instance the hypothesis that $\underline{\tilde{e}}^s_{t+\frac{\tau}{2}} = \frac{\underline{\tilde{e}}^s_{t+\tau} + \underline{\tilde{e}}^s_t}{2}$).

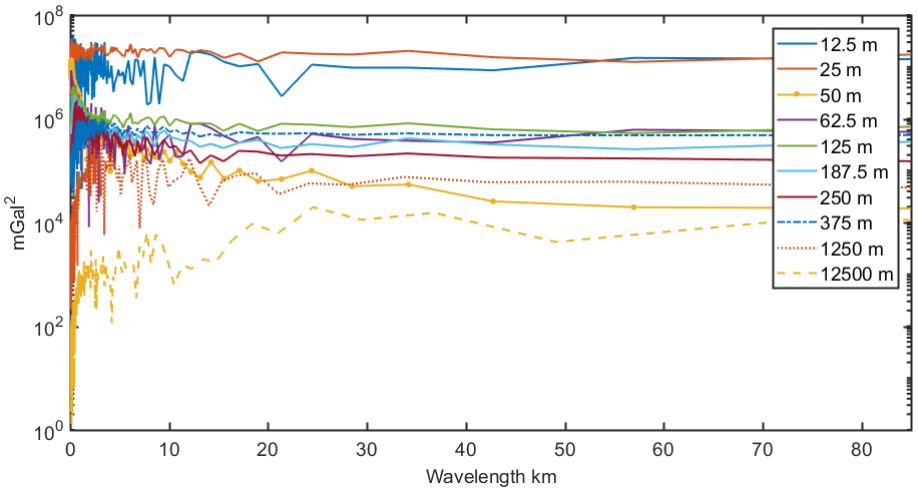

Figure 7.2: Power spectra of GNSS accelerations in z-direction estimated with different time step interval

7.3 Test on the GNSS multi-constellation approach

In last decades, the continuous increase of available GNSS satellites constellations have led to an improvement in navigational applications. Nowadays in fact, all the orbiting GNSS satellites consent to achieve high position accuracies thanks to the increased number of available satellites, compared to GPS-only positioning. The use of multiple GNSS constellations in fact improves the success rate of positioning, by receiving a higher number of satellite signals even in harsh environments (i.e. urban canyon), and it improves also the robustness against interferences, by using different frequency bands.

Within the developed methodology, it was decided to adopt this approach to estimate the GNSS accelerations. The implemented algorithms allow the user to select satellites of different constellations, e.g. GPS, GLONASS and Beidou. Different combinations have been tested and the results are presented here in the following. To evaluate the advantages in the estimation of the GNSS accelerations of the multi-constellation approach, the same ground station used for the previous test has been chosen and 1 hour dataset has been processed. As seen in the previous section, since the accelerations of a ground fixed station should be zero, it was possible to evaluate the performances of the various tested configurations and consequently to drawn some considerations from the obtained results.

Table 7.1 shows the standard deviations of the estimated accelerations derived

from different combinations of GNSS satellites. From these statistics it can be noticed how the combination of more than one GNSS constellation clearly improves the estimates. This is a consequence of the fact that, as stated before, the increasing number of available satellites improve the geometry of the problem. However, note also that in these tests the GPS plus Beidou combination performs better with respect to the GPS plus GLONASS combination (and with respect to the GPS+GLONASS+Beidou combination too). This effect can be explained considering the two following aspects. First of all, the improvements in the geometry of the system seems "to go to saturation", once reached a certain number of available satellites. Furthermore, the different observation errors, if not properly tackled, appear to degrade the final result. Different GNSS constellations in fact probably present a different error, that, within our computations, has not been considered. Looking at the standard deviations obtained from our tests, the observation errors of GPS and Beidou constellations results more similar and in general smaller than those of GLONASS constellation.

GNSS combination	STD $[ms^{-2}]$
GPS	$1.229 \cdot 10^{-5}$
GPS+GLO	$1.173 \cdot 10^{-5}$
GPS+BEI	$8.751 \cdot 10^{-6}$
GPS+GLO+BEI	$1.051 \cdot 10^{-5}$

Table 7.1: Standard deviations of accelerations derived from different combination of GNSS constellation for one hour data of a ground permanent station

From these considerations, we decided to use for our computations the GPS and Beidou combination, leaving the problem of the estimate of the optimal weights to combine different systems to future developments. A plot of the derived accelerations in the z-direction for the test station is shown in Fig. 7.3. In details, the green line is the vertical acceleration estimated from GPS-only observations and the red one is the vertical acceleration from GPS+Beidou observations. The advantage of the multi-constellation approach is evident since the red values are almost always within the variation range of the green ones. Note that to compute the statistics reported in Table 7.1 these accelerations have been filtered, by the application of spline interpolation first and then of the convolution theorem in the frequency domain, to reduce the observation noise and enhance the valuable signal actually used for the final gravity acceleration estimation.

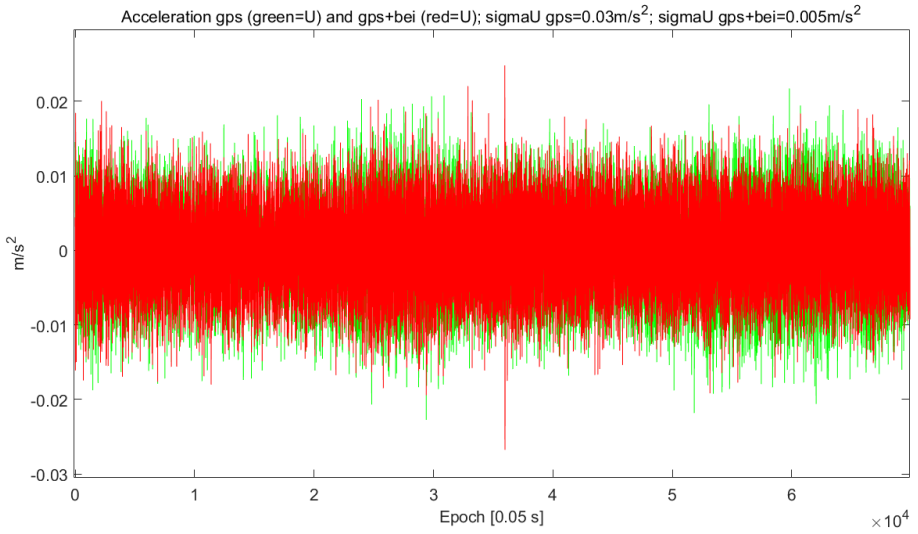

Figure 7.3: Comparison between accelerations in z-direction derived from GPS-only data (green) and GPS+Beidou data (red)

7.4 Test on L_{cut} for the gravity signal reduction

At the beginning of the processing procedure to filter and grid the aerogravimetric observations, there is the remove step, which consists in separating from the acquired data all the gravity signals that can be considered known. The first signal removed is basically the one derived from the GGMs. These models in fact, after the recent satellite gravity missions (i.e. GRACE and GOCE), are considered the most reliable representation of the Earth's gravity field, especially for the low frequencies component of the signal. Once removed this component, the medium-high frequencies signal is instead estimated from GGMs of the gravity effect of topography and it is removed too. The parameter that separates the low frequencies from the medium-high ones is L_{cut} (see Sec. 5.1). The proper choice of this parameter, as explained in Chapter 5, can be done by empirically fixing it on the basis of the formal error of the GGM or by estimating it as a function of the dimension of the investigated area.

Considering that the remove step is performed on both the observed and the reference signals, and that this last one is used to built the Wiener filter, it is interesting to understand how the L_{cut} parameter can potentially affect the filtered signal and consequently the resultant final predicted one. To investigate this effect different L_{cut} have been tested, analyzing the differences between predicted

gravity disturbances.

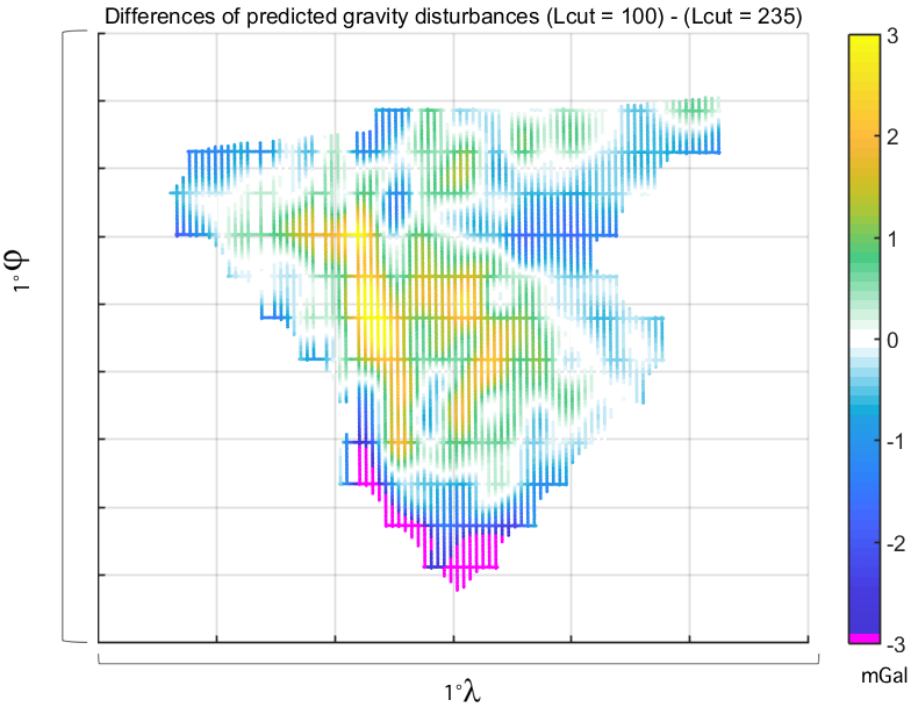

Figure 7.4: Differences of predicted gravity disturbances obtained using $L_{cut} = 100$ and $L_{cut} = 235$

Fig. 7.4 shows the difference between the along track predicted gravity disturbances derived using in one case an L_{cut} equal to 100 and in another case L_{cut} equal to 235, corresponding to wavelengths of 380 km and 160 km respectively (using Eq. 5.3). The standard deviation of these differences is 1.17 $mGal$. Neglecting the border effects, highlighted in purple, this figure however proves that L_{cut} has only minor effects on the final estimates. The choice of a lower L_{cut} is in general preferred since the higher L_{cut} (i.e. in this test 235) clearly includes not only a low frequency signal but also a medium-high frequency component, that in this way is basically taken away within the remove step. Using a small L_{cut} value, i.e. in this case 100, these medium-high frequencies are not replaced by the Wiener filter, leaving the Least Squares Collocation step to recover also this part of the signal from the airborne survey data. After the analysis of the results obtained within this test, we decided to use for our computations a value

for L_{cut} of 100.

7.5 Test on the along-track Least Squares Collocation solution

To predict grids or sparse points of gravity disturbances the Least Squares Collocation has been used. As exposed in Chapter 5, this method requires the manipulation of quite big matrices for the estimation of the predicted signal and its relative error. Eqs. 5.53 and 5.54 in fact show that the estimated signal can be computed by means of the product between two matrices, with one of them that has to be previously inverted.

For a real aerogravimetric dataset, the covariance matrices of the actual signal and of the observation noise (which have to be summed up and then inverted) result to be quite big, considering that the number of gravity disturbances observations can reach 800000. Furthermore, the cross-covariance matrix between the estimated signal and the actual signal, depending on the amount of prediction points, can be quite big too. Consequently, from the computational point of view, the inversion of these matrices is in general problematic, depending also on the available computational power of the working machine. The easiest solution, here implemented to deal with this kind of problem, is the downsampling of the observations which have to be used to build both the signal and noise covariance matrices. With the aim to analyze the effect of the downsampling on the predicted values of gravity disturbances, different downsampling factors (5, 10, 20, 50, 80, 100) have been tested and the errors with respect to the solution obtained using the smallest downsampling factor allowed by our working machine (i.e. 5) have been analyzed. The Fig. 7.5 shows the standard deviation of the differences between two Least Squares Collocation solutions, the first one performed using the downsampling factor indicated along the x-axis and the second one performed with a downsampling factor equal to 5. Analyzing this plot we can say that the error committed using a downsampling factor below 20 results to be always smaller than 1 $mGal$ (for example, with a downsampling factor equal to 20 the maximum error committed is $3\sigma = 3 \cdot 0.24 = 0.72\ mGal$). The plot shows, as expected, also that at the increase of the downsampling factor, the prediction deteriorates, with an error that exceeds the $mGal$ level.

The results obtained with this test suggest that the downsampling of the observation is not a problematic issue and it should be handled according to the available computational power and time.

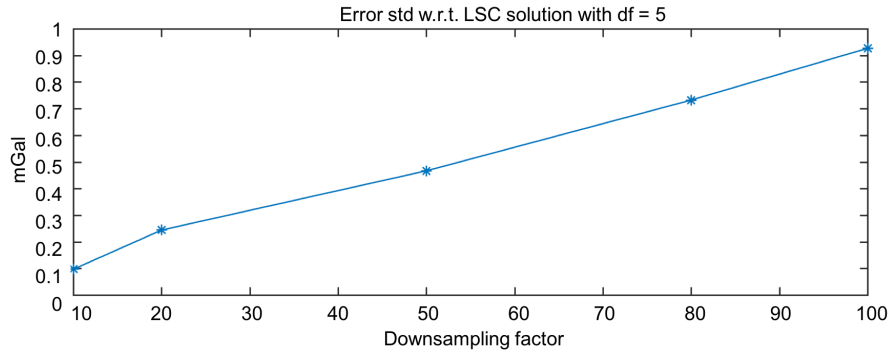

Figure 7.5: Error standard deviation with respect to the Least Squares Collocation predicted signal obtained using a downsampling factor of 5

7.6 Test of the VIKING software suite on a real aerogravimetric dataset

The complete set of algorithms presented in the previous Chapters have been tested on a real airborne acquisition performed in 2014-2015 by a contractor of Eni S.p.A.. The various computations have been performed on a single node of a super-computer equipped with two 8-cores Intel Haswell 2.40 GHz processors (for a total of 16 cores) with 128 GB RAM.

The along track raw gravity disturbances observations are computed by means of the variometric and the gravimeter processing modules. By the subtraction of GNSS derived aircraft accelerations from the inertial ones, applying the Eötvös and the lever arm correction terms and removing the normal gravity effect, the raw gravity disturbances are estimated. The Fig. 7.6 shows each term of Eq. 3.10 of a single flight track used to derive the raw gravity disturbances observations. Note that the gravimeter inertial accelerations and the GNSS ones are dominated by noise (being the order of magnitude of the accelerations of 10^4 $mGal$), even though they have already been downsampled and smoothed by means of splines interpolation. The complete dataset of raw gravity disturbances can be seen in Fig. 7.7. From this figure it can be noticed that the anomalous gravitational potential, in particular its functional the gravity disturbance, is largely dominated by noise (as expected). Moreover it can also be observed that the noise is characterized by both low and high frequencies components. This characteristic makes the filtering process a complex process. Note that, as stated in previous chapters, no a priori information on the stochastic properties of the observation noise are available.

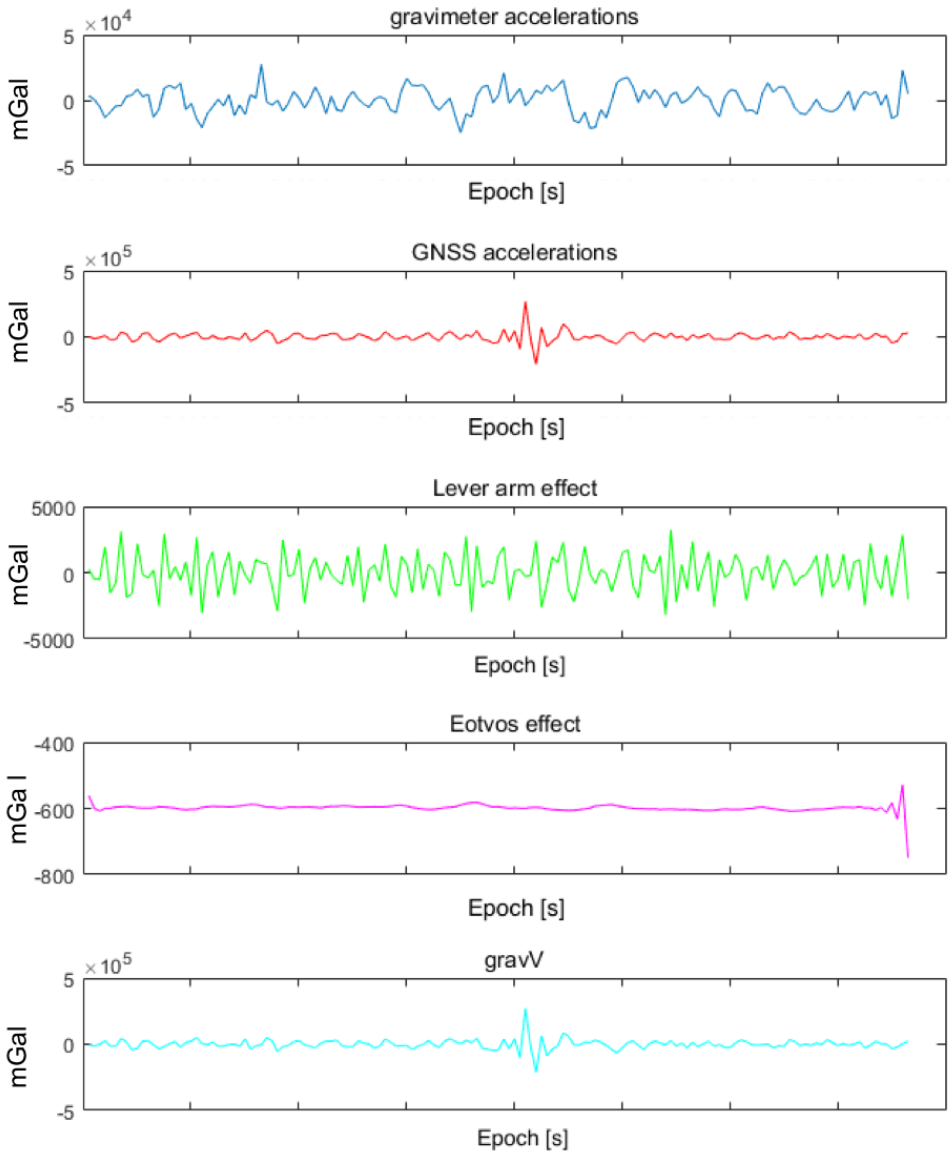

Figure 7.6: Sample of estimated parameters of a single flight track to derive the raw gravity disturbances within the VIKING pre-processing

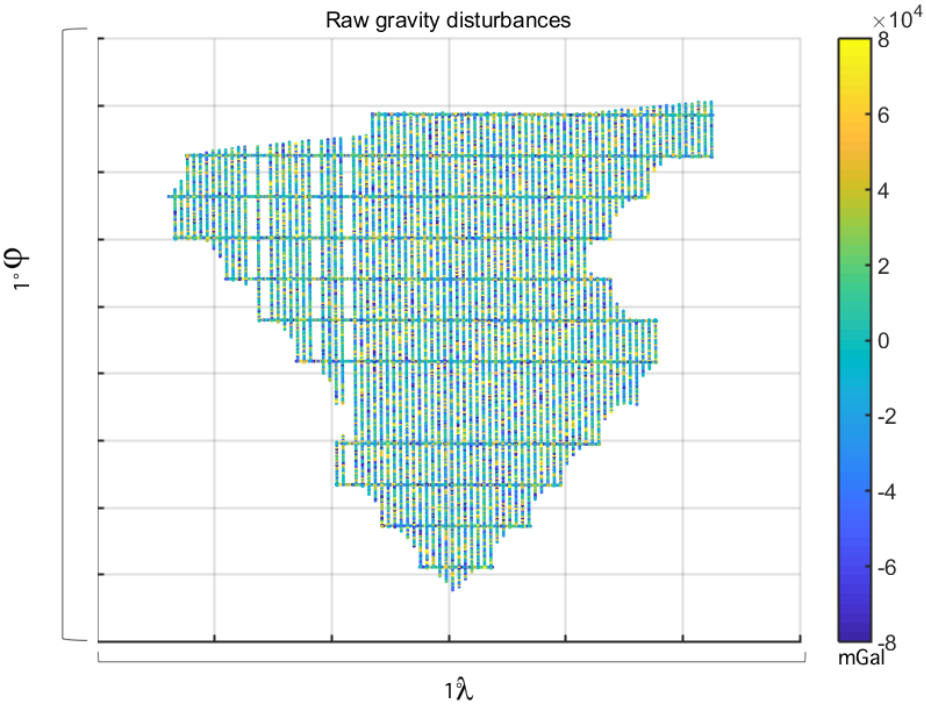

Figure 7.7: Along track raw gravity disturbances observations

As described in Chapter 5, the first step of the developed processing procedure consists in computing the reference signal on the whole set of observation points. This is done by applying the spherical harmonics synthesis to estimate the gravity disturbances from the chosen GGM and by adding to it a residual terrain correction. In this work the GGM used was the GECO model [20], up to its maximum degree/order (i.e. $L_{max} = 2190$). The synthesis has been performed by the spherical harmonics toolbox developed in parallel C language. The computation of this harmonic synthesis up to degree and order 2190 on the whole points (more than 800000 points) takes about 40 minutes, however the software is able to properly downsample the observations (according to the GGM maximum degree and the distance between two points on the same line) thus reducing the computational time up to 10 times on a HPC. For the residual terrain correction (RTC), the terrain correction module was used. In details, RTC has been computed as the difference between the full resolution DTM (we used etopo1 [2] with 1 $arc - minute$ resolution) and the smoothed DTM obtained by applying a moving average window of about 10 km. The etopo1 model has a resolution

of about 1.5 km which is acceptable for the present case study since the offshore investigated area has an averaged depth of about 2 km.

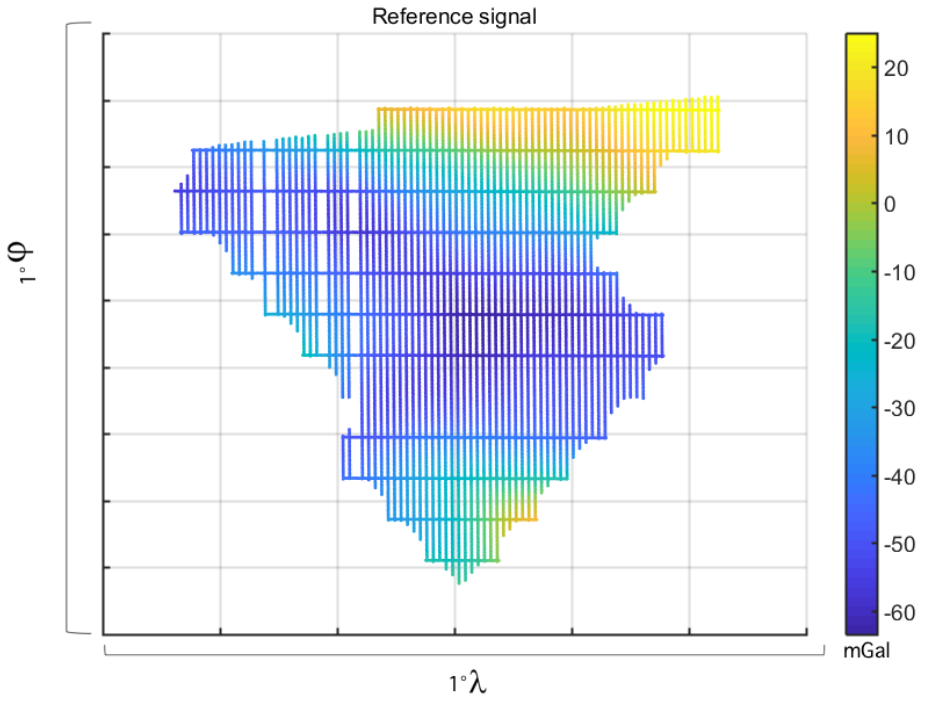

Figure 7.8: Along track reference gravity disturbances signal

Fig. 7.8 shows the reference signal generated. It can be seen that the actual gravity signal should present a signal to noise ratio that is of the order of 1% with respect to the raw noisy observations, shown in Fig 7.7.

The second step of the processing procedure is the reduction of both observations and reference signals, for the low and mid-high frequencies. The first component (i.e. the low frequencies) is derived by using again the GECO model, which is known to have very well estimated low frequencies signal, due to the fact that it is derived from GOCE observations and EGM2008 (which contains GRACE data). It has to be underlined that for these frequencies, satellite gravity data are more reliable with respect to airborne local ones since they have a global coverage. The mid-high frequencies component instead has been synthesized using dV_ELL_RET2012 model from L_{cut} and L_{max} (i.e. 100 to 2190).

After the remove step the Wiener filter was applied along track. From the computational time point of view, the Wiener filtering, exploiting the properties

of the FFT, requires about 1 s for each flight lines for a total amount of few minutes for the whole dataset. Fig. 7.9 reports, for a sample flight line, the observed gravitational field, the synthesis from the GECO model up to degree 2190 and the reference signal (i.e. derived from GECO plus the residual terrain correction). Again it can be noticed how the observed gravity disturbances are completely dominated by the observation error, which contains not only very high frequencies but also trends and biases.

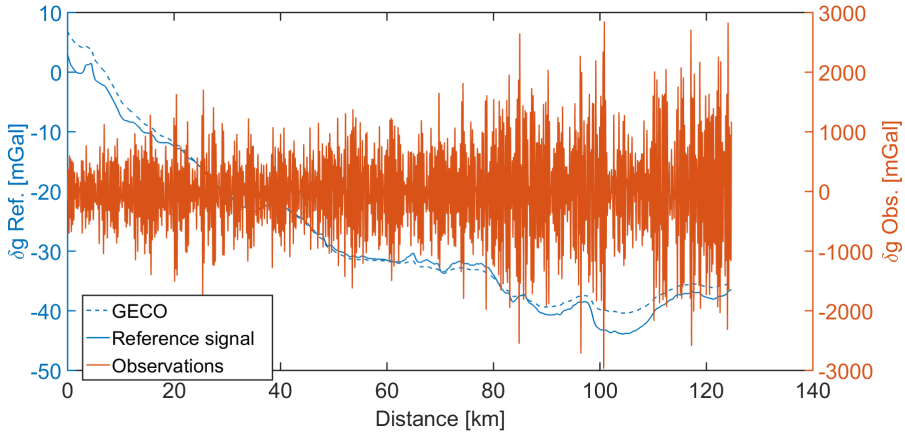

Figure 7.9: Along track reference and observed gravity disturbances signals

In Fig 7.10 the filtered reduced signal is compared to the reference one thus showing the improvements due to the airborne observations, with respect to the initial GGM-based reference signal. The order of magnitude of this improvement is of 2.65 $mGal$ (standard deviation), for the considered flight track, which is coherent with the expected accuracy of the GECO model.

Once filtered the reduced gravity disturbances, the crossover analysis was then applied. A total number of 557 crossovers has been identified and analyzed to derive the empirical covariance function of the observation noise. From this analysis emerged that the along-track colored noise presents a standard deviation of 4.81 $mGal$ and a correlation length of about 2 km. As for the covariance function of the reduced signal, it has been computed by means of the two methods described in Chapter 5 and it is shown in Fig. 7.11.

The main differences between the two covariances are due to the fact that the two methods use different inputs (filtered airborne along-track observations and grid of the reference model respectively) and use also different regions to estimate the signal covariance. For the Least Squares Collocation solution, the chosen signal covariance function was the one obtained with the first method, with

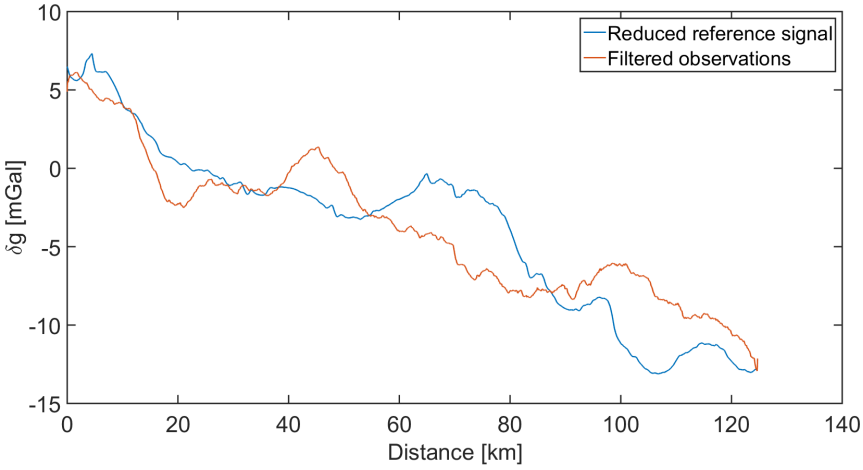

Figure 7.10: Along track reference and filtered gravity disturbances signals

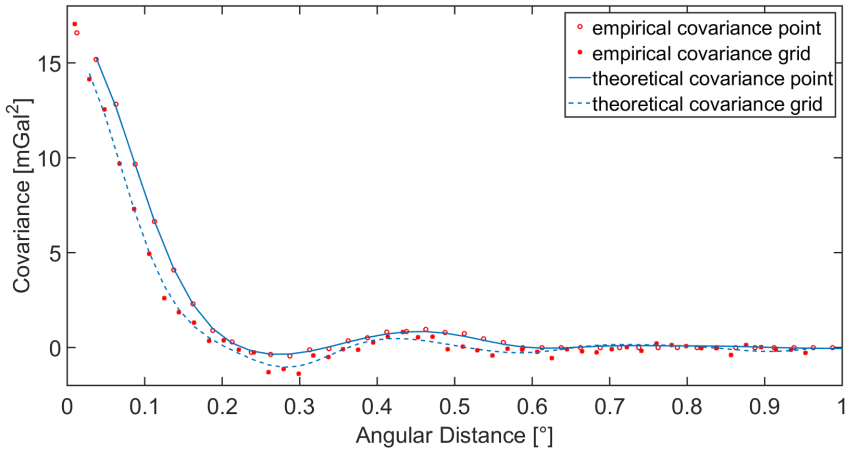

Figure 7.11: Covariances of the reduced filtered gravity disturbances signal

the objective to reduce the influence on the final solution of the GGM adopted.

In order to compute the final results by means of the Least Squares Collocation, the dataset has been downsampled by a factor 10 according to the consideration made in Section 7.5. In this way the observations dataset has been reduced

to about 80000 points. This is justified also by the fact that the initial dataset is sampled at 2.5 m and it is corrupted by a noise with approximate correlation length of about 2 km. As a consequence the contribution to the final estimate of points closer than 25 m can be assumed to be quite limited. On our working machine, the Least Squares Collocation algorithm, together with the covariance function estimation and modeling, took about 45 minutes to compute the final gravitational field on the whole observation points (800000).

The final results in terms of along-track reduced gravity disturbances and their predicted errors are shown in Figs. 7.12 and 7.13. From these figures it can be seen that the predicted error is of the order of 1.3 $mGal$ at a spatial resolution of about 1 km, increasing in proximity of the borders of the surveyed area, accordingly to the signal covariance length, due to the lack of observations in these regions. This final spatial resolution has been identified from a comparison between power spectra of noise and signal, as the minimum resolution at which the signal spectrum results to be larger than the noise one. The obtained

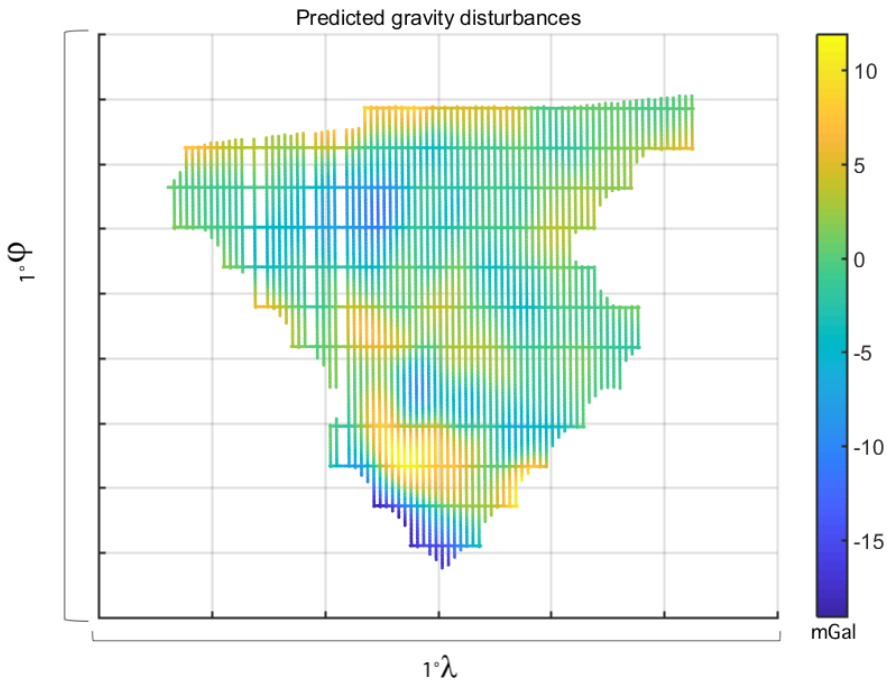

Figure 7.12: Predicted gravity disturbances signal for along-track points

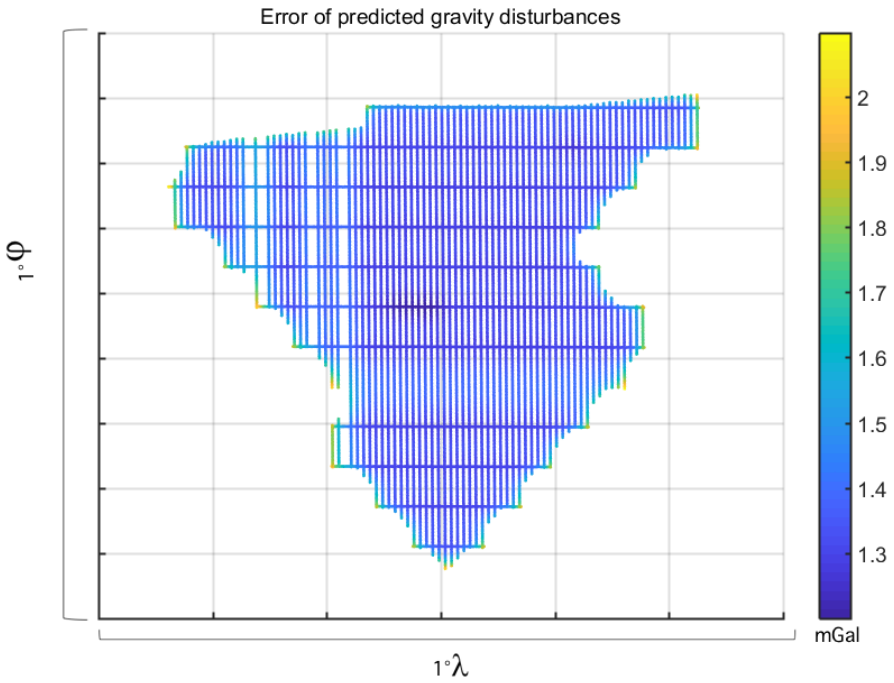

Figure 7.13: Accuracies of the predicted gravity disturbances signal for along-track points

accuracy is greater than the objective goal of the VIKING procedure, however it should be considered that it is directly influenced by the spacing among the flight track, that within this dataset was not sufficient to reach a sub *mGal* level of accuracy.

Chapter 8

Summary and Outlook

The airborne gravimetry represents nowadays one of the most efficient techniques ideal to collect gravity observations close to the Earth's surface, in a fast and cost-effective way. With the advent of GNSS technology that drastically improved the accuracy of navigational data, the aerogravimetry technique achieved a wide spread. Among the principal reasons of this diffusion there is its capability to provide gravity measurements over relative wide regions with a few days survey and the possibility to use it also in challenging environments which can be difficult to access otherwise, such as mountainous areas, rain forests and polar regions. The gravity data acquired with an airborne system have a much higher resolution than the one of those data coming from satellite missions, due to the fact that they are collected closer to the Earth's surface with respect to the latter ones. As a consequence, they found various applications from the classical scientific ones, such as the regional gravity field modeling, to commercial applications for the oil and gas industries, like geophysical studies finalized to the resources exploration.

The traditional airborne measuring system has three principal components: an accelerometer, i.e. the gravimeter, to measure the specific force, a system to evaluate the accelerometer attitude and a GNSS receiver to derive the inertial acceleration of the aircraft. Combining gravimeter and GNSS data, the gravity observations can be derived. Nowadays other measuring systems are available and represent an interesting topic to be investigated for the scientific community, however for resources exploration purposes this system remains the standard to be adopted.

The present work proposes a new methodology for processing airborne gravity measurements, named Very Improved KINematic Gravimetry (VIKING). VIKING is based on an innovative approach for estimating the accelerations of a single GNSS receiver by means of the so called variometric solution that only requires the observations of a single GNSS receiver and the standard GNSS products (orbits and clocks provided with the satellites navigation message).

The variometric algorithm is based on the assumption that the time single-difference of carrier phase observations displays the changes in the geometric range between the satellite and the receiver, so by dividing for the time interval between two epochs, it can be related to the averaged receiver velocity. In the same way, applying this concept to aerogravimetry, the double differences in time can be considered a valid estimator of the receiver acceleration. In this way, the variometric approach basically consents to use the GNSS receiver as a velocimeter as well as an accelerometer.

The VIKING methodology does not only consists in the application of the variometric approach for GNSS processing, but it includes also a complete procedure to process the aerogravimetric data, from the initial pre-processing phase (to derive the raw gravity accelerations) to the filtering and gridding phase (finalized to estimate grid or along track gravity disturbances).

The developed algorithms used to pre-process raw GNSS acquired data are basically obtained by manipulating the classical GNSS observation equation to derive a new expression sensitive to the receiver acceleration (which corresponds to the vehicle acceleration) but almost insensitive to its actual position. Moreover they have been thought for a multi constellation approach, to exploit the various available GNSS constellations and to improve the derived acceleration estimate. Regarding the gravimeter data pre-processing instead, the algorithms implemented consent to compute all the corrections terms (i.e. the Eövös and the lever arm effects) that can not be neglected to properly combine gravimeter and GNSS observations. The optimal combination is performed applying the tuned developed algorithms that deal with the different sampling rate of these two dataset.

The implemented processing procedure is based on a combination of an along track Wiener filter with a classical Least Squares Collocation adjustment. Moreover, since the stochastic properties of the observation error are in general unknown, the developed algorithms include a method that on the basis of the crossovers analysis serves to empirically evaluate them. The principal issue related to airborne gravity data is their signal-to-noise ratio which is commonly lower than $\frac{1}{1000}$. The standard solution to this problem is a remove-compute-restore procedure that consents to disentangle the noise from the actual gravity signal. The VIKING processing solution has the same characteristics of this type of procedure and from the exploitation of the information coming from the

available GGMs allows to first recover the valuable signal from the raw gravity accelerations and then to extrapolate them on grid or sparse points.

During the implementation of the whole processing procedure, it was decided to define a methodology not strictly dependent on the GGM used and based as more as possible on the acquired airborne observations. With this purpose, for instance the estimation of the empirical covariances of both the observation noise and the observed signal have been performed by fully exploiting the airborne data, without involving the GGM-derived reference signal.

An important part of the whole research project regarded the implementation of a suitable software for airborne gravity data processing. The first preliminary version of this software has been developed and tested in Matlab programming environment, and then the final code has been converted in parallel C programming language. The software is organized in a set of toolboxes, which can be run independently from all the other ones, or in sequence to perform the whole processing.

In order to evaluate the performances of the proposed approach and the implemented software suite, various numerical tests have been performed. The dataset used is a real airborne dataset, acquired by one of the major operator providing airborne geophysical surveys for petroleum and mineral exploration. The different tests are mainly focused on the analysis of the optimal choice of some parameters involved in the computation and on the performances in terms of accuracy and computational times of the various modules.

From the test on the optimal time step to be chosen to compute the time double differences from GNSS data emerged that a 1 s interval is preferable, since, after the analysis of the GNSS accelerations power spectra, it resulted to be the one that maximize the high frequencies content of the signal. The advantages of the multi constellation GNSS processing have been evaluated too, by means of the second test here presented aimed to estimate the acceleration of a static point (which is clearly zero). The results of this test have shown that the optimal combination that improves the accuracy of the derived acceleration is GPS and Beidou, while GLONASS introduces some kind of observation errors that degrade the estimates. The L_{cut} parameter has been investigated as well with a test which proved that its value slightly influence the final predicted values of gravity disturbances (the differences of the results with different L_{cut} are below the 1 $mGal$ level). However from the obtained results emerged that it should be chosen as low as possible since it is related to the presence of some medium-high frequencies, that is better to maintain and not remove before the application of the Wiener filter. In conclusion, once set the various parameters on the basis of the performed tests, the entire methodology has been tested to derive the final prediction of gravity disturbances and their corresponding errors. The obtained results show a predicted signal with accuracies of about 1.3 $mGal$ at a spatial

resolution of about 1 km that degrade, as expected, with the increase of the distance from the airborne observations.

Outlook

Looking for future improvements of the VIKING methodology, all the principal issues emerged from the development of the procedure and the results of the numerical tests performed have been taken into account. The analysis of all these aspects has highlighted the following topics that would be interesting to investigate more in details in the future:

- about the GNSS processing, from the numerical test done to evaluate the advantages of the multi constellation approach, emerged that an analysis of the errors characterizing the various GNSS observations as well as a proper weighting of the GNSS observations belonging to different constellations could be an interesting research problem; these analysis in fact seem to be necessary to benefit from the multi constellation approach and to improve the reachable accuracies of the derived accelerations;
- about the remove-compute-restore procedure, the optimal choice of the L_{cut} parameter in particular by exploiting the full covariance of the global model error, is an issue that could be further investigated too;
- another aspect could be the upgrade of the terrain correction module, that actually works only in planar approximation, to introduce also the spherical approximation and the multi resolution approach, that are currently been tested and investigated in Matlab environment; this would improve the modeling of the terrain and consequently its corresponding gravity effect;
- from the theoretical point of view, another improvement regards the extension of the presented methodology to other functional of the anomalous potential, such as its second derivatives in the various directions or the geoid undulation;
- in the end, the downward continuation, which is the operation of moving gravity observations in the vertical direction, commonly adopted in the processing of gravity data for both geodetic and geophysical applications, could be an interesting matter to be examined and implemented in the future within the VIKING methodology.

List of Acronyms

BLUP	Best Linear Unbiased Predictor
CHAMP	CHallenging Minisatellite Payload
DGPS	Differential Global Positioning System
DTM	Digital Terrain Model
ESA	European Space Agency
FFT	Fast Fourier Transform
FOC	Full Operational Capability
GGM	Global Gravity Model
GLONASS	GLObal'naya NAvigatsionnay Sputnikovaya Sistema
GNSS	Global Navigation Satellite Systems
GOCE	Gravity Field and Steady-State Ocean Circulation Explorer
GPS	Global Positioning System
GRACE	Gravity Recovery And Climate Experiment
HPC	High Performance Computing
ICGEM	International Center for Global Gravity Field Models
IGFS	International Gravity Field Service
IAG	Internationa Association of Geodesy
IGS	International GNSS Service
IMU	Inertial Measurement Units
INS	Inertial Navigation System
LSC	Least Squares Collocation
MMSE	Minimum Mean Square Error
NAVSTAR	NAVigation Satellite Time and Ranging
NNLS	Non Negative Least Squares
NRL	Naval Research Laboratory
PPP	Precise Point Positioning
RTC	Residual Terrain Correction

S/A	Selective Availability
SINS	Strapdown Inertial Navigation System
TEC	Total Electron Count
UAV	Unmanned Airborne Vehicles
US	United States
VIKING	Very Improved KINematic Gravimetry

Acknowledgments

This work is the result of three years of research. I would like to express my gratitude to all the people that helped me, in all various and different ways.

First of all, I would like to thank the management of Eni Upstream and Technical Services for the permission to realize this research project and concretely apply it to real problems within the resources exploration.

I would like to express a special thank to my Supervisor, Professor Mattia Crespi, and my Co-Supervisor, Emeritus Professor Fernando Sansó, that led me throughout this experience.

Then, I am totally aware that this work substantially benefited from the precious help of Dr. Daniele Sampietro and from his wide knowledge of many topics related to gravity field modeling. His encouragement, suggestions and discussions have been essential for the finalization of this work.

I would like to thoroughly thank Professor Mirko Reguzzoni and Dr. Andrea Gatti of Politecnico di Milano, that have been a fundamental source of informations and advices. I am particularly gratefull to Dr. Gatti for useful conversations and important suggestions which helped me within the development of the C VIKING software.

I shared the last three years of my working and studying experience with other researchers and Ph.D. candidates of the Department of Civil and Environmental Engineering of Politecnico of Milan and with all the members of the GReD srl. The nice, productive and cooperative atmosphere that I experienced is due to each of them. Thank you.

Finally, I would like to acknowledge all the people that supported me, day by day: my family, friends. All of you helped me, in different ways, within this experience. Thank you.

Bibliography

[1] Alberts, B., 2009. *Regional gravity field modeling using airborne gravimetry data*. NCG, Nederlandse Commissie voor Geodesie.

[2] Amante, C., & Eakins, B. W., 2009. *ETOPO1 1 Arc-minute global relief model: Procedures, data sources. and analysis*. Tech. Rept. NESDIS NGDC-24, National Geophysical Data Center, National Oceanic and Atmospheric Administration (NOAA), Boulder, Colorado.

[3] Arabelos, D., & Tziavos, I. N., 1992. *Gravity field approximation using airborne gravity gradiometer data*. Journal of Geophysical Research: Solid Earth, 97(B5), 7097-7108.

[4] Barthelmes, F. & Köhler, W., 2016. International Centre for Global Earth Models (ICGEM), in: Drewes, H., Kuglitsch, F., Adam, J. et al., *The Geodesists Handbook 2016,* Journal of Geodesy (2016), 90(10), pp 907-1205, doi: 10.1007/s00190-016-0948-z.

[5] Blakely, R. J., 1996. *Potential theory in gravity and magnetic applications*. Cambridge University Press.

[6] Blewitt, G., 2007. *GPS and Space-Based Geodetic Methods.Treatize on Geophysics.* Academic Press, Oxford, UK, 2007, vol. 3., ch. 3, pp. 351-390. Editor Thomas Herring, Ed.-in-chief Gerald Schubert.

[7] Brozena, J. M., 1992. *The Greenland Aerogeophysics Project: Airborne gravity, topographic and magnetic mapping of an entire continent*. In From Mars to Greenland: Charting Gravity With Space and Airborne Instruments (pp. 203-214). Springer New York.

[8] Brozena, J. M., Peters, M. F., & Salman, R., 1997. *Arctic airborne gravity measurement program*. In Gravity, Geoid and Marine Geodesy (pp. 131-138). Springer Berlin Heidelberg.

[9] Bruton, A. M., 2000. *Improving the accuracy and resolution of SINS/DGPS airbone gravimetry.* University of Calgary.

[10] CarbonNet Project Airborne Gravity Survey, 2012. *Gippsland Basin Nearshore Airborne Gravity Survey, Victoria, Australia.* Victoria: Department of primary industries, Victoria State Government.

[11] Chen, D., & Plemmons, R. J., 2009. *Nonnegativity constraints in numerical analysis.* The birth of numerical analysis, 10, 109-140.

[12] Bell, B., & Clark, J., 2002. *Bringing command and control of unmanned air vehicles down to earth.* In Digital Avionics Systems Conference, 2002. Proceedings. The 21st (Vol. 2, pp. 7E1-7E1). IEEE.

[13] Colon, C. R., 1999. *An efficient GPS Position determination algorithm* . Ph.D. dissertation (No. AFIT/GE/ENG/99M-33), Air Force Institute of Technology, Wright-Pattersonafb, OH.

[14] Colosimo G., 2012. *VADASE-Variometric Approach for Displacement Analysis Stand-Alone Engine.* Ph.D. dissertation, University of Rome "La Sapienza", Italy.

[15] Davis, P. J., 1975. *Interpolation and approximation.* Courier Corporation, New York.

[16] Dow, J. M., Neilan, R. E., Weber, R., and Gendt, G., 2007. *Galileo and the IGS: taking advantage of multiple GNSS constellations.* Advances in Space Research (2007).

[17] Dow, J. M., Neilan, R. E., & Rizos, C., 2009. *The International GNSS Service in a changing landscape of Global Navigation Satellite Systems.* Journal of Geodesy 83 (2009), 191-198.

[18] Forsberg, R., & Kenyon, S., 1994. *Evaluation and downward continuation of airborne gravity data-the Greenland example.* In Proc. of International Symposium on Kinematic Systems in Geodesy, Geomatics and Navigation (KIS94) (pp. 531-538).

[19] Forsberg, R., & Kenyon, S. C., 2002. *Arctic Gravity Project.* Eos Trans. AGU, 80, 46.

[20] Gilardoni, M., Reguzzoni, M., & Sampietro, D., 2016. *GECO: a global gravity model by locally combining GOCE data and EGM2008.* Studia Geophysica et Geodaetica, 60(2), 228.

[21] Glennie, C. L., 1999. *An analysis of airborne gravity by strapdown INS/DGPS*. University of Calgary.

[22] Glennie, C. L., Schwarz, K. P., Bruton, A. M., Forsberg, R., Olesen, A. V., & Keller, K., 2000. *A comparison of stable platform and strapdown airborne gravity.* Journal of Geodesy, 74(5), 383-389.

[23] Götze, H-J., and Lahmeyer, B., 1988. *Application of three-dimensional interactive modeling in gravity and magnetics*. Geophysics, 53, 1096-1108.

[24] Grafarend, E. W., 2006. *Linear and nonlinear models: fixed effects, random effects, and mixed models*. de Gruyter.

[25] Forsberg, R., 2003. *An overview manual for the GRAVSOFT Geodetic Gravity Field Modelling Programs*. DNSC - Daniosh National Space Center.

[26] Grubbs, F. E., 1950. *Sample criteria for testing outlying observations*. The Annals of Mathematical Statistics, 27-58.

[27] Gumert, W. R., 1998. *An historical review of airborne gravity*. The Leading Edge, 17(1), 113-116.

[28] Hammer, S., 1983. *Airborne gravity is here!*. Geophysics, 48(2), 213-223.

[29] Harlan, R. B., 1968. *Eotvos corrections for airborne gravimetry*. Journal of Geophysical Research, 73(14), 4675-4679.

[30] Heiskanen, W. A., & Moritz, H., 1967. *Physical geodesy*. Bulletin Geodesique (1946-1975), 86(1), 491-492.

[31] Hirt, C., Featherstone, W. E., & Marti, U., 2010. *Combining EGM2008 and SRTM/DTM2006. 0 residual terrain model data to improve quasigeoid computations in mountainous areas devoid of gravity data.* Journal of Geodesy, 84(9), 557-567.

[32] Hofmann-Wellenhof, B., Lichtenegger, H., & Wasle, E., 2007. *GNSS-global navigation satellite systems: GPS, GLONASS, Galileo, and more*. Springer Science & Business Media.

[33] Huang, Yangming, et al., 2007. *SGA-WZ: A new strapdown airborne gravimeter*. Sensors 12.7 (2012): 9336-9348.

[34] Jekeli, C., 1998. *Algorithms and preliminary experiences with the LN93 and LN100 for airborne vector gravimetry*. OHIO STATE UNIV COLUMBUS DEPT OF CIVIL ENGINEERING.

[35] Karaim, M., Karamat, T. B., Noureldin, A., & El-Shafie, A., 2014. *GPS Cycle Slip Detection and Correction at Measurement Level.* British Journal of Applied Science & Technology, 29(4), 4239-4251.

[36] Kaula, W. M., 1966. *Tests and combination of satellite determinations of the gravity field with gravimetry.* Journal of Geophysical Research, 71(22), 5303-5314.

[37] Klobuchar, J. A., 1996. *Ionospheric effects on GPS. Global Positioning System: Theory and applications.* 1, 485-515.

[38] Krarup, T., 1968. *A framework for least-squares determination of the potential of the earth.* International Association of Geodesy, Copenhagen, Denmark.

[39] Krarup, T., 1969. *A contribution to the mathematical foundation of physical geodesy.* Geod. Inst. Copenhagen, Medd., No. 44, 80 p., 44.

[40] Lambeck K, 1990. *Aristoteles: an ESA mission to study the earth's gravity field.* ESA J 14:1-21.

[41] Lawson, C. L., & Hanson, R. J., 1995. *Solving least squares problems.* Society for Industrial and Applied Mathematics.

[42] Leick, A., Rapoport, L., & Tatarnikov, D., 2015. *GPS satellite surveying.* John Wiley & Sons.

[43] Longman, I. M., 1959. *Formulas for computing the tidal accelerations due to the moon and the sun* Journal of Geophysical Research, 64, 2351-5.

[44] MacMillan W.D., 1930. *Theoretical Mechanics, vol. 2: The Theory of The Potential.* MacGraw-Hill, NewYork (1930). Reprinted by Dover Publications, New York (1958).

[45] Moritz, H., 1972. *Advanced least-squares methods* (Vol. 175). Columbus: Department of Geodetic Science, Ohio State University.

[46] Nagy D., 1966. *The gravitational attraction of a right rectangular prism.* Geophysics, 31, 362-371.

[47] Nassar, S., Schwarz, K. P., & El-Sheimy, N., 2004. *INS and INS/GPS accuracy improvement using autoregressive (AR) modeling of INS sensor errors.* In Proceedings of ION-NTM (pp. 936-944).

[48] Nettleton, L. L., LaCoste, L., & Harrison, J. C., 1960. *Tests of an airborne gravity meter.* Geophysics, 25(1), 181-202.

[49] Offord, A. C., 1935. *On Hankel Transforms.* Proceedings of the London Mathematical Society, 2(1), 49-67.

[50] Olesen, A. V., 2002. *Improved airborne scalar gravimetry for regional gravity field mapping and geoid determination.* Doctoral dissertation, Faculty of Science, University of Copenhagen.

[51] Report 2015-2016. *PolarGap 2015/2016 -Filling the GOCE polar gap in Antarctica (and ASIRAS radar flight for CryoSat support).*

[52] Robinson, G. K., 1991. *That BLUP is a good thing: the estimation of random effects.* Statistical science, 15-32.

[53] Reguzzoni, M., Tselfes, N., 2009. *Optimal multi-step collocation: application to the space-wise approach for GOCE data analysis.* Journal of Geodesy, 83(1), 13-29.

[54] Rummel, R., Balmino, G., Johannessen, J., Visser, P. N. A. M., & Woodworth, P., 2002. *Dedicated gravity field missions-principles and aims.* Journal of Geodynamics, 33(1), 3-20.

[55] Saastamoinen, J., 1972. *Atmospheric correction for the troposphere and stratosphere in radio ranging satellites.* The use of artificial satellites for geodesy, 247-251.

[56] Sampietro, D., Capponi, M., Triglione, D., Mansi, A. H., Marchetti, P., & Sansó, F., 2016. *GTE: a new software for gravitational terrain effect computation: theory and performances.* Pure and Applied Geophysics, 173(7), 2435-2453.

[57] Sampietro, D., Capponi, M., Mansi, A. H., Gatti, A., Marchetti, P., & Sansó, F., 2017. *Space-Wise approach for airborne gravity data modelling.* Journal of geodesy, 91(5), 535-545.

[58] Sander, S., Argyle, M., Elieff, S., Ferguson, S., Lavoie, V., & Sander, L., 2004. *The AIRGrav airborne gravity system.* In Airborne Gravity 2004-Abstracts from the ASEG-PESA Airborne Gravity 2004 Workshop: Geoscience Australia Record (Vol. 18, pp. 49-54).

[59] Sansò, F., 1997. *Il trattamento statistico dei dati.* CittáStudi.

[60] Sansó, F., & Sideris, M. G., 2013. *Geoid determination: theory and methods.* Springer Science & Business Media.

[61] de Saint-Jean B., Verdun J., Duquenne H., Barriot J., Melachroinos S., Cali J., 2007. *Fine analysis of lever arm effects in moving gravimetry.* Dynamic Planet, 809-816.

[62] Schwarz, K. P., Sideris, M. G., & Forsberg, R., 1990. *The use of FFT techniques in physical geodesy.* Geophysical Journal International, 100(3), 485-514.

[63] Schwarz, K. P., Colombo, O., Hein, G., & Knickmeyer, E. T., 1992. *Requirements for airborne vector gravimetry.*. In From Mars to Greenland: Charting Gravity With Space and Airborne Instruments, 273-283, Springer New York.

[64] Schwarz, K., & Li, Z. , 1997. *An introduction to airborne gravimetry and its boundary value problems.* Geodetic boundary value problems in view of the one centimeter geoid, 312-358.

[65] Schüler, K., & Li, Z. , 1997. *On ground-Based GPS Tropospheric delay estimation.* Ph.D. dissertation,Universität der Bundeswehr München.

[66] Skaloud, J., Colomina, I., Parés, M. E., Blázquez, M., Silva, J., & Chersich, M., 2016. *A Method of Airborne Gravimetry by Combining Strapdown Inertial and New Satellite Observations via Dynamic Networks.* Part of the series International Association of Geodesy Symposia pp 1-12.

[67] Smit M, Koop R, Visser P, van den IJssel J, Sneeuw N, Muller J, Oberndorfer H, 2000. *GOCE End-to-End Performance Analysis, Final Report.* ESTEC Contract No. 12735/98/NL/GD.

[68] Smith, D. A., 2007. *The GRAV-D project: gravity for the redefinition of the American Vertical Datum.*

[69] Tegedor, J., Ovstedal, O., & Vigen, E., 2014. *Precise orbit determination and point positioning using GPS, Glonass, Galileo and BeiDou.* Journal of geodetic science, 4(1).

[70] Thompson, L. & LaCoste, L., 1960. *Aerial gravity measurements.* J. geophys. Res., 65, 305-322.

[71] Tian, Y., 2016. *Online estimation of inter-frequency/system phase biases in precise positioning.* M. Sc. Technische Universität Berlin.

[72] Tsoulis D., and Petrovic S., 2001. *On the singularities of the gravity field of a homogeneous polyhedral body.* Geophysics, 66, 535-539.

[73] Uieda L., Bomfim E.P., Braitenberg C. and Molina E., 2011. *Optimal forward calculation method of the Marussi tensor due to a geologic structure at GOCE height*. Proceedings of the 4th International GOCE User Workshop.

[74] Uieda, L., Oliveira V. C. Jr, and Barbosa, V. C. F., 2013. *Modeling the Earth with Fatiando a Terra*. Proceedings of the 12th Python in Science Conference, pp. 91 - 98.

[75] Watts A.B, 2001. *Isostasy and Flexure of the Lithosphere.* Cambridge University Press, Montpelier.

[76] Watson G.N., 1995. *A treatise on the theory of bessel functions.* Cambridge University Press, Montpelier.

[77] Wei, M., & Schwartz, K. P., 1998. *Flight test results from a strapdown airborne gravity system.* Journal of Geodesy, 72(6), 323-332.

[78] Yao, Y., He, Y., Yi, W., Song, W., Cao, C., & Chen, M., 2017. *Method for evaluating real-time GNSS satellite clock offset products.* GPS Solutions, 1-9.